UNIVERSITY OF OKLAHOMA

GRADUATE COLLEGE

DRAINAGE BEHAVIOR OF AQUEOUS, POLYMERIC, AND OIL-BASED NITROGEN FOAMS: THEORETICAL AND EXPERIMENTAL INVESTIGATION

A DISSERTATION

SUBMITTED TO THE GRADUATE FACULTY

in partial fulfillment of the requirements for the

Degree of

DOCTOR OF PHILOSOPHY

By

ABHISHEK GOVINDU

Norman, Oklahoma

2019

DRAINAGE BEHAVIOR OF AQUEOUS, POLYMERIC, AND OIL-BASED NITROGEN FOAMS: THEORETICAL AND EXPERIMENTAL INVESTIGATION

A DISSERTATION APPROVED FOR THE

MEWBOURNE SCHOOL OF PETROLEUM AND GEOLOGICAL ENGINEERING

BY

Dr. Ramadan Ahmed, Chair

Dr. Ramkumar Parthasarathy

Dr. Subhash Shah

Dr. Catalin Teodoriu

Dr. Saeed Salehi

Dr. Mahmood Amani

Dr. Bor-Jier Shiau

A book is never read for the letter last.

ACKNOWELDGEMENTS

This research was made possible by NPRP grant 10-0115-170165 from the Qatar National Research Fund (QNRF). I would like to express my utmost gratitude to QNRF for their sponsorship without which this work would not have seen the light of day. Further, this work is a culmination of efforts of various people who have either directly or indirectly shaped my life at the University of Oklahoma. Without Dr. Subhash Shah's encouragement in 2009, I would probably never have pursued higher education after obtaining my undergraduate degree. Dr. Ramadan Ahmed taught me my first class at OU, making me realize that there is much more to the career path I had chosen than I had reckoned as a freshly graduated twenty-year old. I would like to thank them both for their patience with me, motivation, and support. Dr. Shah taught me tubing flow data analysis and how to present technically. I have built on that over the past several years resulting in the work produced for various projects at the Well Construction Technology Center (WCTC) and at my internships. Dr. Ahmed taught me how to write technically, be it my MS thesis, journal papers, or this current document. I am greatly indebted to them both. I cannot imagine my current career path without their guidance during my time spent at OU, and I am confident they will play a role in any future paths that I might tread.

I credit Dr. Kumar Parthasarathy for helping me understand the fundamentals of fluid mechanics. I still remember my first class with him where my answer to his question on defining viscosity proved inadequate. If I ever stumble upon a teaching profession, I know who I am going to try to emulate. I thank Dr. Saeed Salehi, Dr. Catalin Teodoriu, Dr. Mahmood Amani, and, Dr. Bor-Jier Shiau, for serving as my committee and for their suggestions to improve the quality of my work. I express my thanks to Jeff McCaskill and the late Joe Flenniken for their help in conducting every experiment at WCTC. Jeff McCaskill always tries to teach students how to

handle various tools as well as explain the right way to perform the tasks necessary to design tests, construct equipment, and execute experiments. This information is invaluable and cannot be acquired in the classroom. I also thank Gary Stowe for providing me with surface tension measurements, without which the mathematical modeling portion of this work could not have been accomplished. I would also like to acknowledge Dr. Sarkis Kakadjian who gave me the opportunities of interning for Trican Well Service and Keane Group, as well as his team at the Woodlands, notably Jarrett Kitchen, Amanda Flowers, and Antonio Pontifes, among others. Various students and graduates at WCTC have also helped shape skills that went into preparing this document. I acknowledge Feyi Fakoya, Rida Elgaddafi, Vineet Sinha, Soham Pandya, Harsh Patel, Sarvesh Naik, and various others, who in their own way have encouraged and supported me over the years.

In my personal life, I have been lucky to be surrounded by amazing people who have helped me in various ways over the years. My first year at OU I met Mark and Kim Klein who have welcomed me into their family. I will always cherish the memories of time spent at their home with – Britt and her growing little family; Braden and her husband; Chandra and her beautiful family; Brent; Aunt Susan; the late Grandma Helen; among others, and the fun conversations that we have had over the years. It is hard to list all the incredible people I have fostered relationships with during my time at OU. These friends – Abhijit, Lauren, Sarith, Auda, Alex, Shi Qi, Shendi, Emily, Armando, Tara, Marija, Adwaita, Himanshu, KV, Aditya, Priyavrat, Ruchir, Jyot, Neira, Salah, Sunayna, Saurabh, Karma, Sheila, Andrea, Delcio, and many many more, have been there during the good times. A lot of them have been there as well for support when times were not so good.

Lastly, I wish to acknowledge my family who have been a pillar of strength, and without whom I would have lacked the courage to achieve anything meaningful. Members of the Lee family – Jason, Richard, and, Janice, among others, have opened their doors and literally fed me for months. My sisters and cousins – Kavitha, Kalpana, Venkesh, Shailu, as well as others including Kayra, have always been there when I had nowhere to turn in a foreign land, and have done everything they can to provide an ideal environment as I complete this manuscript. My amazing parents have done everything in their power to make me the person I am today. They have always shown a keen interest in my work and have been a great source of comfort. My little brother, who is not so little anymore, has always reminded me that I need to be the best version of the both of us and shaken away any fears or indecision that tend to creep up. Whatever life may have in store, I could not wish for better people than these to share it with. They say you cannot choose family, but I certainly did with Jessica Govindu. This incredible person has, over the years, made me feel invincible thanks to her unwavering belief in me that borders on incredulous. She is certainly the reason that makes me feel like I am on the top of the world and that there is nothing I cannot do. She does all this despite her work in Washington D.C. being certainly much more relevant in today's world than mine as she takes on the fight for indigenous people's rights with lawmakers and members of the United States Congress.

I am certainly very fortunate to call on each and every one of you as mentors, friends, and family. This is as much your achievement, as it is mine. Thank you.

TABLE OF CONTENTS

LIST OF TABLES

LIST OF FIGURES

ABSTRACT

Foams can be formulated to have a wide range of densities and viscosities. This unique behavior makes foam suitable for underbalanced drilling where pressure exerted on formation is maintained below pore pressure and at the same time, favorable conditions for a good hole-cleaning can be established in the wellbore. Foams are also used as in fracturing, cementing, and, enhanced oil recovery applications. However, the disadvantage of foam is its inherent instability. The stability of aqueous foams in vertical conduits has been extensively investigated. However, in many industrial applications such as underbalanced drilling foam is used in inclined configurations. The stability of foams inclined conduits is not well understood. The effect of geometry is often ignored. In addition, polymer-based and non-aqueous foams with more complex flow and stability behavior are becoming more common. As a result, there is a strong need to investigate foams to better understand the effects of different operational factors (inclination, conduit geometry, base fluid type, and shearing) on their stability. Thus, the main goal of this study is to investigate each of these factors with respect to their impact on foam stability.

To achieve this, foam stability experiments were conducted in concentric annulus and straight pipe sections. The pipe section is manufactured from a fully transparent PVC pipe, enabling visual inspection of foam structure and liquid drainage. The annulus is made of stainless steel casing and a rotating inner PTFE (polytetrafluoroethylene) rod. Three types of foams (aqueous, polymeric-based and oil-based foams) were used in the investigation. All tests were performed at 400 KPa and ambient temperature (22 ± 2^{o}C). Foam quality was ranged from 40 - 80%, except for oil-based foam which was limited to 70% due to instability at high qualities. Foam rheology data was obtained from pipe viscometers before conducting stability tests. Two inclination angles (0^{o} and 30^{o}) were considered in this study. For tests conducted in the annulus,

the rotation speed of the inner rod was varied (0, 4, and 7 rpm) to examine the impact of shearing on foam stability. Hydrostatic pressure data measured from the annular test section is converted into density profiles, which are used to determine the drained liquid volume as a function of time. In straight pipe sections, the volume of drained liquid was measured using a measuring tape. A digital camera with a microscope was used to capture images of foam in real-time to examine the process of foam decay (i.e. the degree of bubble coarsening and coalescence).

Foam stability increased with quality. For a given quality, foam prepared with polymeric fluid was the most stable, while oil-based foam was the least. The wall effects can hinder bubble and drained liquid motion and consequently delay drainage. As a result, foam drained more slowly in the annulus than in pipe. Inclining the test sections resulted in much faster drainage, possibly due to the formation of a liquid layer between foam structure and container walls that flows down due to gravity, effectively avoiding the hydraulic flow resistance of foam structure. The effect of shearing on drainage was minimal for the level of shear rate applied. Channel-dominated model developed in this study is suitable for all foams considered (40-80%). Node-dominated model is not recommended for these wet foams as it tends to over predict liquid volume fractions at early time steps.

CHAPTER 1

INTRODUCTION

Foams are a common occurrence in industrial processes that involve gas-liquid fluid systems. When naturally occurring or generated as by-products, foams are often considered problematic (e.g. – crude oil foaming in refineries or wastewater foaming in sewage). On the other hand, specially formulated foams are used in various industrial and domestic applications due to their low densities and/or high viscosities (e.g. firefighting foam and shaving foam). In the oil and gas industry, foam can be encountered or applied at all stages of hydrocarbon recovery including drilling, cementing, hydraulic fracturing, production operations, enhanced oil recovery, transportation, and processing. Stable foams used as drilling fluids are designed to lubricate the bit, carry cuttings to the surface, control formation pressure, and exert pressure on the formation to stabilize the wellbore.

Foam generated for a specific application at one stage of hydrocarbon recovery can be useless in the next stage. For example, because of their high-viscosity, foams are created in-situ for enhanced recovery operation to improve the volumetric sweep efficiency of reservoirs. However, undesirable foams encountered at the surface in oil-water separators and distillation towers in refineries create problems, and they are often broken down to their constituent fluids using chemicals. It is essential that foam retains its properties when specifically applied at a particular stage, and loss of properties can lead to costly remedial operations. For instance, if foam breaks down during drilling operation it can lead to excessive formation damage and wellbore instability issues.

1.1 Foamability of Foam and Thermodynamically Unstable Foams

Foams are a colloidal dispersion with gas as the dispersed phase and liquid as the continuous phase (Bhakta and Ruckenstein 1997; Weaire and Hutzler 1999). Solid foams are a special type of foams where gas is dispersed in a solid. These foams are not discussed in this study. As a colloidal species foams belong to the same family as dispersed bubbles, particles, or droplets, where at least one substance is insoluble and microscopically dispersed (with diameters typically between 10 and 1000 μm) in another. Bubble sizes in foam can often exceed the upper limit, especially as foam approaches its collapse. All foams eventually collapse, if left on their own as they are thermodynamically unstable.

The ability of a solution to produce foam is termed foamability. To create foam, energy is added to a gas-liquid system, which leads to an increase in the gas-liquid interfacial area (Wang et al. 2016). Energy can be added to gas-liquid solution through physical (mechanical foaming or phase transition), chemical, or biological means (Drenckhan and Saint-Jalmes 2015). The foaming technique chosen affects the dispersion of bubbles in liquid (monodispersed or polydispersed) as well as their size distribution. Therefore, the properties of foams generated greatly depend on the method used to produce them. In addition, the foaming method greatly influences the rate of foam generation. Examples of foam used in daily life, generated using various methods of generation are shown in Table 1.1. Usually, energy added to the gas-liquid solution is mechanical and it can be simple agitation, injection of gas into liquid, or application of shear. Since energy is added to the system and results in a net increase in surface energy (Eq. 1.1) this process is not spontaneous. Hence:

$$E = \sigma A \tag{1.1}$$

where E is the surface energy; σ is the interfacial tension; and, A is the interfacial area. The produced foam is at a higher energy state than its constituents (liquid and gas phases with a lower interfacial area between them), and hence, it is thermodynamically unstable. The system tries to achieve a lower, more stable energy state by minimizing the gas-liquid interface. This occurs by gas bubbles merging to form larger bubbles and downward draining of liquid due to gravity, lowering gas-liquid contact area. Ultimately, the two phases are completely separated, and the system achieves its most stable state with the least interfacial area between the phases. The separation of the phases due to gravity and bubble merging are the drainage/decay mechanisms of foam. These processes are thermodynamically favored and spontaneous.

Table 1. 1: Foaming Methods (Drenckhan and Saint-Jalmes 2015)

Process	Example(s)
Physical	Culinary foam created using kitchen blender (mechanical)
Chemical	Baking powder added to water
Biological	Rising of dough due to carbon dioxide produced by yeast processing sugars

Foams formed with pure liquids and gases collapse almost immediately. Merging of bubbles in such mixtures is instantaneous with no flattening of the interface between them (liquid film present between bubbles ruptures instantly). The addition of surfactants to a gas-liquid system and subsequent adsorption along the interfaces leads to the development of resistance to film rupturing (Schramm and Wassmuth 1994). Bubbles are pushed against each other and deformed due to the persistence of the liquid films between them. This persistence prolongs the life of foam, resulting in a pseudo-stable or metastable state (temporary kinetic stability), where the separation of phases is slowed and delayed, and so by comparison (timescale), foam can be considered stable. For example, shaving foam is stable as there is no noticeable separation of phases while shaving. As opposed to this, foam generated when beer or soda is poured into a glass is unstable as it dissipates almost instantaneously. Relating this to surface energy, surfactants lower interfacial tension

(Anazadehsayed et al. 2018) and, therefore, surface energy, making it easier to produce foam, i.e., increase the foamability of a solution. Since less energy is required to produce foam, the resultant foam is more likely to exist temporarily at a metastable state.

1.2 Classification of Foams

Preparing foam from its constituents (gas and liquid phases and surfactant) is a process which involves adding energy to the mixture. The difficulty arises when maintaining the stability of the created foam. A simple injection of gas into liquid results in the formation of spherical bubbles surrounded by liquid. As long as the injection rate is maintained higher than the drainage rate of liquid from between the bubbles, the foam structure can be generated.

The shape of bubbles in foam structure is one of the criteria for classification foams. When foam exhibits a structure consisting of well-separated spherical bubbles with a film thickness comparable to or greater than bubble diameters, the foam is called wet foam (Schramm and Wassmuth 1994). As liquid between bubbles drains from the wet foam, the bubbles come together. If the bubbles resist coalescence (due to thin liquid film persistence), they deform and form polyhedral shapes with very low liquid volume fraction in foam structure (as most of it has drained away). Such foam is called dry foam and is characterized by thin, flat liquid films between the polyhedral bubbles. The stability of foam structure is directly related to thin film persistence, and therefore, on the formation of dry foam.

Foams can be further classified based on their relative lifespans and effectiveness of foaming agent (surfactant). Addition of surfactant results in the formation of foam due to the lowering of surface tension and the increase in surface elasticity. The elasticity of thin film that exists between bubbles results in resistance to its rupturing and delays foam decay. Such foams

are called stable foams. However, if the elasticity of thin film is not sufficient to counteract gravity and capillary forces, the thin film between bubbles ruptures and foam formed decays quickly. Foams with short life spans are called unstable foams. The liquid phase used to prepare foam can also be used as a criterion to classify foams. The liquid phase can be aqueous (water or water-based solution) or oil. Stable aqueous or oil foams can be termed stiff foams if polymer(s) are used to viscosify the liquid phase to enhance foam properties and prolong its life.

Table 1. 2: Classification of Foams

Criteria	Nomenclature of Foam	
Bubble Shape	Wet	Dry
Relative Lifespan	Evanescent	Persistent
Liquid Phase	Aqueous	Oil
Polymer Viscosification	Stable	Stiff

1.3 Properties of Foam

The unique properties presented by foam are the reasons why it is utilized widely in various industries. These properties are dependent on physical properties of the two bulk phases that constitute foam, gas-liquid volume fraction, foam structure, the surfactant used, pressure, temperature, additives, and contaminants present (Rojas et al. 2001). In this section, a brief introduction to the properties of foam: quality, bubble size, density, rheology, stability, and carrying capacity is presented. Furthermore, the effect of pressure and temperature on foam properties, particularly stability is discussed.

1.3.1 Quality

Foams are characterized by quality and texture (bubble size distribution). Quality is the gas volume fraction in foam. Wet foam has high liquid content and is of lower quality than dry foam, which has high gas content. The stability of foam depends on its quality. High-quality dry foams have complex structures that enable viscous resistance to liquid drainage. This results in stable dry

foams with very low densities and high viscosities. However, increasing quality improves stability up to a limit beyond which the foam becomes unstable. At qualities of beyond 98%, foam splits into slugs of lower quality foam and gas (Beyer et al. 1972). At a critical quality, gas-liquid solution reaches inversion point and flow turns into mist (continuous gas phase with liquid dispersed in it). The upper limit of foam quality is variable. It depends on gas-liquid phase properties, additives and contaminants, pressure and temperature, and energy added to the system.

Increasing the shear rate (mechanical energy input) of flow helps create higher quality foams (Okpobiri and Ikoku 1986). It is hard to define a lower quality limit for stable foams. Under static conditions, gas bubbles can stably exist in foam at almost negligible gas volume fractions. In foam flow, bubbles do not interact until the quality exceeds 55% (Mitchell 1971). Foam flow is dominated by deformation of adjacent bubbles when quality exceeds 75% and foam viscosity increases nearly exponentially with foam quality (Rankin et al. 1989; Bonilla and Shah 2000).

1.3.2 Bubble Size

Bubbles in dry, stable foams (low liquid volume fraction), are polyhedral in shape and not spherical. However, it is convenient to use 'bubble diameter' when describing their size distributions. Gas bubbles in foams tend to have 'diameters' ranging from 10-1000 μm. Foams are often characterized and classified according to the shape of the bubbles dispersed in them (Sebba 1987). For example, wet foams are classified as spherical foams. Although it is simple and convenient to characterize foams this way, bubbles are never monodispersed (uniform shape and size), and there is always a size distribution. Given enough data (photographic methods), bubbles can be characterized by a distribution function or simple histograms. Foam stability is not directly related to bubble size. However, bubble size distribution and its variation with time is a good indication of stability. Foams with small average bubble size are the most stable. Change in bubble

size distribution with time can be used to mathematically indicate stability of foams. Bubble size distributions also influence the viscosity of foams, which is another measure of stability. For a given quality of foam, if gas bubbles interact electrostatically in a foam network, viscosity increases with decreasing bubble size (Schramm and Wassmuth 1994). This is because smaller bubbles correspond to a larger interfacial area; therefore, a narrower film with higher flow resistance. In addition, for a given foam quality, viscosity increases with an increase in the uniformity of bubble size.

1.3.3 Rheology

Rheological properties of foam are a combination of elastic, viscous, and yielding phenomena (Saintpere et al. 1999). These phenomena mainly depend on the properties of constituent gas and liquid phases, additives added, the surfactant used, the method of foam generation, shear rate, pressure and temperature (Ozbayoglu 2005). Higher viscosity is associated with an increase in the stability of foam as viscous forces impede liquid movement in foam network and oppose drainage. Foam rheology can be measured using Couette–flow rheometers (cone and plate, coaxial cylinders) or pipe viscometers (Hutchins and Miller 2003). In Couette–flow viscometers, foam is first generated by agitation or shear and then rheological measurements are made. In pipe viscometers, foam is generated and measurements are made while foam is flowing in either single pass or re-circulation mode.

Usually, water or oil is used to make up the liquid phase of foam with additives that do not alter its Newtonian viscosity. Foams created with these liquids exhibit Newtonian behavior at low qualities (wet foams) and shear rates. Einstein's equation for a dilute dispersion of spheres can be used to estimate viscosities of wet foams with spherical bubbles. The effective viscosity of wet foams is constant and applicable if bubbles are small and spaced apart such that there are no

electrostatic interactions. The exception to this is stiff foam, which is generated using viscosified liquid phase. The foam viscosity of stiff foams increases with increasing liquid phase viscosity (Reidenbach et al. 1986).

With increasing quality, foam exhibits non-Newtonian, pseudoplastic behavior and its viscosity increases due to the generation of highly dispersed bubble structure (Sherif et al. 2015). Some foams also possess yield stress, and their flow behavior can be described by the Bingham Plastic model (Krug and Mitchell 1972). The rheology of intermediate quality foams (70-80%) can be characterized by power law model (Raza and Marsden 1967; Wendorff and Ainley 1981) while those of high-quality foams (over 90%) can be represented by Bingham Plastic model (Ozbayoglu 2000). For flowing foam, quality and flowrate have the most impact on its rheology (Clark 1947; Beyer et al. 1972). Other process variables that affect the flow behavior of foams include pressure and temperature. These parameters influence rheology by altering foam quality and liquid phase viscosity.

1.3.4 Density

Foams find applications in various industries, primarily due to their low densities. Foam density depends on the gas and liquid volume fractions, and hence, can be characterized by quality. For simplicity, the mass of dispersed gas phase is ignored in foam density calculations, as it can be assumed to be negligible compared to the mass of the liquid phase. Foam density can then be calculated as the mass of liquid phase over total foam volume (Eq. 1.2). This equation can be re-arranged to express density as a function of gas volume fraction or foam quality. Increase in foam quality increases the gas volume fraction and leads to lower density. Density change with time is an indication of foam drainage. Loss of liquid volume from foam structure lowers its overall

density. Since gravity–induced liquid phase drainage occurs as soon as foam is generated, the foam becomes heterogeneous with time, and its density varies in the vertical direction.

$$\rho_f = \frac{m_g + m_l}{V_f} = \frac{m_l}{V_f} = \varepsilon\rho_l = (1-\varphi)\rho_l \quad (1.2)$$

where m is mass; V is volume; ρ is density; ε is liquid volume fraction; and, φ is gas volume fraction or quality. The subscripts are used to identify the phases as: f – foam; g – gas; and, l – liquid.

1.3.5 Stability

Despite the numerous benefits of foams over conventional fluids in oil field operations, the flow behavior and stability of foam fluids are more complicated, especially at elevated pressures and temperatures. Foam is destabilized upon the moment it is generated and starts to drain, followed by decay (Exerowa and Kruglyakov 1997; Weaire and Hutzler 1999). Foam drainage is the reduction in liquid volume fraction of foam due to gravity, forcing gas bubbles together and creating a complex structure comprised of – thin liquid films between two bubbles, Plateau borders between three bubbles, and nodes. Foam decay is the loss of bubbles due to bubble merging and diffusion of smaller bubbles into larger ones (Krustev and Muller 1999; Saint-Jalmes 2006).

These three mechanisms of foam destabilization through drainage and decay are termed: (i) gravity separation, (ii) coarsening, and (iii) bubble coalescence (Argillier et al. 1998). In the first, liquid phase accumulates at the intersection zone of closely packed bubbles (Plateau borders) due to the pressure difference, and it drains due to gravity. This liquid drainage down the film between bubbles depends on bulk and surface viscosity, and capillary pressures (capillary forces directly oppose gravity). High liquid viscosity impedes its downward movement and delays the drainage process, making the foam to last longer. Coarsening is a mechanism in which small gas

bubbles diffuse into larger ones through the liquid film due to the pressure difference between the two (gas is under higher pressure in a smaller bubble). Coalescence occurs when the film between two bubbles starts thinning as it loses liquid and ultimately ruptures resulting in one larger bubble. Parameters that control these mechanisms affect drainage and decay, and hence, the stability of foam fluid. These are interfacial and bulk properties, film elasticity, surfactant interaction with other surfactants or polymers, and presence of liquid or solid impurities such as clay, salts, crude oil, resins or asphaltenes (Rojas et al. 2001). Under static conditions, if the rate of decay and drainage are comparable, then foam is short lived and is called transient foam (loss of both liquid and gas). If the rate of decay is much slower than the rate of drainage, the gas volume fraction increases creating a stable dry foam. In such dry foams, bubbles are so closely packed that they lose spherical shape and take on a polyhedral form resulting in the formation of Plateau borders and nodes mentioned earlier (Koehler et al. 2000; Kruglyakov et al. 2008).

1.3.6 Carrying Capacity

The advantage of foam as drilling fluid over other fluids such as air or mist is its superior carrying capacity. This is due to their high viscosity resulting from bubble interference and structure. The carrying capacity of foam depends on foam quality, well inclination, hole geometry, the density of solids, and their size distribution. However, when foam structure and properties change over time due to drainage and coalescence, foam loses its carrying capacity resulting in poor hole cleaning. It is important that foam retains its properties while circulating in the wellbore to prevent well stability problems. In a stable foam, settling velocity of a single solid particle increases as particle diameter increases, and decreases with increasing quality (Herzhaft et al. 2000). The Herschel-Bulkley model can be used to describe the rheology of high-quality foams and the yield stress is a good indication of their carrying capacity (Saintpere et al. 2000). However, in horizontal and

inclined sections of a well, despite the solid suspending ability of foam, a stationary solids bed is formed under most flow conditions (Ozbayoglu 2003). Particularly in inclined wells, hole cleaning efficiency is poor when the angle of inclination lies between 40 and 60^{o} (from the vertical). However, increasing foam flow to sufficient rates helps erode solids bed in horizontal and inclined wells (Martins et al. 2000; Martins et al. 2001). Lower quality foams are better in eroding and removing solids in horizontal and inclined wellbore sections because higher foam mass flow rates can be achieved (Capo et al. 2006).

1.3.7 Pressure and Temperature

Increasing pressure decreases the gas phase volume, and subsequently foam quality (Beyer et al. 1972). When quality is maintained constant, pressure indirectly affects foam stability by having some influence on dynamic surface properties such as surface elasticity and surface rheology (Ruckenstein and Jain 1973, Wasan et al. 1994). Surface elasticity prevents rupturing of thin films, and surface viscosity retards the flow of liquid in film, lowering rate of drainage and bubble coalescence, thereby, increasing the stability of foam (Joly 1964). Furthermore, aqueous foam flooding experiments show that the stability of foam increases with an increase in system pressure by limiting capillary pressure effects (Holt 1996).

Temperature has two contrasting effects on foam quality and foam viscosity. The gas phase of foam expands with increasing temperature and increases foam quality. When quality is kept constant, increase in temperature, up to a critical value, results in a significant drop of the apparent viscosity of foam (Ross and Morrison 1988). Beyond this critical temperature, which is a function of gas-liquid phase properties, there is little effect on foam rheology. Increase in temperature has

a similar thinning effect on surface rheology of liquid films. Therefore, an increase in temperature negatively affects foam stability by interacting with surface and bulk viscosities.

1.4 Applications of Foam

In the oil and gas industry, foam has wide application and is usually used as a superior replacement to conventional fluids. The density of foam, by nature, lies between the values of constituent gas and liquid. For applications where the viscosity of fluid plays a vital role, usually for carrying solids into the formation or out of the wellbore, foam offers superior solids suspension ability compared to clean or polymer viscosified liquid (Beyer et al. 1972; Abbott 1974; Rankin et al. 1989). In this section, various industrial applications of foam including drilling, cementing, hydraulic fracturing, and enhanced oil recovery, are briefly discussed.

1.4.1 Drilling

Foams have been used as drilling fluids since the early 1960s due to their high solids carrying capacity, large formation fluid handling capacity, effective sealing properties in lost circulation zones (low leak-off), and variable densities (Hutchison 1972; Bentsen and Veny 1976; Lincicome 1984; Anderson 1984). Such properties have enabled application of foam drilling fluids in extended reach and deep-water drilling. In offshore wells, where there is a high risk of lost circulation due to weighted conventional fluids, pre-formed foam fluids have been pumped successfully due to their low leak-off (Hall and Roberts 1984). Foam drilling fluids have also been utilized in reservoirs where compressible fluids are preferred due to low pressures, extensive natural fractures, and high risk of formation damage since the late 1980s. In such cases, foam fluid is used to drill underbalanced as a special type of aerated fluid with better solids carry capacity and lower risk of wellbore instability than air drilling (Nugroho et al. 2017).

Foam drilling fluids enable operators to control fluid loss, minimize differential sticking of pipe, increase the rate of penetration, prevent formation damage, and produce reservoir fluids while drilling (Paknejad et al. 2007). There are several economic benefits to drilling wells with foam fluids over conventional ones. Low leak off results in less fluid use, and hence, lowers costs. Reduced risk of formation damage, higher drilling rate, and superior well cleaning, result in less rig time, higher production rate, better recovery, and lower operational expenditure (Sui et al. 2000). Using stable foams over air when drilling underbalanced can help prevent corrosion of tubulars and downhole equipment due to excessive contact with formation water and air (Meng et al. 2005). Foams cut down corrosion rate by lowering air input, encapsulating gas bubbles, and by serving as a medium for corrosion inhibitors.

1.4.2 Cementing

Cementing with foam enables the economical design of wells with low density and high strength material. Primarily, foam cementing is utilized when weak or highly fractured zones are encountered and it is critical to place strong cement, to fill vugs, porous thief zones, or to use as a lightweight, inexpensive, slurry (Peskunowicz and Bour 1987; Olanson 1985). In such reservoirs, which have low fracture gradients, conventional cement slurries with 11 ppg or more density cannot be used. Gas phase, usually nitrogen, acts as a lightweight compressible additive in foam cement, without adversely affecting its physical properties such as thickening time or compressible strength (McElfresh and Boncan 1982).

For cement jobs in coal bed methane wells, care must be taken to control fluid invasion, particularly because cementing is performed slightly overbalanced to prevent gas migration into the cement column. For such wells, foam cement is recommended to prevent fracturing the coal and prevent loss of cement to the formation (Kumar and Kumar 2013). Foam cement shows greater

resistance to cyclic and thermal stress cracking. It is, therefore, recommended in thermal project wells that have frequent cycling of steam, and are subject to high temperatures that can cause strength retrogression and chemical decomposition of cement sheath (Miller and Frank 1998). Foam cement is frequently used in deep offshore wells (where weak and unconsolidated formations have low fracture gradients) to prevent fluid leak off, mitigate shallow water flows, and prevent formation fracture (Moore et al. 2000; Waheed et al. 2002; Green et al. 2003; Doherty 2007; Taiwo and Ogbonna 2011; Doan et al. 2016).

1.4.3 Hydraulic Fracturing

Foam has properties that are desirable in hydraulic fracturing operations. In low permeability reservoirs, foam fluids are preferred as they exhibit extremely low fluid leak off. With the low fluid loss to the formation, all the treatment volume is available to generate and propagate fractures, creating longer fractures and larger fracture area (Bullen and Bratrud 1976). Furthermore, during flow back, most of the fluid is recovered with very little contact with the reservoir. This is extremely advantageous in fluid sensitive reservoirs with the risk of formation damage. The high-volume content of gas in foam enables rapid flow back of fluid as mist, enabling early production. The expansion of the gas phase in pores results in expulsion of hydrocarbons from pore spaces, increasing production rate and ultimate recovery.

Settling velocity of proppant particles in foam is very low, minimizing the risk of screen outs and lowering proppant requirements. Usually, fracturing foams are prepared with nitrogen as the gaseous phase, although carbon dioxide and natural gas are used as well (Pankaj et al. 2018). Nitrogen gas is inert and not very soluble in formation fluids. Therefore, the gas poses a negligible risk of combustion or explosion hazard. The liquid phase is generally water containing small quantities of foaming surfactants. In water sensitive formations, KCl inhibited aqueous foam or

oil base foam are used to prevent clay swelling (Driscoll et al. 1980). The stability of fracturing foams is improved by increasing the surfactant concentration and/or by adding a gelling agent to the base fluid.

1.4.4 Enhanced Oil Recovery

Enhanced recovery methods are employed to recover hydrocarbons after the natural energy of a reservoir has depleted on initial production. In these methods, generally, energy is externally supplied to the reservoir by injecting fluids (water, nitrogen, carbon dioxide, or methane) into the formation, enhancing reservoir pressure and limiting undesirable gas mobility, thereby, increasing oil production and ultimate recovery (Bedrikovetsky 1993). Gas injection is preferred over water due to its superior microscopic sweep which results in lower residual oil saturation in pores (Lake 1989). However, gas has poor volumetric sweep efficiency as compared to water due to which a large portion of the oil is not contacted (Rossen and Duijn 2004). Injecting foam instead of either liquid or gas alone solves the problem associated with either phase. Foam has a higher viscosity than gas or liquid, and therefore, has better hydrocarbon displacement ability. Furthermore, it blocks fluid from high permeable zones, where foam has low mobility, and diverts it into the low permeability layers, improving volumetric sweep efficiency (Farajzadeh et al. 2012; Farzaneh and Sohrabi 2013).

1.5 Statement of the Problem

Foam has diverse applications within the oil and gas industry due to its unique properties. It exhibits variable density, which allows greater flexibility when dealing with changing in-situ pressures; has low leak-off rate into the formation; exhibits high viscosity, due to its highly dispersed bubble network; and it is economically preferable fluid in drilling low-pressure depleted

formations. Nitrogen gas is the main cost driving factor in foam applications, and its requirements; and therefore, cost increases with deeper wells and longer laterals. However, the cost of foam application is offset by its many benefits which result in early and better production, lower loss of expensive fluid to the formation, and eliminating the need for expensive stimulation operations. The main disadvantage of foam is the need for precise prediction of foam properties (stability, rheology, and density) that are required for proper design and execution of the job. Due to the strong coupling between these properties, making an accurate prediction is very challenging.

As stated earlier, all foams are unstable thermodynamically and will dissipate over time. The half-life of foam, which is the time it takes for foam to lose half of its initial volume by drainage, is a critical parameter that is often used to assess the stability of foam. Hence, the half-life of foam needs to be considered and it is sensitivity to wellbore condition needs to be analyzed before undertaking the job. It is critical that half-life of foam exceed circulation time in drilling operations. In cementing and hydraulic fracturing, foam half-life should be greater than the time taken for it to reach targeted zones (it is beneficial for foam to dissipate post-fracturing so as to quickly flow back the fluid as its constituents). Ignoring temperature effects, as the wellbore temperature more or less stabilizes after multiple hole volume circulations, in-situ pressure plays an important role in foam properties, and therefore, on its half-life. However, operators should accurately predict foam half-life under borehole condition and modify gas-liquid injection rates at the surface, to sustain stable foam for the job in concern. At present, a method that accurately predicts foam stability under downhole conditions is lacking. Surface personnel do not have a reliable method to account for the effects of different downhole parameters on foam stability. As a result, the success of underbalanced drilling is limited. A considerable portion of wells drilled underbalanced with foam still exhibit formation damage. Some of these downhole parameters

(pipe rotation, wellbore geometry, and inclination) are considered in this study and their effects on stationary foam are monitored under ambient temperature conditions.

1.6 Objectives and Scope of Work

An innovative and new method of measuring liquid drainage rate from trapped stationary foam was developed during this investigation. The principal objective of this study is to investigate the effects of foam quality, the type of liquid phase, geometry, shearing, and inclination on drainage behavior of foam and ambient temperature.

i. Quality – Foam fluids were formulated at various qualities by changing the gas-liquid volumetric ratio. Changing quality influenced foam properties, specifically viscosity and density. The effect of quality on foam drainage rate was studied by comparing the drainage curves of foams.

ii. Type of Liquid Phase – Three types of base liquids (water, polymer suspension, and oil) were used to formulate foams in this study. Aqueous foam was prepared with tap water and polymer foam was prepared by adding hydroxy ethyl cellulose (HEC) to water. Oil-based foam was generated using a mixture of mineral oil and diesel as the base liquid. Effect of liquid phase on foam drainage rate was studied by comparing drainage curves obtained from pipe and annulus and studying them at each quality.

iii. Geometry – Prepared foams were trapped in annular and straight pipe sections. Drainage curves produced for each type of test foam at a given quality from pipe and annulus were compared to study the effect of geometry and container walls on foam drainage rate.

iv. Shearing – The effect of shear was studied only in the annular section. The shear was stimulated by rotating inner pipe at 4 and 7 rpm in the annulus and subsequently observing drainage curves produced for each type of foam keeping quality constant.

v. Inclination – The experimental setup was designed to enable rotation 0 to 90^{o} from the vertical. Effect of inclination on drainage rate was studied by comparing drainage curves obtained from annular and pipe sections at 0 and 30^{o} (from the vertical), keeping quality constant for each type of foam.

Furthermore, the objective of this study was also to investigate instability of foam caused by decay mechanism using images of bubble distribution captured at fixed time for aqueous and polymer foams. Lastly, information gathered from drainage and decay studies was to be used to modify existing channel and node dominated models (Koehler et al. 2000) that predict liquid volume fraction distribution with time in vertical foam column for aqueous and polymer foams. Specifically, the assumption of constant bubble size and shape in foam structure was modified by incorporating correlations developed that account for bubble coarsening of various quality foams with time.

CHAPTER 2

LITERATURE REVIEW

This chapter starts with the description of basic units that form the structure of foam. It is important to discuss this structure, albeit an idealized one, as it forms the conduit through which liquid drains. Following this, the physical processes occurring at the moment of foam generation are explained. These processes play an important role in determining if the generated foam is stable (i.e. drainage rate is faster than the rate of decay) or transient (i.e. foam collapses quickly by coarsening and ultimate diffusion of gas from bubbles into the atmosphere). All the foams generated and studied in current work can be considered to be stable. Next, these two mechanisms – drainage and decay, which lead to destabilization of foam are briefly explained. This is followed by a brief account of various measuring methods utilized to study these mechanisms. In the same section, the current methods developed to study foam drainage and bubble coarsening are explained. Lastly, a literature review on foam drainage and the effects of various factors are presented.

2.1 Structure of Foam

It is important to understand the basic structure of foam before examining its drainage behavior. Foams contain disordered bubbles of varying sizes and are usually termed as polydispersed foams. In wet foam, bubbles are well separated by liquid and barely touch one another. As liquid volume fraction reduces, bubbles come closer and the structure can be idealized to be a random packing of similar spheres (Bernal packing). As more liquid drains out, and foam gets drier, the bubbles are tightly packed and develop a polyhedral shape (Weaire and Hutzler 1997). Such a packing gives rise to the basic structural units that are referred as lamellae, Plateau borders or channels,

and nodes. A highly idealized two-dimensional view of general foam structure overlapped by bulk gas phase at the top and bulk liquid phase at the bottom is shown in Fig. 2.1.

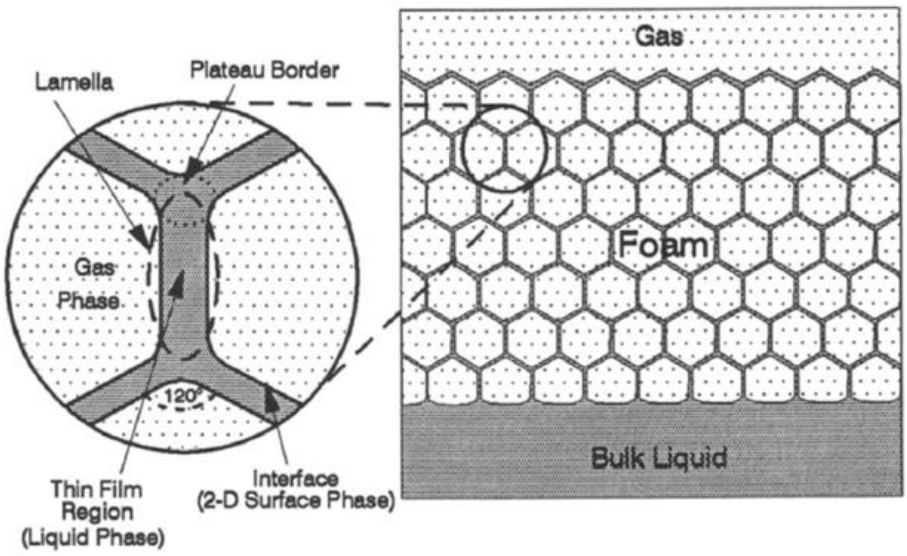

Figure 2. 1: Generalized Foam Structure (Schramm 1994)

A lamella is a region that encompasses thin film (which is where the liquid resides), two gas-liquid interfaces on either side of the film, and part of a junction (Fig. 2.1) shared with other lamellae (Schramm 1994). This junction between lamellae is termed Plateau border (sometimes referred to as a channel). In dry foams, three lamellae intersect to form the channel or Plateau border at approximately 120^{o}. The intersection of four Plateau borders is called a node. This intersection is usually at an approximate angle of 109.28^{o} in dry foams (Kraynik 1983). These approximate angles of intersection of lamellae and channels are valid when surface tension is uniform across the foam structure. Figure 2.2 shows an idealized polyhedral bubble, foam structure unit showing four half-length Plateau borders or channels intersecting to form a node, and dog-bone shaped foam structure unit which contains one channel with one-fourth of a node at each end. Channels can be approximated as tubular structures which expand when liquid drained from films accumulates and elongate/thin at mid-section as liquid drains down ultimately resulting in the formation of the dog-

boned structure shown. The factors leading to this elongation and thinning will be discussed in the next chapter. All the liquid present in the foam structure is contained within these lamellae, nodes, and channels. The bubble is shown in Fig. 2.2 has a tetrakaidecahedral shape and monodispersed foam with such bubbles is called Kelvin foam (Koehler et al. 2000). The denotation 'L' indicates the channel or Plateau border length while 'r' indicates Plateau border radius (Fig. 2.3). These denotations will be used in the rest of the manuscript and will be of importance in Chapter 4 where a detailed mathematical analysis of the units introduced here is presented.

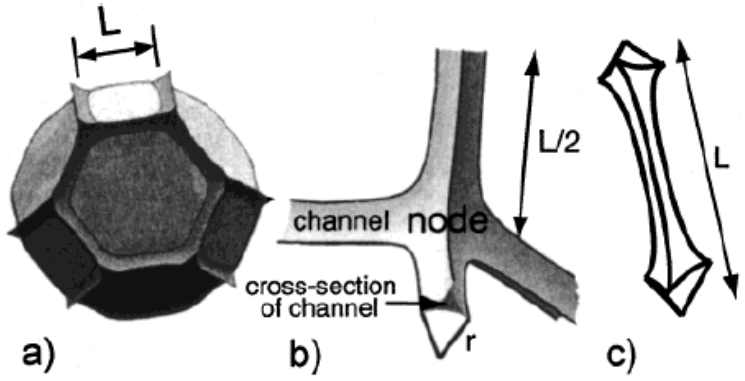

Figure 2. 2: (a) Polyhedral bubble with edge length L (channel); (b) Structure unit showing four half-length channels intersecting to form a node; and (c) Dog-bone shaped structure unit showing one channel and one-fourth of a node at each end (Koehler et al. 2000)

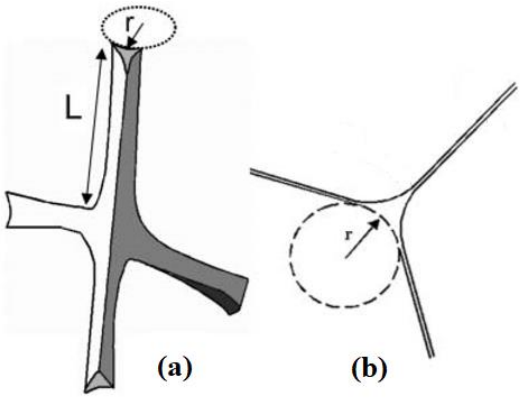

Figure 2. 3: (a) Structure unit defining Plateau border/channel length and radius; (b) Cross-section of the channel showing its radius and three films attached to it (Saint-Jalmes 2006)

2.2 Formation of Foam

Foam is generated when bubbles resist diffusion or coalescence on collision and shearing. These small bubbles form the foam structure along with the liquid trapped between them. If no further energy is added to the system, the liquid starts to drain from between the bubbles, and this is followed by decay of foam structure due to the aforementioned diffusion/coalescence. The loss of liquid from films between bubbles thins the films and pushes bubbles together. Eventually, after enough liquid is lost, bubbles start to deform and lose their spherical shape to gain a polygonal one. Such a tightly packed foam structure gives rise to channels (also called Plateau borders) and nodes explained earlier. At this stage, there is very little liquid left between bubbles (thin films) to offer any resistance to bubble merging. If thin films rupture, there is no barrier between bubbles and foam collapses completely. Therefore, liquid drainage, which results in thinning of liquid films, always precedes decay of foam structure and fast drainage leads to quick decay of foam (Deshpande and Barigou 1999). This is of importance because it indicates that the liquid drainage rate is a good indication of overall foam stability. It is easier to study drainage from standing foams than to study coarsening/decay of foam structure. Foam drainage experiments can be reasonably replicated but it is very hard to ensure that bubble structure generated each time for specific quality foam remains or looks the same.

2.3 Mechanisms of Foam Destabilization

Foam destabilization occurs through two processes: drainage and decay. Drainage is the loss of liquid from the structure of foam and is driven by gravity and capillary forces. The decay of foam is the loss of bubbles in foam structure due to diffusion of small bubbles into larger ones

(coarsening) and/or coalescence due to film rupturing. It occurs due to the pressure difference between the gas phase trapped in bubbles of various sizes.

2.3.1 Foam Drainage

As mentioned in the previous chapter, foam is thermodynamically unstable, and it starts to dissociate into its component phases upon the moment of generation. However, this does not mean that drained liquid is observed at the bottom of foam column or free gas is noticeable at the top immediately after foam generation. There is a delay (lag time) since it takes some time to form the first drop of draining liquid. High-quality foams exhibit long lag times. Intuitively, this is expected since high-quality foams have low liquid volume fraction and that liquid volume must traverse a more complex bubble network (due to higher gas volume fraction) and thin liquid films on its journey downwards. During drainage, the flow of liquid occurs predominantly through Plateau borders and nodes with the driving force for this flow being gravity and capillary pressure (Hutzler et al. 2005). This is because liquid tends to drain from films where the pressure is high due to the curvature of the gas-liquid interface and collect at Plateau borders where the pressure is low. Surface tension also plays a role in this accumulation of liquid at Plateau borders.

The liquid present in the network of channels or Plateau borders flows downward due to gravity. This downward movement induces a gradient in liquid volume fraction, which increases in the downward direction. In sections of foam structure with higher liquid volume fraction, Plateau borders are larger (larger radius) as compared to ones in drier parts. Hence, the liquid in these larger Plateau borders/channels experiences higher capillary pressure as compared to liquid in the drier part of the foam (given by Young-Laplace equation). Therefore, capillary forces arise due to the gradient in liquid volume fraction and induce flow from regions with high liquid volume fraction to those with lower ones (Weaire and Hutzler 1999; Koehler et al. 2000), effectively

opposing gravity. However, the net flow of liquid is still in the downward direction and is due to the combined effects of gravity and capillary effects, while it is resisted by viscous dissipation that occurs in the flow network. The flow starts with the accumulation of drained liquid from films into channels, followed by liquid influx from different channels merging at the nodes before splitting to flow through other channels, across the entire foam structure. Viscous dissipation is the resistance to flow of liquid occurring at the walls of channels (Bhakta and Ruckenstein 1995). It is stronger in high-quality foams due to a tighter bubble packing with thinner films and elongated channels. This impediment to flow depends on the liquid phase viscosity. Therefore, increase in base liquid viscosity results in the reduction of drainage rate and prolongs foam life (Monnereau et al. 1999).

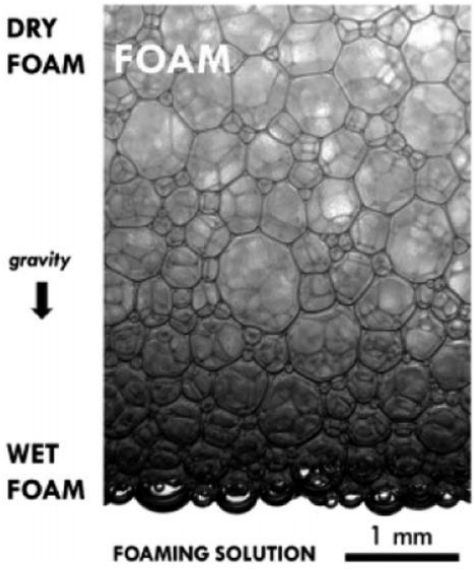

Figure 2. 4: A typical standing foam showing liquid drainage (Drenckhan and Hutzler 2015)

As drainage progresses, foam becomes progressively drier due to liquid removal from its structure, increasing quality. This increase in quality is a function of drainage rate, and hence, a function of time, provided foam does not decay at a similar rate (Fei et al. 2017). Normally, drained liquid collects at the bottom of foam column and a small portion is sucked back into the foam

structure due to capillary effects acting at liquid/foam interface (Saint-Jalmes 2006). At the interface, a section of wet foam exists and is characterized by almost spherical bubbles (Fig. 2.4). At some point an equilibrium state is achieved and foam structure retains residual liquid. At the interface of liquid/foam structure, capillary drive flow of liquid into foam is balanced by gravity. However, since foam structure is subject to change with time (decay), multiple equilibrium states are achieved over the life of foam with the residual liquid volume gradually decreasing with time until foam collapses.

2.3.2 Foam Decay

After foam is generated and liquid starts to drain after an initial lag-time, a new mechanism comes into play which alters the foam structure. During drainage, the structure deforms as its basic units expand, thin, or elongate, with the influx or efflux of liquid. However, during the decay of foam, existing units dissipate and reorganize due to diffusion and coalescence of bubbles (Fig. 2.5).

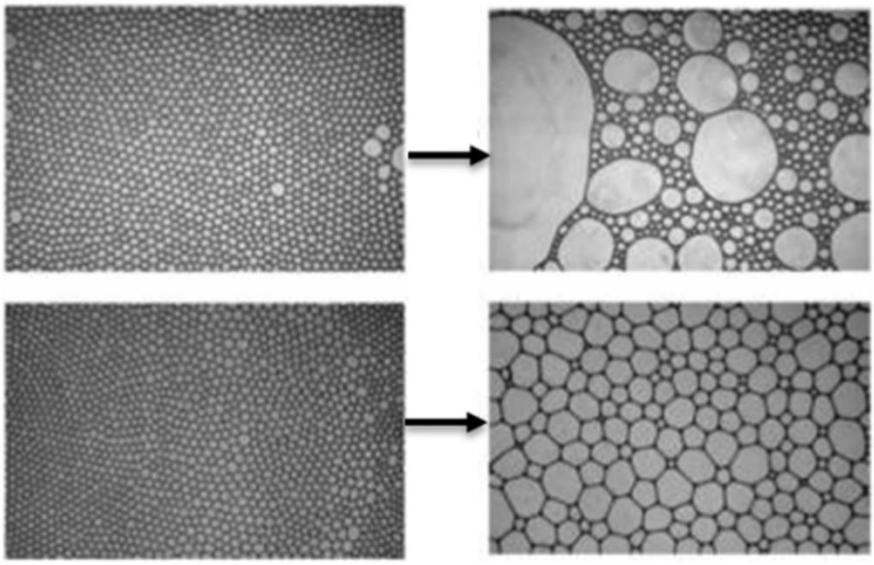

Figure 2. 5: Coalescence (top) and coarsening (bottom) of bubbles (Hill and Eastoe 2017)

Coarsening

Diffusion is the process of bubble merging in which gas diffuses through the thin films (Prud'homme and Khan 1997; Weaire and Hutzler 1999; Saint-Jalmes et al. 2005). Bubbles in foam choose the smallest path to diffuse through thin films (Rio et al. 2014). It occurs due to the pressure difference between the gas phase trapped in small and large bubbles (Laplace pressure). The Young-Laplace equation can be used to express this differential pressure. The process of increasing the size of bubbles by gas diffusion from smaller bubbles is called coarsening. It is sometimes also called Ostwald ripening, although this term is for solid solutions rather than foams.

The overall volume of gas in foam remains constant during coarsening. The factors that affect coarsening rate are quality, average bubble size or bubble size distribution, and physical chemistry of component gas-liquid phases (Cantat et al. 2013). Aqueous foams prepared with water-soluble gases (e.g. carbon dioxide) tend to coarsen at a higher rate than those prepared with nitrogen, which is not very soluble in water. Carbon dioxide and other water-soluble gases can easily transport across water films, thereby, increasing the risk of diffusion. Adding small amounts of nitrogen to carbon dioxide before generating foam increases foam stability due to delayed gas diffusion across thin films (Weaire and Pageron 1990). 'Nitro' beers are a good example of this in day-to-day life which are prepared with carbon dioxide/nitrogen mixtures and produce thick/creamy foam head.

Coalescence

Unlike coarsening, coalescence does not involve gas diffusion through thin films. It occurs due to rupturing of thin films between bubbles. This process gradually decreases gas volume in the foam, until foam completely collapses (Cantat et al. 2013). Since it is difficult to rupture films when foam has a high liquid content, this process usually comes into effect when drainage is complete, and the equilibrium state achieved (Rio et al. 2014). Films between bubbles are very thin at that

point and are susceptible to rupturing. The rate of coalescence is not affected by bubble size (not directly at least) but, clearly, depends on the rate of drainage, and below a critical liquid volume fraction increases dramatically (Carrier and Colin 2003). From this, it can be inferred that the rate of coalescence can be delayed by generating foams which take longer to drain and reach the critical liquid volume fraction (Hill and Eastoe 2017).

2.4 Foam Drainage Measuring Methods

Foam drainage studies can be classified as either microscopic or macroscopic. Microscopic studies are at the scale of a single Plateau border or channel and are usually focused on a single foam liquid film. Macroscopic studies consider several bubbles and liquid contained between them if not the whole foam column. The experimental study conducted in present work is at a macroscopic scale, investigating the drainage behavior of standing foam.

2.4.1 Microscopic or Single Foam Film Approach

Studying drainage characteristics of thin films and investigating their stability can give insights into the complex mechanisms of foam drainage and decay. An early method of studying single film cell is interferometry which involves comparing intensities of light shined onto a film to the one reflected from it. Mysels et al. (1959) used this method to study the thinning of soap films. Clark et al. (1990) improved the method by using laser beams. The components of white light passing through a liquid film are reflected at different angles based on their wavelengths and the thickness of the film. The reflected spectrum of white light is seen as colored fringes and can be used to study variation in film thickness (Isenberg 1978).

If a film has a large thickness (>120 nm) then white light passing through will split into components of the visible spectrum. As thickness decreases (30-120 nm), the visible spectrum is

reduced to colored fringes with longer wavelength components disappearing. As the thickness of the film is reduced to value lower than that of the light beam (~30 nm), colored fringes disappear, and it appears as a black film. At about 30 nm, it achieves metastable thickness. On further thinning (~5 nm) it reaches a more stable thickness and is called a Newton black film. Comparing the intensity of monochromatic light, reflected at an angle from the liquid film, to the maximum intensity of incident light, the film thickness can be determined using Eq. 2.1 (Isenberg 1978). Results from such experiments can be correlated to obtain information on foam structure and can even be used to measure foam decay. In Eq. 2.2, the ratio of reflected to incident light intensity is used to measure the number of foam lamellae per unit length traversed by light.

$$t_f = \frac{\lambda}{2\pi r_i cos\theta} sin^{-1}\left(\frac{I_R}{I_O}\right)^{1/2} \tag{2.1}$$

$$\frac{I_O}{I_R} = an_F + b \tag{2.2}$$

where a, b are correlation constants; I_R is the intensity of reflected monochromatic light; I_O is the maximum intensity of incident light; n_F is the number of foam lamellae per unit length; r_i is a refractive index; t_f is film thickness; λ is the wavelength of monochromatic light; and, θ is the angle of reflection.

Yamanaka et al. (1994) used infrared spectroscopy to study foam films. This method is only applicable to aqueous foams as it measures the absorption of infrared light shone on liquid film due to its water content. This method enables measuring of film thickness as well and is particularly useful in studying Newton black films. Another method that uses a similar concept involves exposing the liquid film to X-rays and measuring their reflectivity (Belorgey and Benattar 1991; Platikanov et al. 1993). Barigou and Davidson (1994) and Barigou et al. (2001) used an

electrical resistance technique to measure the drainage of foam films. They generated a thin film in the annulus between two electrodes and measured its electrical resistance by applying voltage. They postulated that resistance of the thin film is a function of its thickness and estimated film thickness from measurements obtained. By measuring changes in film resistance with time, they were able to monitor thinning of film. This method is restricted by models used to define film structure and their limiting assumptions. Proper interpretation of measurements obtained is necessary to get meaningful results. Another limitation is the reproducibility of experimental data. It is difficult to consistently generate similar single free foam cells. Some methods used by investigators to generate these films are drawing out a film in a frame from a surfactant solution, pulling apart two uniaxial cylinders, and withdrawing two concentric cylinders from a solution.

2.4.2 Macroscopic or Bulk Foam Approach

Early methods of measuring liquid drainage from foams are simply monitoring liquid volume drained after a specific time (Bikerman et al. 1973). This method was evolved to monitor liquid volume fraction in foam column with time as well as the liquid drained (Weaire et al. 1997). Drained liquid volume measurements made with time can then be used to generate drainage curves (Jacobi et al. 1956; Miles et al. 1945; Bhakta and Ruckenstein 1995; Argillier et al. 1998; Hilgenfeldt et al. 2001; Saint-Jalmes and Langevin 2002; Vera and Durian 2002). Figure 2.6 shows a typical drainage curve, reproduced from measurements made by Argillier et al. (1998) using a foam-filled graduated cylinder. Drainage curves obtained from draining foam column can typically be classified into three regimes. In the first regime (Regime I), liquid drains slowly from the standing foam column. The drainage rate then sharply increases after a few minutes. The second regime (Regime II) is characterized by, more or less, constant rate of liquid drainage. In the first two regimes, the primary mechanism is gravity drainage. The last regime (Regime III) is

characterized by a gradual decrease in drainage rate as most of the liquid has separated. Bubble coalescence and coarsening are dominant factors in determining foam drainage in this regime. The slope of the curve obtained from experiments for the third regime is dependent on the initial bubble size distribution. The duration of these regimes are dependent on gas and liquid phases, the surfactant used, and the presence of drainage influencing additives such as polymers.

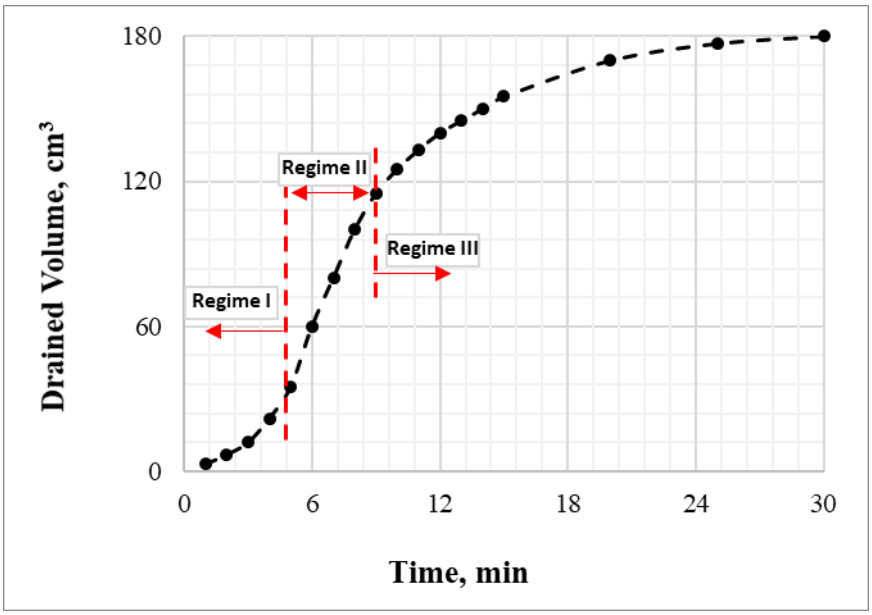

Figure 2. 6: Typical foam drainage curve (reproduced using data from Argillier et al. 1998)

For non-conducting foams, Hutzler et al. (1995) provided a relationship between the capacitance of foam column and liquid volume fraction. They used a segmented capacitance resistor to measure foam capacitance. To ensure foam was non-conducting, they prepared foams with a non-ionic detergent solution. This method was limited by the effect of liquid conductivity on measured capacitance resulting in poor reproducibility of results. Since the foam must be non-conducting, the application of this method is rather limited. In contrast, the electrical conductivity of foam has also been used to gather information on the liquid volume fraction profiles in standing foam, since conductivity is directly proportional to the water content in foam structure (Chang and

Lemlich 1980; Datye and Lemlich 1983; Weaire et al. 1995; Wilde 1996). In this method, two electrodes are inserted into the wall of the container that houses foam column. Voltage is applied and local resistance is measured as a function of time. However, since during drainage a thin liquid layer exists at the walls of container electrical resistance profiles may not be reliable.

Magnetic resonance imaging (MRI) was used by McCarthy (1990), Barigou et al. (1993), and Prause et al. (1995) to measure density profiles in standing foams. Liquid volume fraction can be estimated from such density curves since a linear relationship exists between density and liquid content in foam. This method is limited by the high cost of MRI which can narrow its application to small scales.

2.4.3 Present Work

The present work uses bulk foam approach to measure drained liquid volume, liquid volume fraction, and hydrostatic pressure profiles with time. Since density is linearly related to liquid volume fraction, the primary aim while designing experiments for current work was to obtain density profiles for a standing foam column. To accomplish this, an annular section was built were foam was to be trapped and allowed to drain free from external influence. Differential pressure transducers were installed at fixed lengths across this section and hydrostatic pressure exerted by draining foam column was measured. As the density of foam column is directly proportional to the hydrostatic pressure exerted by it, this information was used to generate density profiles with time. In addition to providing information on liquid content held up in the foam column, density profiles were also used to estimate the volume of drained liquid. This method is simple to use and much more cost effective than MRI. Limitations of this method are – the time scale of each experiment, sensitivity/reliability of pressure transducers, and, number of pressure transducers that

can be used. A detailed description of the experimental test section constructed, and procedure adhered to is given in Chapter 5.

2.5 Foam Decay Measuring Methods

One means of measuring stability in static foams is to monitor the rate of foam decay. The decay rate is measured by analyzing the change in size distribution of gas bubbles in foam structure over time. Various methods (photographic, optical fiber, pressure measurements, light transmission, and others) used by investigators to measure bubble size distributions.

2.5.1 Photographic Methods

Chang et al. (1956) proposed a simple but tedious method to measure size distributions in static foams which involves flash freezing the foam with liquid nitrogen. Columns of frozen foam samples are sliced carefully at the top to obtain a flat surface and the cell structure is observed under a microscope. Extreme care must be taken to ensure frozen foam does not melt by keeping it in contact with liquid nitrogen. Optical fibers are used to provide light to view the foam surface to prevent additional heat sources. The microscope used is placed in a dry box and continuously flushed with nitrogen to eliminate water vapor condensation. This method is useful in determining size distributions in a stable foam. Nishioka et al. (1996) proposed a correction to the size distribution obtained, arguing that a plane cut through foam will preferentially hit larger cells.

An easier method of studying bubble size distribution is to observe foam cells on a glass wall. However, any observations made by such a method are influenced by segregation of large bubbles in foam cells due to wettability of glass wall (Chang et al. 1956). In recent years, with advancements in still image technology, high-resolution photographs of foam cross-sections can be used to analyze bubble size distributions. Glare spots break in bubble boundaries, and images

of bubbles below those in the plane being analyzed must be edited out to prevent erroneous conclusions (Gido 1989).

2.5.2 Optical Fiber Methods

Bisperink et al. (1992) used optical fiber probes to measure size distribution in foams. The method involves inserting a probe of known dimensions at a particular speed and constantly measuring the amount of light reflected from the tip. There is no reflection if the tip is in liquid, and partial reflection if it is in gas. As tip goes from liquid to gas in the foam, an alternating analog signal can be produced, which contains information of bubble size distribution in foam layer. The results obtained from this method are used to statistically extrapolate bubble size distribution in foam after suitable corrections. It is assumed that the probe is completely wet by the liquid phase and does not disrupt the bubbles in foam while measuring. However, it is not possible to measure bubbles which are smaller than the probe diameter using this method.

2.5.3 Measurement of Pressure in Head Space

A foam under static conditions in a column or container decays over time, losing its dispersed gas to the bulk gas phase. This dispersion of gas leads to a rise in pressure in the headspace above the static column of foam, which can be measured by utilizing equations of state for foams (Ross 1969; Hollinger 1991). The rate of decay is calculated in terms of foam container cross-sectional area from pressure increase measurements (Kruglyakov and Taube 1965; Nishioka and Ross 1981). Kruglyakov and Taube (1965) were the first to use this method and they measured increments in pressure with a water manometer. This method is difficult to reproduce and replicate the results obtained (Monsalve and Schechter 1988, Princen 1988, Lachaise et al. 1990). Additionally, it is only valid for dry foams with polyhedral bubble distributions as in wet foams with spherical bubbles hydrostatic pressures come into play and must be considered in foam equations of state.

Exceptional care must be taken to ensure measurements are made at a constant temperature to get meaningful results.

2.5.4 Light Transmission and Reflectance

Light beams entering foam structure undergo reflection and refraction at gas bubble walls. If absorption effects are ignored, the light exiting the foam should be uniform over its surface. Therefore, the intensity of light entering and exiting the foam is directly proportional to its surface area. In light transmission methods, the change in intensity of light passing through foam is used as a measure of change in the total area of foam. Changes to relative total foam area with time is a measure of foam decay rate (Ross and Cutillas 1955, Nishioka and Ross 1981, Lachaise et al. 1990). Durian et al. (1991) modeled transmittance of light through foam as a diffusion process and showed that the mean free path traversed by the light beam is proportional to the average bubble diameter. Multiple light scattering of foams was then used by them study the arrangement and rearrangement of bubbles over time in foam giving insight into internal dynamics within the bubbles. This experimental method is easy to reproduce and is not dependent on temperature fluctuations or hydrostatic effects. Different studies have produced correlations that relate reflectance of foam to other physical properties that affect its stability.

2.5.5 Other Methods

Changes in density of foam can be monitored by measuring the electrical conductivity of foam with time, which is a measure of liquid content in the foam structure (Chang and Lemlich, 1980). Racz et al. (1982) proposed a method of measuring pressure distribution in plateau borders using manometers to estimate liquid drainage from foam with time. Magnetic resonance imaging (MRI) can be used as a non-invasive means of probing foam structure to circumvent the model dependence of Durian et al. (1991) method which utilized multiple light scattering. This method

involves sampling the polarization density of nuclear moment as a function of position. Using this topology of foam structure can be reconstructed at various times enabling visualization of foam coarsening (Gonatas et al. 1995). Limitation of the MRI method is the resolution of images produced which means very small bubbles tend to be ignored leading to potential errors in estimating average bubble size. Banhart et al. (2001) and Lambert et al. (2005) used in situ X-ray tomography to capture images of real-time coalescence of bubbles in aqueous and metallic foams. However, with this method as well very small bubbles tend to be not counted and is subject to human error as images are inspected by eye. To remedy this Myagotin et al. (2009) developed a method which involves spatiotemporal analysis of radiographic projection images in real time. Bubble coalescence is detected using breaks in the spatiotemporal image analysis.

2.5.6 Present Work

The main experimental work taken upon in this study focused on drainage from standing static foam and not on foam decay. However, during the experiments conducted with aqueous and polymer foams, it was possible to capture images of standing foam that could be seen through a visual port. These images were captured at fixed times measured from the instant foam was trapped (videos as well, in some instances). They show the upward movement of bubbles initially, followed by coarsening of the foam structure. It is difficult to pinpoint the exact mechanisms occurring that led to bubble coarsening as this secondary work was limited to visual observation. However, using these images and by analyzing them with image processing software (ImageJ), it was possible to measure bubble diameters (assuming them to perfectly spherical). Therefore, photographic information was converted to bubble size distribution data that varies over time. The limitations of this method are human error as images are inspected by eye and poor resolution which can result in very small bubbles not being captured.

2.6 Factors Affecting Foam Stability

The experimental portion of present work mainly focusses on measuring liquid drainage rate from standing foams while varying quality, base liquid phase, inclination, container shape, and shear. In this sub-section, the effects of these factors on foam stability and liquid drainage are discussed.

2.6.1 Quality

Higher qualities indicate a larger volume fraction of gas phase which generates a foam structure with a lower volume of liquid trapped between tightly packed bubbles. Tight packing is due to a large fraction of compressible gas trapped in a constant pipe or annular section volume. The drainage rate is low at a higher quality because there is not much liquid in foam, and what remains is trapped between bubbles experiencing higher viscous resistance, capillary effects, and other impediments to liquid flow due to a more complex structure with thinner films.

2.6.2 Liquid-Phase Viscosity

Foams that are prepared using a viscous liquid phase are called stiff foams. Aqueous and stiff foams have a similar foam structure. However, the structure of still foams is more stable due to increased viscosity of its liquid phase. This is due to an increase in viscous forces in the liquid film that oppose gravity drainage and prevent rupturing. Higher quality foams can be created, without risk of liquid phase becoming discontinuous, using viscosified liquid phase (Russell 1993). Due to increased viscosity, drainage is reduced in stiff foams.

2.6.3 Inclination

In a vertical column of foam, the liquid must pass through a complex network of foam structure to reach the bulk liquid phase accumulating at the bottom. Flow is hindered due to viscous dissipation experience by liquid at Plateau border/channel walls. One means of enhancing foam drainage is

inclining the foam column. In inclined conduits, liquid volume fraction is not spatially uniform (Stevenson 2007). It significantly varies in both axial and lateral directions. By contrast, when said conduit is vertical, liquid content in foam only varies in the axial direction (lateral variation is usually negligible). In an inclined column, foam gets progressively drier as it moves in both axial and lateral directions. Drained liquid follows the path of least resistance. Hence, it drains laterally toward the conduit wall, forming a flowing liquid film as shown in Fig. 2.6 (Dickinson et al. 2010). Once the liquid reaches this film, it does not experience any viscous dissipation (bypasses foam structure) and is free to flow down to the accumulating bulk liquid phase. Therefore, drainage is enhanced or exacerbated (based on if it is desirable or undesirable) in inclined conduits as compared to vertical ones. Hence, inclined conduits are utilized in foam fractionation techniques where the goal is to enhance the separation of liquid from foam column (Mukhopadhyay et al. 2010).

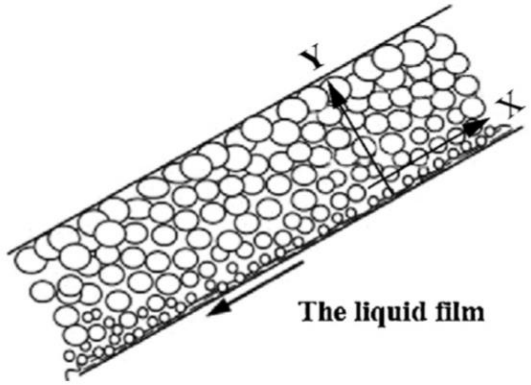

Figure 2. 7: Flowing liquid film in inclined foam column (Wang et al. 2013)

The angle of inclination significantly affects the rate of drainage from an inclined foam column (Jiang et al. 2011; Wang et al. 2013). Wang et al. (2013) conducted foam drainage experiments with very wet foams in inclined conduits at various inclination angles (0-60^{o}). They generated foam by bubbling air into the wastewater held in an inclined column (0-60^{o}). Once foam was generated, the bubbling was stopped, and the liquid height recorded. Subsequently, the

increasing liquid height was recorded at intervals of 30 seconds. Based on the experimental results, they identified 45^o as the critical angle at which drainage rate was most accelerated (Fig. 2.7). The superficial drainage velocity is estimated using incremental liquid height and time (Eq. 2.3).

$$j_{dave} = \frac{dh}{dt} \tag{2.3}$$

where, dh is incremental liquid height; and dt is incremental drainage time.

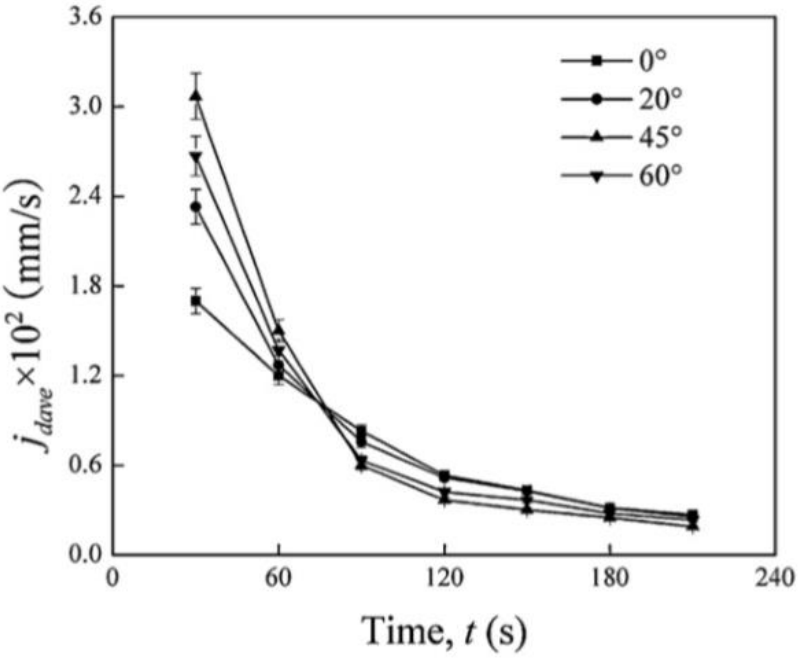

Figure 2. 8: Effect of inclination angle on superficial drainage velocity (Wang et al. 2013)

2.6.4 Wall Effects

Wall effects that affect bulk liquid drainage from foam can be classified into three categories: diameter and height; container shape; and, the wettability of container walls (Papara et al. 2009). Very limited information is available in the literature regarding these factors on foam drainage. On a microscale, the motion of individual particles in foam (liquid or gas) is influenced by container walls, gas-liquid interface, and the presence of other particles. Although it is not specifically aimed

at foams, Clift et al. (1978) present a critical review of various factors (container, container shape, wettability, and motion of surrounding particle) that affect particle motion in fluid.

Container Effects

Container effects have largely been ignored in the study of foam drainage. Various authors have opted to use cylindrical tubes of different diameters with but there has been no systematic study on the comparison of results obtained until 2001. Brannigan and De Alcantara Bonfim (2001) studied the diameter effect on forced drainage using cylindrical containers with 12.5, 18, 25, and 37.5 mm diameters. In forced drainage experiments, the liquid phase is continuously injected at the top of foam column such that liquid floods the completely drained foam at the top (forced drainage will be presented in Chapter 4). From their experiments, they concluded that drainage rate increased with decreasing diameter when liquid volume fraction was maintained constant irrespective of bubble size. They explained this by the presence of liquid films at container walls which enables liquid to travel down to bulk liquid phase with little resistance as it bypasses the foam bubble network. According to them, the contribution to drainage from these liquid films increased with decreasing diameter. They further postulated that wall effects diminish in containers larger than 37.5 mm. However, they did not validate this with experimental results. Although previous researchers were aware of the effect of wall films in foam drainage, it was assumed that since interstitial films in foam structure greatly outnumber wall films, drainage contribution from wall films can be considered negligible. This assumption, which might hold true when container diameter is large enough, clearly does not work for small diameter containers. Koehler et al. (2004) confirmed these conclusions, adding that wall film drainage is enhanced in foams with rigid gas-liquid interfaces. Rigid or immobile gas-liquid interfaces are characteristically observed in containers with small diameters while they tend to be more elastic in containers with large diameters.

Container Shape

Most drainage experiments with foam are conducted in cylindrical tubes. However, researchers have opted to use different cross-section containers such as square (Durand et al., 1999), or, octagonal (Dame et al., 2005). Saint-Jalmes (2000) investigated the effect of varying container cross-section with height. The container they used had a cross-section that increased exponentially in the vertically downward direction (they described it as 'Eiffel Tower' shaped). They observed that drainage was enhanced on using this container due to the elimination of vertical capillary effects.

Container Wettability

Most investigators opt to use glass (small scale) or Plexiglas when conducting drainage experiments to visually observe the process. Clean glass containers used for such purposes in the lab are fully wettable by aqueous foams and lead to hydrophilic drainage (drainage rate is enhanced). Even when using metal or polymer containers, this problem cannot be avoided as prolonged and repeated use can result in them developing a finite wettability (Papara et al. 2009). Glass containers cannot be used when diagnostic probes (electrodes, optical fibers, and pressure transducers) need to be installed. In such cases, stainless steel containers are used, limiting measurements to be made only at specific locations (Thakur et al. 2003). Since Plexiglas affords visual observation and can be machined to install probes, several researchers have chosen to use them in foam drainage experiments (Fournel et al., 2004). However, Plexiglas is hydrophobic, and the wettability of its surface can vary widely depending on the raw material used, manufacturing process, machining, and surface treatment (Papara et al. 2009). Therefore, it is hard to investigate the effect of its wettability on foam drainage process. It might be necessary to estimate wettability of specific Plexiglas container used before conducting experiments if wall effects are expected to

be significant. This problem might extend to glass, polymer, or metal surfaces as well if they are not properly cleaned after each operation or if surface molecules are adsorbed onto container walls.

Motion of Bubbles

The motion of bubbles near a stationary interface is influenced by bubble-interface hydrodynamic interactions (Happel and Brenner 1965). The extent of this effect depends on (i) the nature of bubbles and interface, (ii) the distance between them, (iii) the size and shape of the interface, and (iv) the direction of bubble motion with respect to interface and direction of gravity. Since experiments conducted in this study are within finite containers, two wall effects must be considered: (i) the effect of container walls parallel to liquid droplet/bubble motion, and (ii) the effect of a gas-liquid interface perpendicular to the direction of bubble motion. According to Clift et al. (1978), the effect of the wall on bubble motion in a cylindrical tube can be corrected using a resistance coefficient correction which depends on the particle (bubble)-container diameter ratio (PCDR). Wall effects have diminishing influence on bubble motion as Reynolds number increases. At high Reynolds numbers and/or low PCDR, wall effects are negligible. Usually, PCDR for bubbles in a liquid column is less than 6%, which is the critical value for a creeping flow (particle Reynolds number < 0.1), and wall effects can be neglected (Malysa 1992). However, wall effects can be significant in foam with its bubble network in which bubbles are close to the container walls, especially as liquid drains and bubbles size increases. Assuming creeping flow and no deformation of interface or bubble, Bart (1968) provided a correlation between resistance coefficient and the distance between a bubble and flat free surface such as a gas-liquid interface. The interference between an interface and bubble or droplet increases with the reduction of the distance between them. At higher Reynolds numbers, the effect of the gas-liquid interface on bubble velocity is negligible and can be ignored.

2.6.5 Shearing

Interstitial liquid in stable foams at rest possesses yield stress which prevents movement of liquid from foam structure. This yield shear stress is overcome when shear is induced to the standing foam. For example, when drilling with foam, the rotation of drill string induces an additional shear on the foam structure. Effect of shear (6-18 s^{-1}) on wet foams in a Couette rheometer (co-axial cylinders with rotating inner cylinder) was studied by Goyon et al. (2010). Bubble movement and size distribution were monitored using MRI. Applying shear to stable foams resulted in rapid drainage.

CHAPTER 3

THEORETICAL STUDY

The stabilization of foam films is critical to the overall stability of foams. The rate of liquid drainage from films and their stability are key factors in controlling foam half-life. Stable foam is characterized by an abundance of Newtonian black films. The transition from a thinning liquid film to a black film depends on the adsorption of surfactant molecules to the film surface. If the population of surfactant molecules on both sides of the film does not reach a critical level necessary for the formation of black films, the film thins until it ruptures. When film thins and reaches nanoscale thickness, weak forces such as electrostatic repulsion and Van der Waals attraction (DVLO theory) come into play and liquid films exhibit both expansion and thinning (Derjaguin and Landau 1941; Verwey and Overbeek 1948). Under certain conditions, other forces affect how liquid films interact with each other; and therefore, play a role in the rate of liquid removal from the films. The significance of this is the development of different forces including ion-correlation, steric, hydrophobic, adsorption, and colloidal structural forces. Ion-correlation forces are a negative correction to electrostatic disjoining pressure arising due to deformation of the electrical diffusive layer (Attard et al. 1988). Steric forces due to disjoining pressure on foam films occur only in stiff foams where polymers are dissolved in an aqueous medium (De Gennes 1985, 1987). Overlapping surfactant adsorption layers result in hydrophobic and adsorption forces acting on foam films (Christenson et al. 1987, 1990; Qu et al. 2009; Karakashev et al. 2013; Tsekov and Schulze 1997). Formation of micelles due to surfactants which attach to either face of foam film leads to colloidal structural forces (Nikolov et al. 1990).

This chapter aims to accomplish two things: (a) explain the significance of Newton black films in foam stability discussions, and (b) briefly define the various factors mentioned above that

act on foam films, and therefore, significantly affect bulk foam stability. Furthermore, miscellaneous factors that influence foam stability (foam generation method and contaminants present) are briefly broached upon.

3.1 Foam Films

The fundamental concepts developed by classical foam investigations have formed the basis of all modern studies on foam films. The black film, which is the most rupture-resistant form of thin liquid films that was first reported by Robert Hooke in 1672 (Hooke 1672). This phenomenon was explained by Newton in his famous manuscript, *Optics*, and termed black films as it reflects almost no light. In his experiments, he used a soap solution to create thin films and explained the colors appearing on such films as analogous to his earlier experiments involving the Newton rings where colors were observed in air trapped between two glass plates (Newton 1730). He reported that these colors formed concentric circles on film in a specific order (Table 3.1). These observations can be made in day-to-day life as the visual spectrum that forms on soap bubbles when seen in sunlight (or any white light). This order of colors starts to dilate with time, spreading over the whole film, resulting in the larger concentric rings to disappear (Fig. 3.1). This was explained by Newton as occurring due to loss of liquid in the film due to gravity. He also observed that as the film thinned, the color rings turned to predominantly black color, with spots of more intense 'blackness'. Newton estimated the thickness of these soap films and concluded that the thickness of the film was inversely proportional to its refractive index. Therefore, as liquid film thins, only larger wavelengths of light are refracted until almost no light passes through film resulting in the black film. The reason Newton black films are very stable compared with thicker films is that when the two interfaces encompassing the liquid film are in close proximity, various weak forces become dominant and resist the rupturing of film. These forces are discussed in the next sub-

section. Significant literature exists on foam films spanning centuries. In this section, a very brief description of the black film is provided as it is important to understand why stable dry foam is characterized by the presence of significant Newton black films.

Table 3. 1: Newton's concentric color bands (Isenberg 1992; Gochev et al. 2016)

Order of succession	Color succession of concentric rings
1	Black, blue, yellow, red, white
2	Violet, blue, green, yellow, red
3	Purple, blue, green, yellow, red
4	Green, red
5	Blue, red
6	Blue, red

Figure 3. 1: Succession of color bands observed in the vertical film (Brewster 1867)

3.2 Effect of Interfacial Properties on Foam Stability

In this section, the various physicochemical factors acting at the interface of gas-liquid phases and the liquid contained between them (films) are discussed. These factors are either directly affected by gravity and capillary forces that act to drain liquid from foam films or tend to strengthen the foam film from rupturing. The first effect limits the mechanism of drainage while the latter impedes foam decay.

3.2.1 Surface Tension

Van der Waals forces of attraction exist between molecules in any liquid phase. These forces are felt equally by each molecule in the liquid phase, except those in the interfacial region, and therefore, pull them into the interior of the liquid. This contracting force is called surface tension and is the reason why droplets of liquids or bubbles of gas tend to be spherical. Liquid or gas surfaces tend to contract and reduce total surface area, thereby, reducing total surface free-energy. From a thermodynamic point of view, surface tension has units of energy per unit area, i.e., expanding surface area requires the addition of energy. When viewing two–dimensional free body diagrams, surface tension is the sum of all contracting forces acting parallel to the interface and has units of force per unit length. Figure 3.1 illustrates surface tension (σ) as surface energy per unit area and surface–contracting force per unit length.

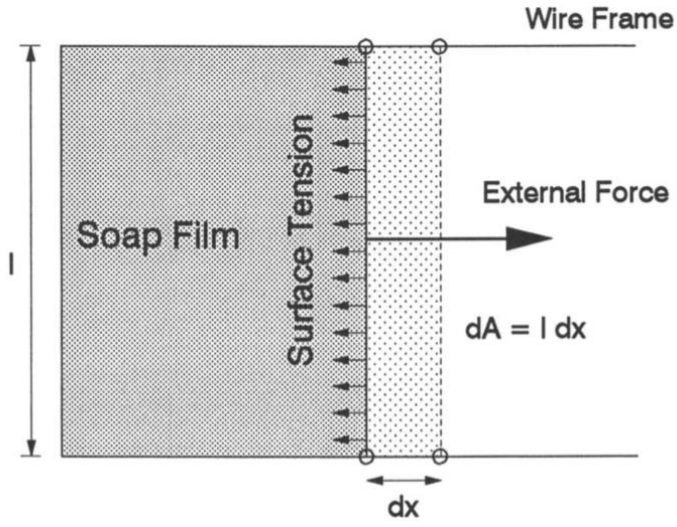

Figure 3. 2: Surface Tension (Schramm 1994)

$$External\ Force * dx = \sigma l dx = \sigma dA \quad (3.1)$$

Lamella in foam structure is composed of thin liquid film and two gas-liquid interfaces, with each interface having its own surface tension. The surface tension of lamella can, therefore,

be expressed as twice the surface tension of the gas-liquid interface and is called film tension. The surface tension of the bulk solution is comparable to that of a thin liquid film surface when the film is thick. As the liquid drains from the foam structure and the film thins, these values diverge from each other.

3.2.2 Young – Laplace Equation

The Young – Laplace equation is the basis for many widely used surface and interfacial tension measuring methods. Some of the commonly used ones are pendant and sessile drop methods, spinning drop method, and maximum bubble–pressure method (Harkins and Alexander 1959, Padday 1969, Miller and Neogi 1985, Cayias and Schechter 1975). Due to interfacial tension, a pressure difference exists along the gas-liquid interface with the pressure on the inside of the bubble being greater. In wet foam with spherical bubbles of radius R, this pressure difference can be expressed as:

$$\Delta P = P_G - P_L = 2\sigma/R \tag{3.2}$$

Equation 3.2 is the Young–Laplace equation, where P_G and P_L are static pressures acting at the interface due to gas and liquid phases, respectively. If the bubbles separated by the interface are not uniform, Eq. 3.2 can be expressed as:

$$\Delta P = P_G - P_L = \sigma\left(\frac{1}{R_1} + \frac{1}{R_2}\right) \tag{3.3}$$

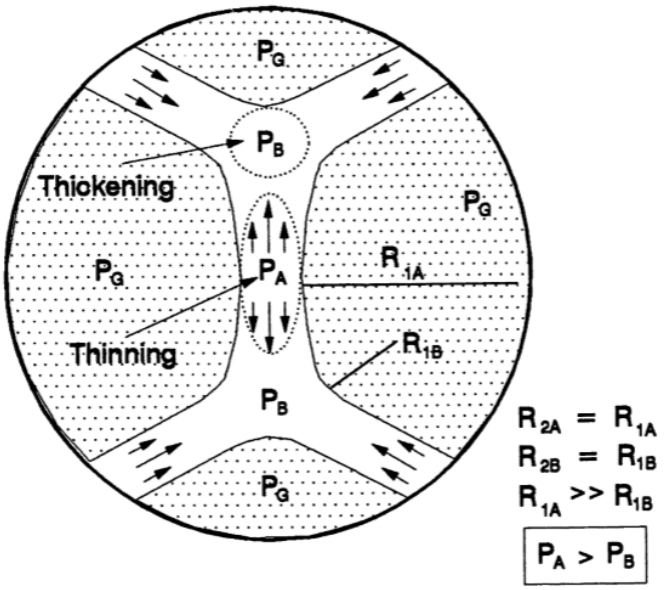

Figure 3. 3: Pressure drop across curved surfaces of lamella (Schramm 1994)

The equation can be further modified to account for an additional pressure difference within the liquid phase. This is shown in Fig. 3.2, where the radius of curvature at the plateau borders (where the pressure is P_B) is very small as compared to the more laminar part of the lamella (where the pressure is P_A). For simplicity, it is assumed here that the bubbles across the thin film are uniform at A and B ($R_{1A} = R_{2A}$ and $R_{1B} = R_{2B}$).

3.2.3 Surfactants

For a given gas-liquid composition, the total surface area of foam, and the free-energy associated with it increases with decreasing bubble size. To create a foam structure with small dispersed bubbles, energy is added to the gas-liquid system (for e.g., mechanical energy input by agitation). If energy addition through mechanical input is insufficient to create the foam structure desired, the free-energy associated with the surface area has to be lowered. Surfactants are chemical compounds that reduce the interfacial free-energy or surface tension when added to the base fluid (water or oil). Therefore, the addition of surfactants to the liquid phase results in lowering of mechanical energy required to create foams.

These chemical compounds have hydrophilic (affinity to a polar group such as water) and hydrophobic parts (affinity to a non-polar hydrocarbon chain, such as diesel). They form micelles, which are a cluster of surfactant molecules arranged in a specific manner when added to the liquid phase. The micellar structure is such that, the hydrophilic parts of surfactant molecules are enclosed by hydrophobic parts (when the liquid phase is aqueous). At the interface, the surfactant molecules arrange themselves such that each part lies in the fluid that it has the most affinity for. This arrangement of surfactant molecules at the interface and within the liquid phase can be seen in Fig. 3.3.

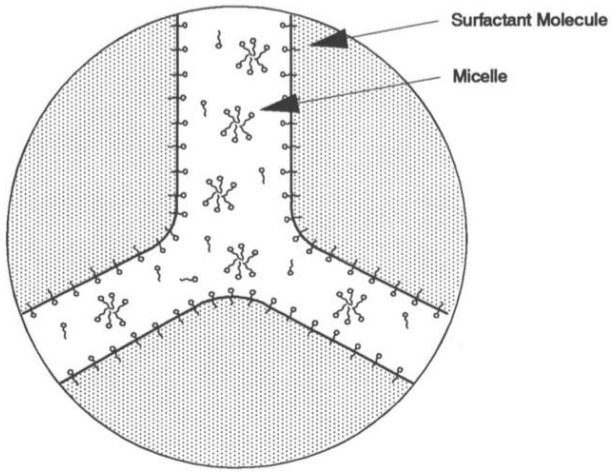

Figure 3. 4: Arrangement of surfactant molecules in lamella (Schramm 1994)

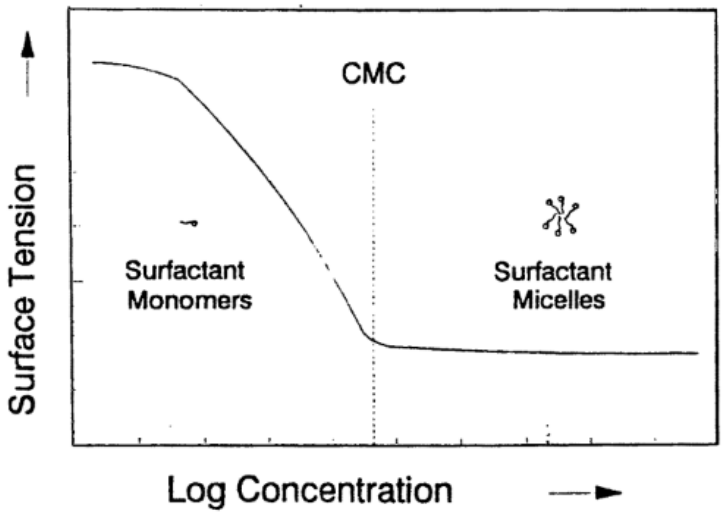

Figure 3. 5: Effect of increasing surfactant concentration in the liquid phase (Schramm 1994)

Surfactants lower interfacial tension by adsorption at the interface which provides an expanding force that acts against surface tension. In addition to lowering interfacial tension, the concentration of surfactants molecules at the interface also impede drainage by increasing interfacial viscosity, which provides mechanical resistance to film thing and rupturing (Schramm 1994). However, there exists a critical concentration of surfactant molecules at the interface (called critical micelle concentration, CMC) beyond which increasing concentration of surfactants in the liquid phase has no effect on foam drainage and stability (Fig. 3.4). Increasing the concentration of surfactant beyond this critical concentration (CMC) results in the formation and increase of micellar structures within the lamellae of foam.

3.2.4 Gravity and Capillary Suction

After the generation of foam, the gravity force drains the liquid phase along the thin film and lamellae of the foam structure. The drainage thins the film and brings the gas bubbles together, changing their shape from spherical to polyhedral, separated by planar lamellae. As the thick lamellae become more planar, capillary forces become significant and aid the drainage of liquid

from the film. This is due to the pressure difference within the lamellae (Fig. 3.2) where the plateau border is at a lower pressure as compared to the laminar portion of the lamellae. This pressure difference can be expressed by the Young-Laplace equation. Liquid flows from higher energy region to a lower energy region, thinning the film, and ultimately leading to rupture and foam dissipation. Therefore, at the scale of foam films, capillary forces assist gravity and result in film thinning. In bulk foam, capillary forces act to resist effects of drainage by trying to restore homogeneity of liquid volume fraction in foam column. Capillary forces were discussed in detail in Chapter 2.

3.2.5 Surface Elasticity

The thin film separating gas bubbles dispersed in foam structure is elastic in nature and can withstand deformations without rupturing to an extent. The elasticity of this film is explained by the surface chemical effect of Marangoni and Gibbs (Clunie et al. 1971). Gibbs–Marangoni or simply Marangoni effect is mass transfer (liquid phase) along the interface of gas-liquid due to surface tension gradient. The gradient may exist if a stabilized film undergoes sudden expansion, increasing its surface area, leading to the expanded region having lower surfactant adsorption as compared to the unexpanded regions. The expanded region has a higher surface tension due to increased surface area, leading to contraction of the surface (thinning). Liquid flows from the low tension to high tension region, resisting thinning and preventing the film from rupturing (Fig. 3.5). This mass transfer due to Gibb–Marangoni effect occurs until surfactant adsorption reaches equilibrium (no surface tension gradient). In thick films, there is enough liquid phase (and therefore, surfactant) for the equilibrium to be achieved quickly. In thin films, there is not enough surfactant available locally, and diffusion from other parts of the foam structure is required to establish equilibrium. To create stable foams, it is important that surface elasticity is of sufficient

magnitude to oppose gravity and capillary forces. If that is not the case, the foam created is short-lived and is termed evanescent foam. The elasticity of films also depends on the container shape and diameter, as explained in the previous chapter. Small diameter containers tend to promote rigidity of films and Plateau borders, accelerating foam drainage (Brannigan and De Alcantara Bonfim 2001; Koehler et al. 2004).

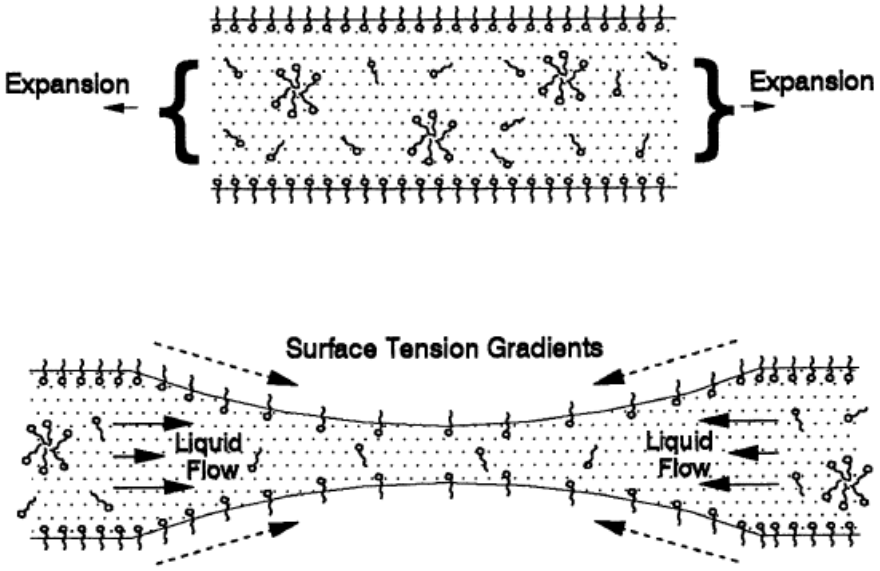

Figure 3. 6: Gibbs–Marangoni effect (Schramm 1994)

3.2.6 Surface Rheology

In addition to elasticity, viscous forces resist expansion and deformation of the thin film, opposing gravity and capillary forces. The interface has two types of viscosities – dilatational viscosity (viscous forces oppose expansion and increase in surface area) and shear viscosity (viscous forces oppose deformation due to applied shear stress). High surface viscosities impede liquid transfer in the thin film, delaying dynamic surface adsorption equilibrium (Gibbs-Marangoni effect), and lowering drainage rate. Therefore, surface rheology helps in resisting film rupture and bubble coalescence, extending the lifespan of foam and improving its overall stability. Surface rheology

is only consequential in thin films and is negligible in thick films (wet foams). In wet foams, bulk viscosity of liquid phase resists film thinning and drainage.

3.2.7 Surface Potential

In a gas-liquid colloidal system, surface potential or charge is the electrical potential difference between the inner and outer surface of the dispersed gas phase (bubble). When ionic surfactants are used to stabilize the thin film, the interface becomes charged. Any such charge at one side of the interface will be carried over to the other side, equally. This charge at the interface creates repulsive forces that resist film thinning. The magnitudes of these forces depend on charge density and the thickness of a liquid film.

Electric Double Layer

A charged interface results in redistribution of ions in the liquid thin film. Ions having the same charge as the interface are repelled while the oppositely charged ions are attracted, leading to the formation of an electric double layer. It consists of an inner layer composed of adsorbed surfactant ions, and an outer layer with ions distributed based on electrical and thermal influences.

Repulsive Forces

As the liquid film thins and gas bubbles come together, the charged interfaces approach one another and their electric double layers overlap. The repulsive forces between these two interfaces become dominant at this point and resist rupturing of the film. In extremely thin films, an additional strong repulsive force called Born repulsion helps stabilize foam. This force is only activated at very short ranges when atomic electron clouds overlap.

Dispersion Forces

The Van der Waals forces are residual weak forces due to attraction and repulsion between neutral molecules and they are caused by three types of molecular dipolar configurations: (i) two permanent dipoles, (ii) dipole-induced dipole, and (iii) induced dipole-induced dipole (London dispersion forces). The forces are only effective at very short distances. In a thin liquid film, dispersion forces are approximated by adding all attractive forces between inter-droplet pairs of molecules (Schramm 1994). The dispersion forces decay much less rapidly at short distances (effective in very thin films) due to Van der Waals forces resisting the rupturing of films.

DLVO Theory

The DVLO theory (named after Boris Derjaguin, Lev Landau, Every Verwey, and Theodor Overbeek), developed by Derjaguin et al. (1941), and independently by Verwey and Overbeek (1948), describes the forces acting between charged surfaces separated by a liquid medium, in aqueous colloidal systems. It combines, previously discussed, Van der Waals attractive and electrostatic repulsive forces acting on liquid film expressed as a function of molecular distances. Broadly, at large film thickness, attractive Van der Waals forces dominate while in thin films repulsive forces are more significant (Born repulsion). However, in very thin films, attractive forces start dominating again and maintain film stability.

Disjoining Pressure

The disjoining pressure is a hydrostatic pressure that exists due to the pressure difference between the gas phase in bubbles and the liquid phase in lamella and is a total of electrical, dispersion, and steric forces acting perpendicular to the two interfaces of lamella (Derjaguin et al. 1987). This pressure is a function of film thickness and is insignificant in wet foams with spherical bubbles

and thicker films. In very thin films, the electrical, dispersion, and steric forces are significant, and the hydrostatic pressure exerted by the two interfaces keep them apart and prevent film rupturing.

3.2.6 Coarsening and Coalescence

Coarsening is the process by which small gas bubbles are integrated into large ones. Bubble sizes are disproportionately distributed in foam structure and there exist concentration and pressure gradients across the films, which separate them. These gradients promote diffusion of small bubbles into larger ones, and ultimately lead to diffusion of the gas phase in foam structure to the bulk gas phase, collapsing the foam structure. On the other hand, the process of coalescence occurs and ruptures the film if all the above-mentioned factors fail to maintain film stability. Bubbles merge when the film between them ceases to exist resulting loss of liquid and gas, hastening the decay of foam.

3.3 Other Effects on Foam Stability

In this section, miscellaneous factors that have an influence on foam stability, directly or indirectly, are briefly discussed. These are methods used to generate foam, and the contaminants present either in liquid or gas phases. It should be noted that the stability of foam depends on how much energy is added to the system and not on the method. A vast literature exists on the influence of liquid (e.g. oil droplets) or solids (e.g. grit, protein aggregates) contaminants on foam stability. Such contaminants can either enhance or retard stability based on their physicochemical interactions with foam films. However, only a brief acknowledgment of this process is provided here as an extensive literature review on this topic is beyond the scope of this study.

3.3.1 Foam Generation Method

To generate foam, energy is added to the system to disperse gas bubbles in the liquid phase. Usually, mechanical energy is added to the system by agitation or shearing to create foam structure. Increasing the gas volume fraction of foam requires high energy inputs. Increasing foam generation shear rate can increase the quality of foam generated (Okpobiri and Ikoku 1986). The use of certain surfactants (foaming agents) lowers the energy requirements for a given gas-liquid solution and quality. The effect of surfactant depends on their chemical composition and their ability to decrease the surface tension of the liquid phase. Adding low concentrations of anionic surfactants such as alpha-olefin sulphonates increases foam stability. Cationic surfactants are not very effective and used at high concentration. They yield poor to moderate foam stability. However, they are used when drilling in water sensitive formations. Increasing concentration of surfactant increases foam quality up to a critical limit. Above this concentration, foam stability decreases (Burcik 1950), although others have reported no measurable effect (Schramm 1994). Other factors that affect foam generation are pressure, temperature, and additives to the liquid phase.

Energy added to create foam can be by injection (Raza and Marsden 1967), coiled tubing (Sanghani and Ikoku 1983), recirculation or single pass (Hutchins and Miller 2005), and needle valve with a static mixer (Sherif 2015). Gas can be injected directly into the liquid or through a porous media to develop bubbles (sprager, glass frit, and steel wool). Coiled tubing adds additional shear to fluid due to the curvature of pipe, and this additional energy generates foam. Foam can be created by passing (shearing) gas-liquid mixture through a flow restriction or long pipe (single pass or recirculation modes). Shearing can also be achieved using a needle valve, porous section, and static mixers. To generate fully developed (equilibrated) foam, high-shear must be provided

for sufficient time (Sherif 2015; Herzaft et al. 2005). When foam is fully developed, it has small bubbles that are tightly packed with ridged structure. The structure improves viscosity and makes the foam stable (David and Marsden 1968).

3.3.2 Contaminants

Contaminants can either be liquids, solids, or emulsions. Contamination can be deliberate (to break or inhibit or enhance foam) or undesirable (influx of formation fines and fluids). When deliberate, contaminants tend to be special systems that are designed to specifically target gas-liquid interface, destabilizing the foam structure. Contaminants that are designed to inhibit or break foam are called anti-foamers. Antifoaming is the action of soluble substances added to a foam system that either: (i) prevent foam from being generated (foam inhibitors), or (ii) reduce foam stability and lead to the collapse of foam structure (breakers and de-foamers). These substances can decrease foam stability by increasing surface tension, decreasing surface elasticity, decreasing surface viscosity, decreasing surface potential, or any combination of these. This can be achieved by partial or complete replacement of surfactant or foaming agent in the interface (e.g., high molecular weight alcohols used as breakers or foam inhibitors), or by actively reacting with the surfactant.

Liquid Contaminants

Liquid contaminants can be oil coming into contact with aqueous foams or water coming into contact with oil-based foams. When this occurs, the contaminant either forms a bead on the surface or spreads to form a film, depending on its affinity to the surface. This destabilizes the foam as the gas-liquid interface is compromised by the insoluble contaminant, and it loses its foam stabilizing ability, becoming less cohesive with higher surface tension and loss of Marangoni effect. The invasion of foam structure with a contaminant can lead to bubble coalescence as it bridges multiples bubbles, rupturing their already weakened films. The liquid contaminant can also spread

over the existing interface and replace the original liquid to create a new interface (water–gas to oil–gas, or vice–versa). This new interface will not have the same foam stabilizing properties leading to destabilization of lamellae and the foam structure. Spreading of low surface tension oil on aqueous foam lamellae (or vice–versa) ruptures it by providing weak spots (Kitchener 1964). Such liquid contaminants (e.g., poly dimethyl siloxane, insoluble in aqueous and some oil-based foams) are prepared as emulsions (to enhance mixing with foam liquid phase) and frequently used in the oil industry as foam inhibitors.

Solids Contaminants

Dispersed solids in foam can increase or decrease foam stability, depending on their effect on liquid phase viscosity and wettability with the foam liquid phase. Solids can increase foam stability by two mechanisms: (i) a stable dispersion of particles in the liquid phase, will increase its viscosity, and help stabilize foam by resisting gravity/capillary drainage (viscous dissipation); and (ii) if solid particles are not completely wetted, they will collect at gas-liquid interfaces, adding mechanical stability to lamellae, resisting thinning and rupturing.

CHAPTER 4

MATHEMATICAL STUDY

It is challenging to develop a generalized model that can be applicable to a wide variety of applications based on experimental measurements alone. One way of establishing a generalized foam stability model is to consider theoretical approaches for formulating mathematical models that can predict drainage characteristics of foams under various conditions. Once validated with experimental measurements, mathematical models can be extremely useful for research and field applications. Even though the effect of temperature was not investigated in present work, it is reasonable to assume that temperature will be uniform in tubing or annulus after circulating few borehole volumes. Therefore, the only major parameter affecting the stability of foam in the field is pressure, which can influence foam quality and other related properties such as density and fluid rheological parameters. In this section, the mathematical formulation of foam stability models is presented starting with the generalized foam drainage equations (FDE). There are two approaches (channel and node dominated methods) in foam drainage modeling and various boundary conditions that yield a number of analytical solutions namely, forced drainage, free drainage, and pulsed drainage solutions. The drainage process studied in the experimental portion of current work is most closely related to free drainage.

4.1 Channel Dominated Drainage Models

Early work on developing an equation to describe the foam drainage process assumes Poiseuille flow in channels with triangular cross-sections, considering only gravity and viscous resistance (Leonard and Lemlich 1965). Velocity profiles in foam column are estimated by applying momentum balance across a typical channel and assuming fixed viscosity (same as liquid

viscosity). Integrating the velocity profiles numerically while accounting for all the disoriented channels in foam structure, the total liquid flow through the foam is estimated. The model also assumed all liquid present in foam accumulates in the channels (no contribution by films or nodes). Furthermore, the model ignored the effect of surface tension and does not consider the deformation of channels as drainage progressed. An analytical solution to this model was developed by Kraynik (1983). Some early channel-dominated drainage models (Princen 1990; Narsimhan and Ruckenstein 1996; Saint-Jalmes et al. 1999) consider container geometry effect on drainage as well. The first true channel dominated foam drainage equation, which takes into consideration the effect of surface tension on foam drainage process was developed by Goldfarb et al. (1988). This model has been evaluated with experimental results and modified by Verbist et al. (1996). However, a recent study (Koehler et al. 2000) has noted that the predictions of this modified model tend to underestimate the drainage rate when compared with the measurements of earlier experimental studies (Kraynik 1983; Desai and Kumar 1982).

To improve the accuracy of the channel-dominated model, Bhakta and Ruckenstein (1995) modeled drainage of foam by considering flow in films in addition to channels. Film drainage is modeled using Reynold's equation for flow between flat circular disks and the effect of van der Walls forces, electric double layer, and other surface properties are considered. A critical thickness value was defined for liquid film, below which it ruptures. They investigated the effect of superficial gas velocities, electrolyte concentration, and bubble size on the half-life of foam. Later, Bhakta et al. (1997) improved the channel dominated model by taking in to account foam collapse and bubble coalescence in addition to gravity drainage. The model also assumed Poiseuille flow in a triangular duct with a no-slip condition at the interface. Results showed that equilibrium can be attained when the gravitational force causing drainage balances the suctioning of the liquid into

channels due to capillary forces. Under equilibrium state, foam stability and collapse are determined by bubble size and surface tension in films (film rigidity). The model considers the flow of liquid phase as occurring due to gravity drainage in channels and upward bubble movement that causes foam to lose liquid as bubbles carry some volume with them.

Using one-dimensional nonlinear partial differential equations (vertical flow assumed), Koehler et al. (2000) presented a foam stability model that considers gravity, surface tension, and viscous forces in its formulation. The model solutions are obtained using boundary conditions taken from three drainage experiments – free drainage where liquid drains from an initially uniform foam of fixed length; wetting of dry foam; and pulsed drainage in which dry foam has a liquid spreading on the surface. Model predictions have been validated with experimental results.

4.2 Node-Dominated Drainage Models

The node-dominated modeling approach is another method commonly used in foam drainage analysis. Node-dominated models assume the presence of a large liquid mass at the nodes where channels intersect. The flow of liquid into nodes from channels is considered as plugs. The contribution of the channel-flow on the drainage process is small as compared to that the nodes. Node-dominated models are rather complex and require solving Navier-Stokes equations to obtain a relationship between liquid flow velocity and liquid volume fraction. Hence, the contribution of channel-flow is assumed minor to simplify the model. Besides this, various assumptions are made based on drainage experiments to simplify the model equations and obtain analytical solutions with meaningful results. Model predictions have been validated with results obtained from forced drainage experiments (Koehler et al. 1999a). Based on experimental observation, the geometry of the foam structure is assumed to be invariable with time. In the experiments, a constant injection of liquid

at the top of a drying foam column was maintained resulting in a downward moving wetting front in the foam. This results in constant liquid volume fraction and liquid velocity in the foam column. The injection was maintained such that liquid velocity was very low to prevent distortion of foam structure.

Later, other studies (Cox et al. 2001; Koehler et al. 2000; Saint-Jalmes et al. 2004) improved the node-dominated model by incorporating different effects including channel flow, viscous effects, and the permeability of foam structure. Cox et al. (2001) incorporated the contribution of channel-flow into the node-dominated model by developing numerical constants (correction factors) to modify the Poiseuille flow used in channel-flow models. Koehler et al. (2000) developed a foam drainage equation that includes viscous effects of flow in node and channels. Saint-Jalmes et al. (2004) used forced drainage experiments on aqueous foam to measure the permeability of foam structure and the viscous resistances of nodes and channels. Recently, Abdolhamid et al. (2017) presented a drainage model for flow in nodes and channels. The liquid velocity was determined by solving the conservation of mass and three-dimensional momentum equations using numerical methods. The predictions of the model were validated with previous experimental data (Koehler et al. 2004; Pitois et al. 2005).

4.3 General Foam Drainage Equation

To develop a general equation that describes the process of liquid drainage from a standing foam column, it is useful to assume the structure of foam to be analogous to porous medium with rigid homogeneous spheres (Zick and Homsy 1982; Larson and Higdon 1989). The permeability of foam structure to liquid flow depends on the interconnected structural units (channels, nodes, and, films) and their concentration. The drainage flow is driven by pressure gradient that is related to average liquid velocity in foam structure by Darcy's law (Koehler et al. 2000):

$$G = -\nabla p + \rho_l g = \mu v/k \tag{4.1}$$

where G is the pressure gradient driving the flow; p is the liquid pressure; ρ_l is the liquid density; g is the acceleration due to gravity; μ is the liquid viscosity; *v* is the average liquid velocity; and *k* is the permeability of foam. However, the problem with equating flow in foam to that of Darcy flow in a porous medium is the assumption that foam structure remains rigid. Channels, nodes, and liquid films, as well as bubbles, deform due to the process of liquid drainage, changing the interstitial flow conduits through which liquid passes. This can be accounted for in Eq. 4.1 by defining permeability of foam as a function of liquid volume fraction, which is a function of time. Therefore, permeability, k(ε) and liquid volume fraction, ε(z, t) vary with time along the vertical axis in a foam column.

The generalized foam drainage equation describes fluid flow in both nodes and channels. The assumptions of the model are: bubbles are monodispersed and foam structure does not deform with time. Conservation of mass can be used to obtain an equation relating liquid volume fraction with liquid flow velocity (Goldfarb et al. 1988; Koehler et al. 1999a):

$$\frac{\partial \varepsilon}{\partial t} + \nabla.(\varepsilon v) = 0 \tag{4.2}$$

Both liquid volume fraction in foam and velocity of draining liquid vary spatially and with time. In Eq. 4.1, Young-Laplace equation can be used to express the pressure exerted on liquid p, as:

$$p = p_{gas} - \frac{\sigma}{r} \tag{4.3}$$

where p_{gas} is pressure in each bubble; γ is surface tension; and, r is the characteristic radius of the curvature of channels in the foam structure. The weight of the foam is considered to be small so

as to not deform the bubbles due to compression (Weaire et al. 1997). Equation 4.1 can be rewritten as:

$$G = \rho g + \nabla\left(\frac{\sigma}{r}\right) \approx \rho g + \frac{\sigma {\delta_\varepsilon}^{0.5}}{L}\nabla\varepsilon^{-0.5} \tag{4.4}$$

where, L is the channel length; and, δ_ε is a constant specific to the geometry of bubble used to relate channel length, L, and channel radius of curvature, r, to the liquid volume fraction, ε. Combining these equations (Eq. 4.1 to 4.4), the generalized foam drainage model can be expressed as (Koehler et al. 2000):

$$\mu\frac{\partial\varepsilon}{\partial t} + \rho g.\nabla[k(\varepsilon)\varepsilon] - \frac{\sigma {\delta_\varepsilon}^{0.5}}{L}\nabla.[\mathrm{k}(\varepsilon)\nabla\varepsilon^{-0.5}] = 0 \tag{4.5}$$

To solve the foam drainage model equation (Eq. 4.5), the permeability of foam needs to be modeled. Hence, permeability models for both modeling methods are presented here. Koehler et al. (2000) developed the following simplified mathematical models assuming flow in the vertical axis and eliminating the second and third order partial differential equations. For channel-dominated flow the following foam drainage equation is presented:

$$\mu\frac{\partial\varepsilon}{\partial t} + K_1\rho g L^2\frac{\partial\varepsilon^2}{\partial z} - \frac{\sigma {\delta_\varepsilon}^{0.5} K_1 L}{3}\frac{\partial^2\varepsilon^{1.5}}{\partial z^2} = 0 \tag{4.7}$$

where K_1 is a dimensionless number that depends on the geometry of foam structural units (channels, nodes, and bubbles). The permeability of foam for channel dominated model is directly related to the liquid volume fraction as:

$$k(\varepsilon) = K_1 L^2\varepsilon \tag{4.6}$$

Furthermore, Koehler et al. (2000) developed the following model to describe node-dominated foam drainage.

$$\mu \frac{\partial \varepsilon}{\partial t} + K_2 \rho g L^2 \frac{\partial \varepsilon^{1.5}}{\partial z} - \frac{\sigma {\delta_\varepsilon}^{0.5} K_2 L}{2} \frac{\partial^2 \varepsilon}{\partial z^2} = 0 \quad (4.9)$$

where K_2 is a dimensionless number which represents the viscous dissipation occurring in channels and nodes. For node-dominated foam drainage, the permeability of foam is expressed as (Koehler et al. 2000):

$$k(\varepsilon) = K_2 L^2 \varepsilon^{0.5} \quad (4.8)$$

The values of these dimensionless constants (K_1 and K_2) depend on the type of drainage and boundary conditions considered. Reasonable values of these constants are obtained from experimental measurements. A detailed analysis of foam permeability is presented by Koehler et al. (2000).

4.4 Foam Drainage Experiments

Three types of drainage experiments have been performed (Koehler et al. 2000; Weaire et al. 1997; Verbist et al. 1996) to develop mathematical models: forced drainage, free drainage, and pulsed drainage. These three scenarios allow for simplification of the complex task of developing a mathematical model that describes foam drainage and provide suitable boundary conditions. Furthermore, liquid volume fraction can be estimated in draining foam column using optical methods (other methods can be used as well and were presented in Chapter 2) which is an essential initial input for any model and can be used to validate said model. Variations to these experiments exist in the literature based on liquid or gas injection rate (Verbist et al. 1996).

4.4.1 Forced Drainage

In these drainage experiments, foam is generated by injecting gas from the bottom into a tube filled with liquid. Forced drainage condition is established by injecting a constant flux of liquid phase at the top of the foam column such that it re-wets the drying foam. Therefore, at the top of the foam column (z = 0), the liquid volume fraction, ε, is assumed constant. However, through the body of the foam column, the liquid volume fraction varies with column height as a drainage wave (Fig. 4.1). The wave consists of three regions: drained region where ε ~ 0 (drained foam); transient region where ε varies with column height (wet foam); and top region where ε is constant (liquid injection).

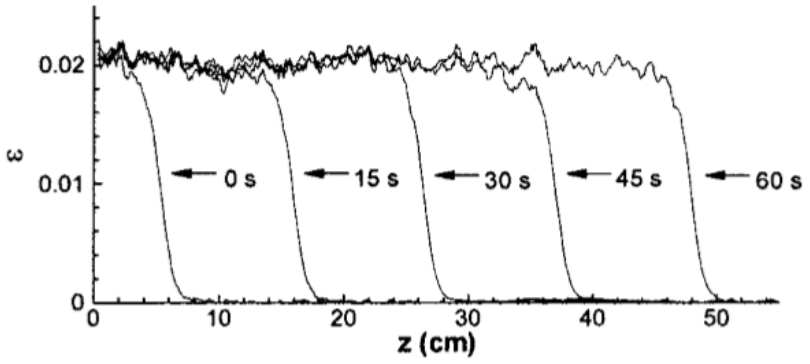

Figure 4. 1: Five drainage waves from forced drainage experiment (Koehler et al. 2000)

4.4.2 Free Drainage

Free drainage is the simplest scenario of foam drainage where a static foam column is allowed to drain and the amount of liquid drained is monitored with time. There is no injection of liquid from the top or gas from the bottom for the duration of the experiment. The liquid volume fraction, ε is homogeneous throughout the foam column at the beginning of drainage experiments (t = 0). Drainage occurs in four main regimes: (i) initial regime where foam releases very little liquid; (ii) second regime with a constant drainage rate; (iii) third regime where the drainage rate gradually

declines; and (iv) fourth regime where drainage rate is exponential (Weaire et al. 1997). Despite being a simple experimental type drainage rate profile, it is difficult to model free drainage due to the inherent complexity of defining suitable boundary conditions. It is useful to divide foam column into three regions: (i) the top region where $\varepsilon \sim 0$ at the top of the column and slowly increases with height; (ii) mid region where ε is constant; and (iii) bottom region where ε approaches 1. The experiments conducted in the present study are similar to free drainage. Results from free drainage experiments of Koehler et al. (2000) are shown in Fig. 4.2.

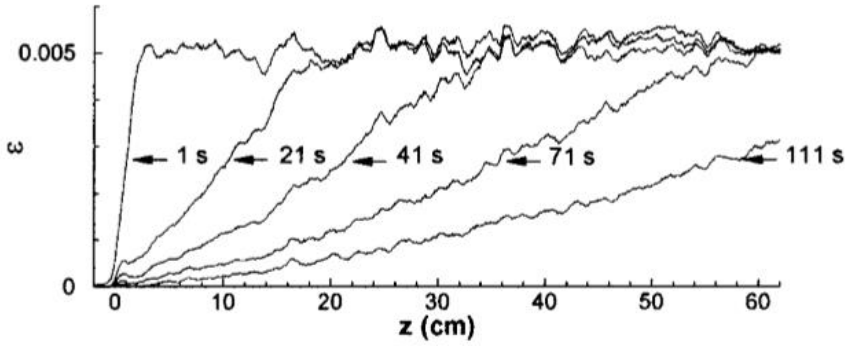

Figure 4. 2: Free drainage results from top to uniform ε region (Koehler et al. 2000)

4.4.3 Pulsed Drainage

In this type of experiment, a very small volume of liquid is injected at the top of foam column. The liquid spreads in all directions within the foam column (Verbist et al. 1996). Using optical methods, large pulses (injected liquid volume) are easier to detect even though they travel fast through the foam column. Smaller pulses slowly travel down but they are difficult to detect due to minimal variations in liquid volume fraction. Results from pulsed drainage experiments by Koehler et al. (2000) are shown in Fig. 4.3.

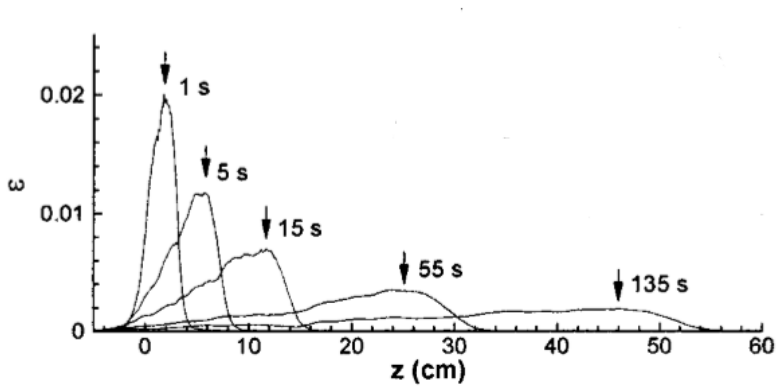

Figure 4. 3: Moving liquid pulse in pulse drainage experiment (Koehler et al. 2000)

4.5 Numerical Techniques

Foam drainage model equations formulated to describe liquid flow in foam network are complex non-linear partial differential equations, requiring numerical techniques to arrive at meaningful solutions. In this sub-section, various techniques (Nishioka et al. 1983; Gubes et al. 2015; Parand and Delkosh 2017; Arbabi et al. 2016) employed to solve these complex equations are discussed.

An early modeling study (Nishioka et al. 1983) used a fourth order Ranga-Kutta method with five back-loops to solve the foam drainage equation. Nishioka et al. (1983) conducted an experimental and mathematical study on foam stability using the rate of reduction foam surface area as a measure of stability. Their experimental study consisted of measuring the rate of loss of foam contained in a fixed volume at a constant temperature by measuring the rate of increase of gas pressure in the headspace above foam. This was also reflected in the mathematical model they employed which assumes inter-bubble gas diffusion to be the dominant mechanism of foam decay.

A recent modeling study (Gubes et al. 2015) used the Reduced Differential Transform Method (RDTM) to solve the non-linear foam drainage equations developed for free and forced drainages. The model assumes channel-dominated flow. They compared their model with the

Adomain and Laplace decomposition methods (ADM and LDM). The concept of RDTM used is derived from power series expansion. They concluded that results obtained from RDTM have better accuracy as compared to ADM or LDM. Also, they compared their model predictions with solutions obtained (Weaire et al. 1997; Verbist et al. 1996) for free and forced drainages.

Another recent modeling study (Arbabi et al. 2016) used Haar wavelets method (HWM) to solve Foam Drainage Equation (FDE) assuming channel flow. Forward difference method has been used to discretize the time derivative of FDE and then quasi-linearization technique was applied to linearize the FDE. The linearized FDE was solved using Haar wavelets by discretizing space derivatives. Their methods were verified by exact solutions available in the literature to the FDEs. They concluded that HWM is more efficient and accurate than homotopy perturbation, homotopy perturbation transform, Adomian decomposition and Laplace decomposition methods (HPM, HPTM, ADM, and LDM).

A more recent modeling study (Parand and Delkosh 2017) presented a solution to the solved FDE using the hybrid numerical method utilizing quasi-linearization and bivariate generalized fractional order of Chebyshev functions (B-GFCF) collocation method. The quasi-linearization was used to transform FDE into a sequence of linear partial differential equations. These linear equations were then solved with B-GFCF collocation method. They concluded that this method is better than the Haar wavelets method used by Arabi et al. (2016).

4.6 Current Work

The tests carried out in the present study can be related to free drainage experiments that were confined to an annular section. For the present study, channel dominated, and node dominated models are developed based on the Koehler et al. (2000) foam drainage equation.

4.6.1 Model Assumptions

The following assumptions are made to obtained numerical solutions to the models:

I. Bubbles are assumed to be monodispersed.

II. For dry foams, channel length, L is expressed as: $L \approx \frac{d_b}{2.8}$, where d_b is the maximum bubble diameter (Koehler et al. 1999a; Koehler et al. 1999b; Koehler et al. 2000; Saint-Jalmes 2006; Nosa 2012). Since the quality of foams considered in this study ranges between 40 to 80%, bubbles are assumed to retain more or less spherical shape rather than polyhedral. Hence, it is reasonable to assume $L < \frac{d_b}{2.8}$. In this study, the channel length is defined as: $L = \frac{d_b(\varepsilon,t)}{3}$. Correlations developed for aqueous and polymer foams to predict average bubble size that account for variation in liquid volume fraction and time are used to determine channel length. Therefore, the new models account for coarsening and coalescence of foam.

III. Surfactant concentration is assumed to be uniform in foam column. Therefore, surface tension is considered constant. Surface tension for water and polymer in contact with air were measured and are presented in Table 4.1.

IV. The flow of drained liquid is assumed to be in a vertical direction.

V. Equilibrium state is assumed to exist after the liquid phase has completely drained from foam such that the liquid volume fraction at the interface of foam and drained liquid is the same as the initial liquid volume fraction in foam column.

VI. Foam is considered to be unbounded. Therefore, geometry of container and wall effects are neglected.

VII. The value of δ_ε used in foam stability models is assumed to be 0.1711. This value has been proposed by (Koehler et al. 2000) using scientific software used to study surfaces shaped by surface tension (Surface Evolver).

Table 4. 1: Measured surface tension of base liquids

Foam Type	Surface Tension, N/m	Temperature, ^oC
Aqueous foam	0.03402	20.8
Polymer	0.03352	21.1

4.6.2 Computational Grid Development

The models developed in this study are used to predict liquid volume fraction at various times along the length of foam column for aqueous and polymer foams at different qualities (40, 60, and 80%). The height of foam column is defined as the total height of annulus used in experimental study multiplied with foam quality. Therefore, the model predicts liquid volume fraction in the top portion of foam column (i.e. between the top of the column to the point where drained liquid level exists after complete drainage). The height of foam is divided into 30 grids (i_1 to i_{30}). For the purposes of numerical modeling, two imaginary grids are added at the top and bottom of the foam column (Fig. 4.4). These imaginary grids enabled defining boundary conditions: $\varepsilon(z,t) = 1 - \varphi$ at t = 0 (initial condition); and, at t = N*Δt, z = H. Here, φ is the foam quality (40, 60, or, 80%); t

is time; z is the position of a computational grid that ranges from 0 at top of foam column to H at the bottom; H is the height of the portion considered, defined as 1.08*φ (total height of foam in the annulus is 1.08 m); N is the number of time steps chosen based on total length of drainage experiments; and, Δt is the timestep. For polymer foam, base liquid apparent viscosity is calculated at a shear rate of 1 s^{-1} using the rheology model parameters obtained from rotational viscometer data. Viscosity for aqueous foams is assumed to be that of water at standard temperature. Permeability constants, K_1 and K_2, are obtained by assuming initial values and comparing modeling results with experiments. These constants are varied for different foams to arrive at meaningful results. The actual foam quality is estimated based on total liquid drained after the complete collapse of foam. These values are shown in Table 4.2 and are used to initialize channel and node dominated models.

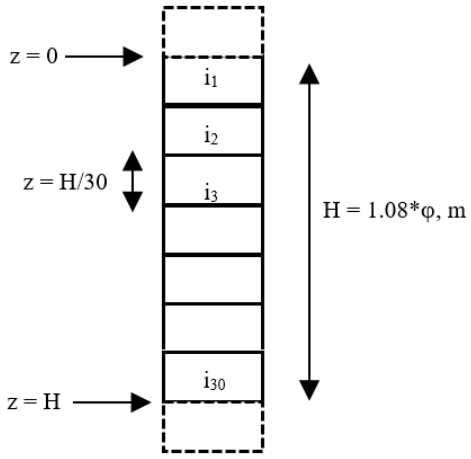

Figure 4. 4: Discretized foam column (30 grids)

Table 4. 2: Foam quality, liquid volume fraction and column height

Foam Type	φ, %	ε	H, m	Δz, m
Aqueous/Polymer	40	60	0.43	0.014
	60	40	0.65	0.022
	80	20	0.86	0.029

4.6.3 Channel Dominated Model

The channel-dominated model equation developed by Koehler et al. (2000) is used in this study. Thus:

$$\mu\frac{\partial\varepsilon}{\partial t}+K_1\rho gL^2\frac{\partial\varepsilon^2}{\partial z}-\frac{\sigma{\delta_\varepsilon}^{0.5}K_1L}{3}\frac{\partial^2\varepsilon^{1.5}}{\partial z^2}=0 \tag{4.10}$$

After simplification, Eq. 4.10 can be rewritten as:

$$\mu\frac{\partial\varepsilon}{\partial t}+2(K_1\rho gL^2)\frac{\varepsilon\partial\varepsilon}{\partial z}-\left(\frac{\sigma{\delta_\varepsilon}^{0.5}K_1L}{3}\right)\left[\frac{\partial}{\partial z}\left(\frac{\partial\varepsilon^{\frac{3}{2}}}{\partial z}\right)\right]=0 \tag{4.11}$$

In Eq. 4.11, the second-order derivative of ε can be further simplified as:

$$\left[\frac{\partial}{\partial z}\left(\frac{\partial\varepsilon^{\frac{3}{2}}}{\partial z}\right)\right]=\left[\frac{\partial}{\partial z}\left(\frac{3}{2}\varepsilon^{\frac{1}{2}}\frac{\partial\varepsilon}{\partial z}\right)\right]=\frac{3}{2}\left[\frac{\partial\varepsilon^{\frac{1}{2}}}{\partial z}\frac{\partial\varepsilon}{\partial z}+\varepsilon^{\frac{1}{2}}\frac{\partial^2\varepsilon}{\partial z^2}\right]=\frac{3}{2}\left[\frac{\varepsilon^{-\frac{1}{2}}}{2}\left(\frac{\partial\varepsilon}{\partial z}\right)^2+\varepsilon^{\frac{1}{2}}\frac{\partial^2\varepsilon}{\partial z^2}\right] \tag{4.12}$$

Therefore, Eq. 4.11 can be rewritten as:

$$\mu\frac{\partial\varepsilon}{\partial t}+2(K_1\rho gL^2)\frac{\varepsilon\partial\varepsilon}{\partial z}-\left(\frac{\sigma{\delta_\varepsilon}^{0.5}K_1L}{3}\right)\frac{3}{2}\left[\frac{\varepsilon^{-\frac{1}{2}}}{2}\left(\frac{\partial\varepsilon}{\partial z}\right)^2+\varepsilon^{\frac{1}{2}}\frac{\partial^2\varepsilon}{\partial z^2}\right]=0 \tag{4.13}$$

Further simplifying Eq. 4.13, yields the following equation:

$$\mu\frac{\partial\varepsilon}{\partial t}+2(K_1\rho gL^2)\frac{\varepsilon\partial\varepsilon}{\partial z}-\left(\frac{\sigma{\delta_\varepsilon}^{0.5}K_1L}{4}\right)\varepsilon^{\frac{-1}{2}}\left(\frac{\partial\varepsilon}{\partial z}\right)^2-\left(\frac{\sigma{\delta_\varepsilon}^{0.5}K_1L}{2}\right)\varepsilon^{\frac{1}{2}}\frac{\partial^2\varepsilon}{\partial z^2}=0 \tag{4.14}$$

Equation 4.14 is the simplified form of the channel-dominated foam drainage equation. It can be expressed in compact form as:

$$A\frac{\partial\varepsilon}{\partial t}+BL^2\frac{\varepsilon\partial\varepsilon}{\partial z}-CL\varepsilon^{\frac{-1}{2}}\left(\frac{\partial\varepsilon}{\partial z}\right)^2-DL\varepsilon^{\frac{1}{2}}\frac{\partial^2\varepsilon}{\partial z^2}=0 \tag{4.15}$$

where, A, B, C, and, D, are constants that are expressed as: A = μ; B = $2K_1\rho g$; C = $\left(\frac{\sigma {\delta_\varepsilon}^{0.5} K_1}{4}\right)$; and, D = $\left(\frac{\sigma {\delta_\varepsilon}^{0.5} K_1}{2}\right)$.

Finite difference method is used to obtain a numerical solution. Equation 4.15 is discretized applying forward difference for first-order derivatives in time and length and the central difference for second-order derivative in length.

$$A\frac{\varepsilon_i^{n+1}-\varepsilon_i^n}{\Delta t} + BL^2\varepsilon_i\frac{\varepsilon_{i+1}^n-\varepsilon_i^n}{\Delta z} - CL{\varepsilon_i}^{\frac{-1}{2}}\left(\frac{\varepsilon_{i+1}^n-\varepsilon_i^n}{\Delta z}\right)^2 - DL{\varepsilon_i}^{\frac{1}{2}}\frac{\varepsilon_{i+1}^n-2\varepsilon_i^n+\varepsilon_{i-1}^n}{(\Delta z)^2} = 0 \tag{4.16}$$

After re-arranging Eq. 4.16, the liquid volume fraction at a future time (n+1) is determined based on the liquid volume fraction at the present time (n) as:

$$\varepsilon_i^{n+1} = \frac{\Delta t}{A}\left\{CL{\varepsilon_i}^{-\frac{1}{2}}\left(\frac{\varepsilon_{i+1}^n-\varepsilon_i^n}{\Delta z}\right)^2 + DL{\varepsilon_i}^{\frac{1}{2}}\frac{\varepsilon_{i+1}^n-2\varepsilon_i^n+\varepsilon_{i-1}^n}{(\Delta z)^2} - BL^2\varepsilon_i\frac{\varepsilon_{i+1}^n-\varepsilon_i^n}{\Delta z}\right\} + \varepsilon_i^n \tag{4.17}$$

4.6.4 Node Dominated Model

The node-dominated foam drainage equation developed by Koehler et al. (2000) is considered in this investigation as an alternative model. This model has been used previously by Ibizugbe (2012), assuming monodispersed bubbles, and provided reasonable predictions of experimental measurements for oil foams. The model equation presented below (Eq. 4.18) is a nonlinear partial differential equation.

$$\mu\frac{\partial\varepsilon}{\partial t} + K_2\rho g L^2\frac{\partial\varepsilon^{\frac{3}{2}}}{\partial z} - \frac{\sigma {\delta_\varepsilon}^{0.5} K_2 L}{2}\frac{\partial^2\varepsilon}{\partial z^2} = 0 \tag{4.18}$$

After simplification, Eq. 4.18 is expressed as:

$$\mu\frac{\partial\varepsilon}{\partial t} + K_2\rho g L^2\frac{3}{2}\frac{\varepsilon^{\frac{1}{2}}\partial\varepsilon}{\partial z} - \frac{\sigma {\delta_\varepsilon}^{0.5} K_2 L}{2}\frac{\partial^2\varepsilon}{\partial z^2} = 0 \tag{4.19}$$

Equation 4.19 is further simplified using constants and expressed as:

$$\alpha \frac{\partial \varepsilon}{\partial t} + \beta L^2 \frac{\varepsilon^{\frac{1}{2}} \partial \varepsilon}{\partial z} - \chi L \frac{\partial^2 \varepsilon}{\partial z^2} = 0 \tag{4.20}$$

where, α, β, and, χ, are constants: α = μ; β =$\left(\frac{3}{2} K_2 \rho g\right)$; and, χ = $\frac{\sigma \delta_\varepsilon{}^{0.5} K_2}{2}$. The finite difference method was used to discretize Eq. 4.20 and obtain a numerical solution. Forward difference method was used for first order derivatives in time and length, and the central difference was used for second order derivative in length.

$$\alpha \frac{\varepsilon_i^{n+1} - \varepsilon_i^n}{\Delta t} + \beta L^2 \varepsilon_i{}^{\frac{1}{2}} \frac{\varepsilon_{i+1}^n - \varepsilon_i^n}{\Delta z} - \chi L \frac{\varepsilon_{i+1}^n - 2\varepsilon_i^n + \varepsilon_{i-1}^n}{(\Delta z)^2} = 0 \tag{4.21}$$

Equation 4.21 can be re-arranged to get Eq. 4.22 which expresses liquid volume fraction at future time step (n+1) based on the liquid volume fraction at the current time (n):

$$\varepsilon_i^{n+1} = \frac{\Delta t}{\alpha} \left\{ \chi L \frac{\varepsilon_{i+1}^n - 2\varepsilon_i^n + \varepsilon_{i-1}^n}{(\Delta z)^2} - \beta L^2 \varepsilon_i{}^{\frac{1}{2}} \frac{\varepsilon_{i+1}^n - \varepsilon_i^n}{\Delta z} \right\} + \varepsilon_i^n \tag{4.22}$$

A computer code, which is implemented in the MATLAB environment, is developed to solve Eq. 4.17 and 4.22. The code is used to estimate liquid volume fraction of profiles of 40, 60, and, 80% quality aqueous and polymer foams. Model prediction obtained from channel and node dominated models are discussed in Chapter 6 by comparing it with experimental measurements. Detailed numerical simulation results are presented in Appendix D.

CHAPTER 5

EXPERIMENTAL STUDY

In this chapter, the flow loop used for experimental studies, the equipment designed to measure foam drainage, instrumentation used for monitoring and controlling various test parameters, materials and chemicals utilized to create stable foams, and test matrix applied during the investigation are presented. The procedure followed when conducting the experiments, and the various equations that were used in analyzing experimental data are also discussed.

5.1 Scope of Experimental Study

In this investigation, test variables were foam quality, drainage column geometry, shear rate level, drainage column inclination, and types of foams. Three types of foams (aqueous, polymer-based, and oil-based foams) were considered in this study. The qualities considered in this study were limited by the capability of equipment used to generate them. For all three types of foams, the minimum quality was 40% as lowering gas volumetric ratio less than this value resulted in the dissociation of gas and liquid in aqueous, polymer, and oil-based foams. For aqueous and polymer-based foams the upper limit of foam quality was 80% and for oil-based foams, it was 70%. Increasing quality beyond this limit resulted in unstable foam. Between these limits of quality, test foams were prepared in increments of 5% quality. Therefore, nine aqueous and polymer-based foams with different qualities (40, 45, 50, 55, 60, 65, 70, 75, and 80%) were tested. For oil-based foam, seven foam qualities (40, 45, 50, 55, 60, 65, and 70%) were considered. Together, twenty-five foams were generated for drainage tests performed in pipe and annular sections under static conditions.

During dynamic tests in the annulus, the shear rate was varied by rotating inner PTFE (polytetrafluoroethylene) rod at different rotational speeds (approximately 4 and 7 rpm). For the dynamic test, foam quality was varied between lower and upper limits by an increment of 10%. Therefore, five foams were generated with water and polymer liquid bases (40, 50, 60, 70, and 80%), and four were prepared with oil based (40, 50, 60, and 70%). The inclination angle considered in this study was only 30^{o}, although the test setup could be rotated up to 90^{o}. This is because it was not possible to obtained consistent pressure measurements and density profiles in the foam column at high inclinations (45 and 60^{o}). Density profiles obtained from preliminary tests conducted at 60^{o} inclination (from the vertical) using 40 and 45% quality foam in annulus are shown in Fig. 5.1. All experiments were conducted under ambient temperature conditions (22 ± 2 ^{o}C) and foam was generated at a system pressure of approximately 689.48 KPa (100 psi).

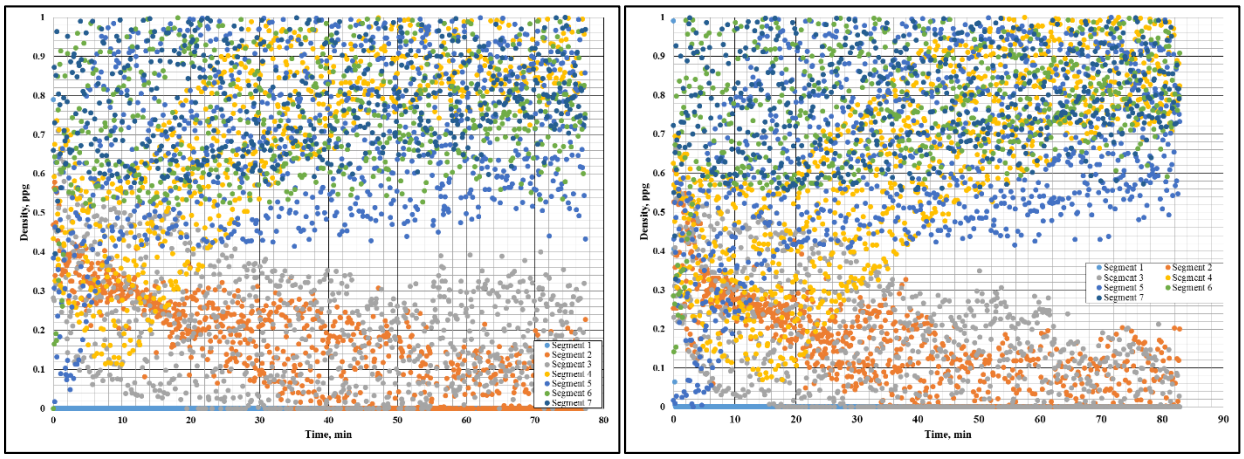

Figure 5. 1: Density profiles obtained from 40 and 45% foam captured in annular section at 60^{o}

5.2 Test Setup

The flow loop (Fig. 5.2) used to perform the experiments consists of liquid reservoir, progressive cavity pump (Moyno), nitrogen supply cylinder, foam generating section (needle valve and two static mixers installed upstream and downstream of the needle valve), pipe viscometers, foam drainage measuring section, and, flow and pressure measuring instruments. A Coriolis mass flow

meter (Endress and Hauser Model F83) was used to measure foam flow rate and density. Four static pressure sensors were used to measure system pressure at different locations. Nine differential pressure transducers (eight Endress and Hauser Model PMD75, and one Rosemount) were used to measure differential pressure in the stability cell and pipe viscometers. Temperature sensor (Omega PRTXD) was used to monitor the system temperature. Flow information was collected using a data acquisition board and transmitted in real time to a computer where it was monitored using an application created in VBA (Microsoft® Visual Basic). The application was also designed to enable control of the foam flow rate in the loop and air supplied to a pneumatic regulator in the foam drainage measuring section. Prior to recording any data, care was taken to calibrate the system to ensure signals transmitted from sensors to the application were accurate and displayed in proper units. The system pressure was monitored using pressure gauges installed on foam generation and foam stability measuring sections.

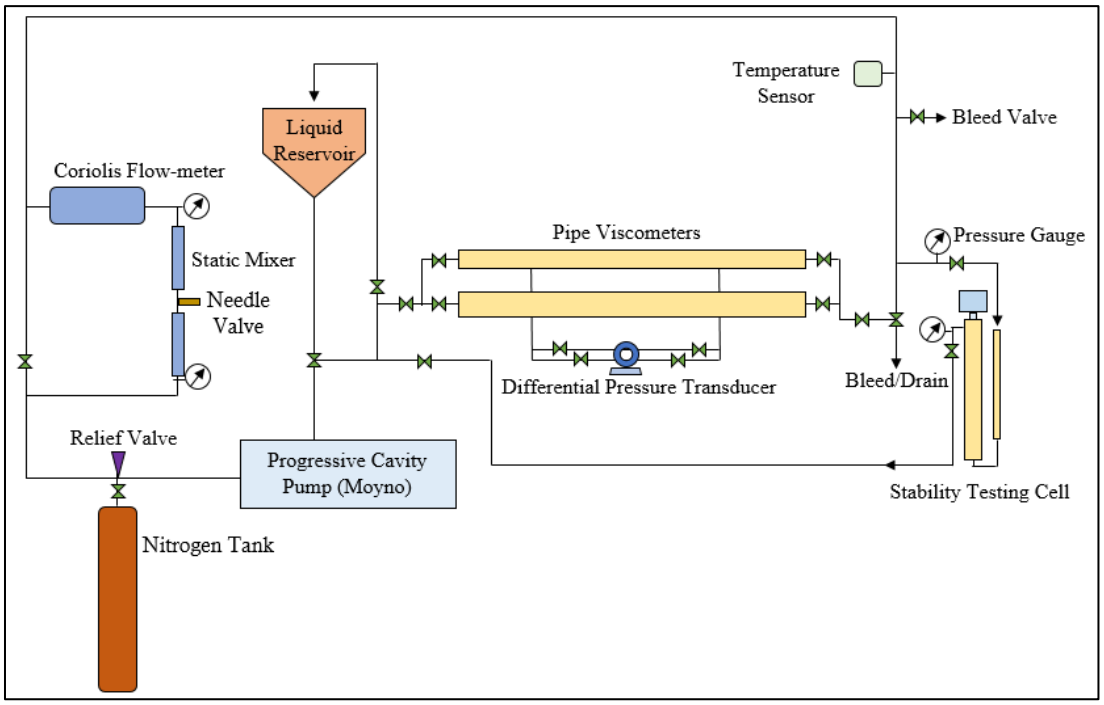

Figure 5. 2: Schematic of flow loop used for experimental study

The liquid reservoir, shown in Fig. 5.3, was used to mix the liquid phase with surfactant solution and supply it to the progressive cavity pump. Return line to the reservoir enabled flow in re-circulation mode and could be disconnected using a valve to switch to a single pass mode. A progressive cavity pump (Fig. 5.4) with a variable speed controller circulated test fluid at the desired flow rate. The pump has a maximum capacity of 113.56 L/min (30 gpm). The gas phase (nitrogen) was injected to the discharge of the pump until system pressure increased to 620.53 KPa (90 psi). The gas injection was regulated using a valve to control the amount of gas entering into the system. Foam generating section consisted of static mixers, needle valve, relief valve, and bypass valve. Needle valve together with two static mixers, shown in Fig. 5.5, generated the foam by maintaining a differential pressure of 206.84 KPa (30 psi) across the foam generation section. The differential pressure provided the necessary shear and mechanical energy to gas-liquid solution for foam generation. Static mixers installed upstream and downstream of the valve provided additional agitation and energy by forcing liquid to flow through a tortuous spiral path. For safety reasons, a relief valve was installed and set to open when pressure exceeded 1103.16 KPa (160 psi). To avoid foam generation during base-liquid circulation, a bypass valve was installed to skip foam generating section. The rheology of foam at different qualities was measured using two 4-meter long pipe viscometers (Pipe #1 and #2) which are shown in Fig. 5.6. The specifications of these pipe viscometers are given in Table 5.1.

Figure 5. 3: Reservoir used to mix liquid phase with surfactant solution

Figure 5. 4: Progressive cavity Moyno pump used to circulate fluids

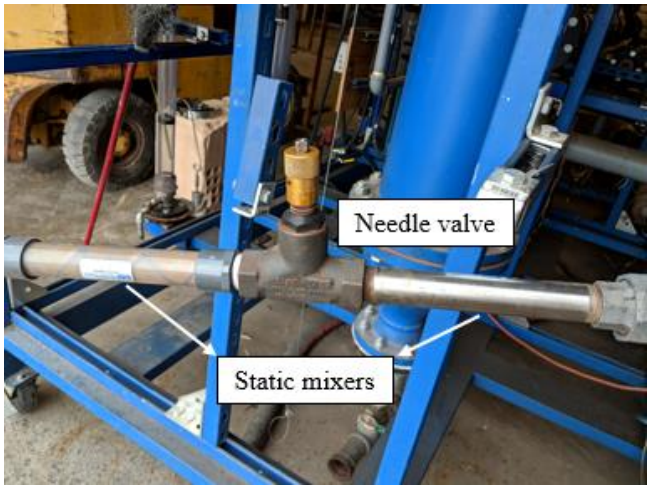

Figure 5. 5: Needle valve and static mixers used to generate foam

Figure 5. 6: Pipe viscometers used to characterize foam rheology

Table 5. 1: Specifications of pipe viscometers

Pipe Nomenclature	Outer diameter, m	Inner diameter, m	Differential length, m
Pipe #1	0.033	0.024	0.051
Pipe #2	0.038	0.032	0.076

The foam drainage section (Fig. 5.7) mainly consists of graduated transparent pipe and non-transparent annulus connected in series. Test foam was circulated and trapped in the drainage section to degrade over time. Visual port installed at the inlet of pipe section enabled capturing still images of static foam using a microscopic camera. The pipe has an inner diameter of 0.025 m (0.985 in.) and is made of clear polyvinyl chloride so that foam could be visually observed (Fig. 5.8). A measuring tape was carefully attached on the pipe wall to measure the drained liquid in the pipe. The outer pipe of the annulus is made of stainless steel which has an inner diameter of 0.076 m (3 in.). The inner cylinder of the annulus is PTFE (polytetrafluoroethylene) rod that has a diameter of 0.051 m (2 in.). The length of the pipe section is 1.08 m (42.46 in.). The annulus is 1.22 m (48 in.) long. The specifications of pipe and annular sections are given in Table 5.2.

Eight differential and two absolute pressure transducers are installed on the annular section. The differential pressure transducers are kept apart at an equidistance of 152 mm (6 inches). One of the absolute pressure transducers was used to measure air pressure coming from an electro-

pneumatic regulator to the low side of the differential pressure transducers. The other one was installed at the top of the annular section to measure foam column pressure. The electro-pneumatic regulator supplied air to the low-side of all eight differential pressure transducers such that the two absolute pressure transducers read approximately the same and the topmost transducer reads zero differential pressure. The measurements made by the transducers were then used to determine the density of foam trapped in the annulus between two consecutive differential pressure transducers.

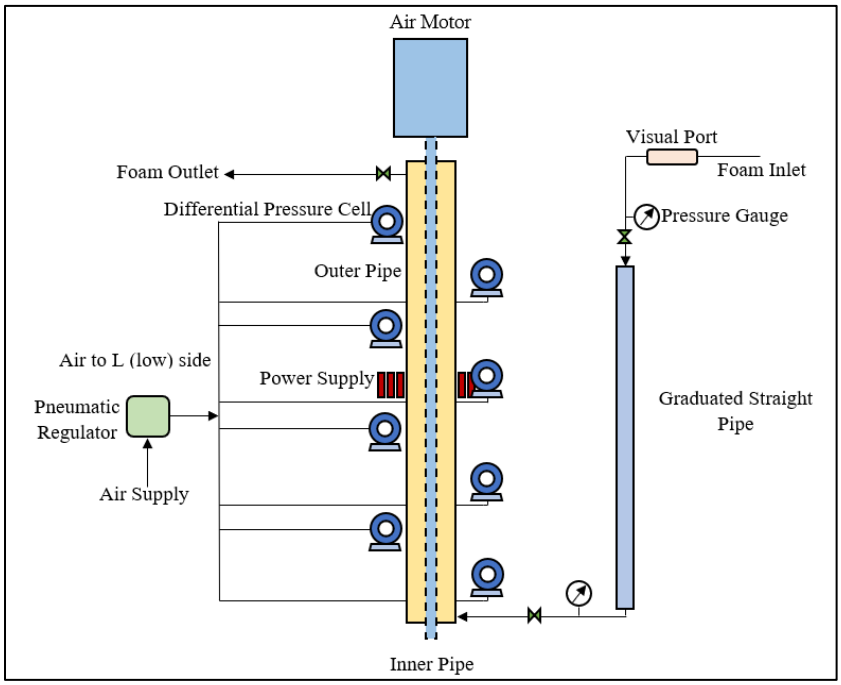

Figure 5. 7: Schematic of foam stability cell

Figure 5. 8: Clear straight pipe with tape measure attached and stainless steel outer pipe of annulus

Table 5. 2: Specifications of pipe and annulus

Test section	Length, m	Inner diameter, mm	Outer diameter, mm
Pipe	1.08	25	33
Annulus	1.22	50	75

5.3 Test Materials

Nitrogen was used as the gas phase for all three types of foam due to its non-flammability, inert nature, and common usage in field operations. Water used to prepare aqueous and polymer foams was tap water. Aqueous foam was generated using 2% (v/v) anionic surfactant (AQF-2, also commonly known in the industry as Howco-suds). Powdered form of hydroxyethyl cellulose (HEC) polymer (0.2% (w/w), anionic surfactant (1% v/v) and biocide (0.025% v/v) were used to prepare the liquid phase of polymer-based foam.

The liquid phase of oil-based foam was prepared by mixing diesel, industry grade light mineral oil (Penreco® Drakeol® LT), and fluorosurfactant (organofluorine surfactants). They were blended together in the volumetric ratio of 88:10:02. Fluorosurfactant was chosen specifically due to its superior foaming properties as compared to other hydrocarbon surfactants. The density of the mixture was 8.3 g/ml when measured using a pycnometer. Density and viscosity values of water were taken from standard tables and were 1 g/ml and 0.001 Pa-s, respectively. The density of polymer gel was the same as water at standard conditions. The rheological properties of base liquids of polymer-based and oil-based foams were measured using rotational viscometer (Fann Model 35). Densities and rheological parameters of all base liquids are shown in Table 5.2.

Table 5. 3: Density and rheology of base liquid phases

Fluid	Density, g/ml	Rheological Model	Viscosity/Rheological Parameters
Water	1.00*	Newtonian	0.001 Pa-s*
0.2% HEC polymer	1.00	Powel law	n = 0.77; K = 0.02 Pa-s^n
Oil	0.83	Newtonian	0.0045 Pa-s

* from standard density and viscosity tables.

Assuming the mass of gas to be negligible, foam quality is determined from density measurement obtained from the Coriolis mass flow meter using Eq. 5.1.

$$Quality\ (\%) = 1 - \frac{foam\ density}{liquid\ phase\ density} \tag{5.1}$$

The foam quality is also back-calculated by measuring the actual liquid volume collected in pipe and annulus after drainage experiment using Eq. 5.2.

$$Quality\ (\%) = 1 - \frac{liquid\ volume}{foam\ volume} \tag{5.2}$$

Within the shear rate range of 30 to 700 s^{-1}, the power law model best fit the rheology data obtained from pipe viscometers. Power law parameters (K and n) presented in Fig. 5.9 are obtained by curve fitting. For aqueous foams, at qualities ranging from 40-45%, it was not possible to determine rheology parameters, as the differential pressure values were too low to provide accurate information. Low-quality aqueous and polymer-based foams showed n values of slightly greater than 1. This could be attributed to the pressure variation and slight expansion of foam in the flow loop as it was circulated. The degree of expansion is proportional to the level of shear stress experienced by foam. As a result, the discrepancy of measured wall shear stress increases with shear rate causing the n values to become slightly greater than 1. The rheology data presented for oil-based foams (34, 41, 50, 61, and, 68%) is from the available database for similar foam (Sherif 2015). Increasing quality resulted in an increase in non-Newtonian behavior for all foams as observed by the decrease in flow behavior index (n) while fluid consistency index increased indicating an increase in apparent viscosity.

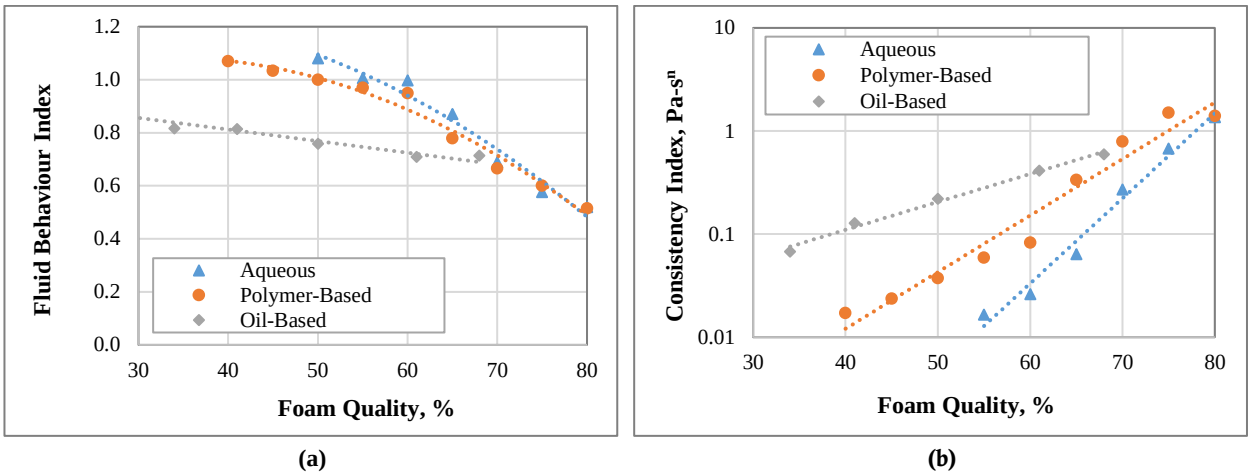

(a) **(b)**

Figure 5. 9: Power-law parameters of test foams: a) fluid behavior index; and, b) fluid consistency index

5.4 Test Procedure

This study includes testing foam stability under static and dynamic conditions. To perform the experiments, the base liquid was first prepared by adding water, polymer suspension or oil mixture, surfactant solution, and other additives at appropriate ratios to the reservoir and circulating the mixture through the flow loop at low flow rates (18.93 L/min) while agitating the mixture in the reservoir to ensure homogeneous mixing. Then, the flow rate was increased to 37.85 L/min (10 gpm) and foam was generated by injecting nitrogen gas into the discharge side of the pump while draining some liquid from the flow loop to increase foam quality. Injection of gas was stopped when the desired foam quality was established in the loop and pressure gauges on the foam generating section read 620.53 KPa (90 psi). The needle valve was then manipulated such that pressure gauge on the high side reads 827.37 KPa (120 psi). Fluid circulation was maintained at 37.85 L/min (10 gpm) for 30 mins to create stable foam. If the pressure in the foam generation section exceeds 965.27 KPa (140 psi), the relief valve would open and eject the foam for safety purposes. Density measurements gathered by the Coriolis mass flowmeter were used to determine

the qualities of test foams. The desired quality foam was prepared by controlling gas injection and liquid drainage from the flow loop.

5.5 Measuring System Calibration

Prior to gathering experimental data from the foam stability cell, the differential pressure transducers were calibrated. Then, the stability cell was aligned at the desired inclination (either 0 or 30 from the vertical) and isolated from the rest of the flow loop. The air supply to the low-side of the transducers was shut off and the system was opened to the atmosphere, allowing any foam, liquid, or gas remaining inside to drain completely. The readings of the pressure transducers were then monitored to ensure they displayed approximately 0 KPa (0 psi), and if they diverged, they were set to zero. After zero calibration, the stability cell was shut off from the atmosphere, re-integrated to the flow loop and air was re-supplied to the low-side of the transducers. The prepared stable foam was then circulated and trapped in the measuring section consisting of pipe and annulus by simultaneously closing the valves and shutting down the pump. On the annular section, air was supplied on the low-side of the differential pressure transducers. Prior to testing foams, pressure measurements obtained from annulus were validated by conducting preliminary testing with base liquid.

The hydrostatic pressure distribution in the base liquid of oil-based foams is shown in Fig. 5.10 (a). A linear distribution was obtained with a density gradient of 0.79 g/ml, which is very close to density measurements made by a pycnometer (0.83 g/ml). Hydrostatic pressure readings obtained for aqueous foam at 55% quality trapped in the annulus at various times are shown in Fig. 5.10 (b). Initially, when the test began (T = 0 min in Fig. 5.3), the annulus was occupied by freshly generated homogenous foam, resulting in a linear distribution of measured pressure

readings. As liquid drained with time and foam became heterogeneous, the linear profile vanished and non-linear pressure distribution across foam column was established.

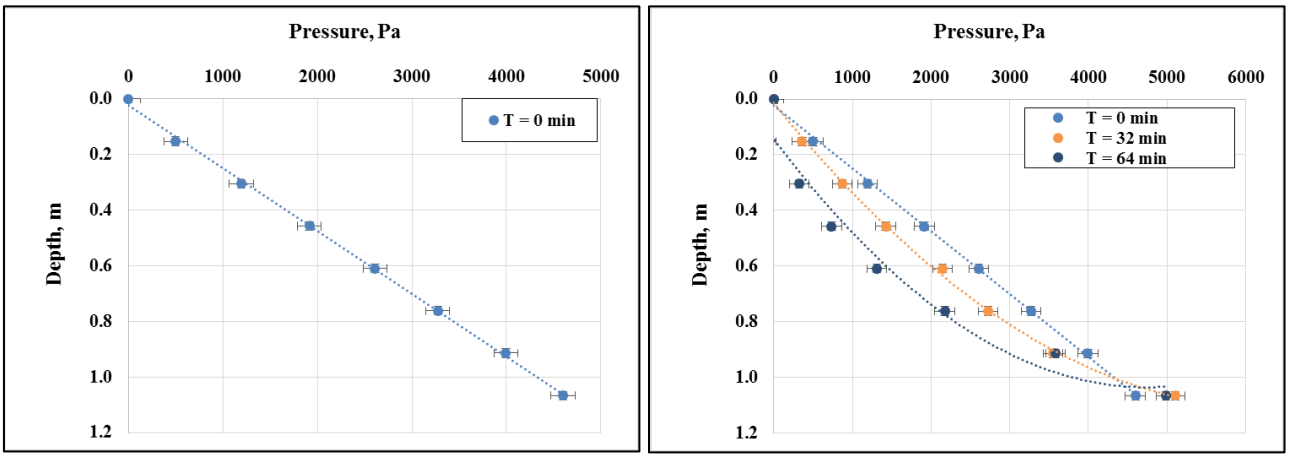

(a) **(b)**

Figure 5. 10: Hydrostatic pressure readings with depth for: a) base liquid for oil-based foam; and, b) 55% aqueous foam

Foam density profile in the annular section is determined using the pressure difference between measurements obtained from two consecutive differential pressure transducers (Eq. 5.3).

$$\overline{\rho_f} = \frac{\Delta p_m}{gh} \tag{5.3}$$

where is $\bar{\rho}_f$ the average density of foam within a fixed height of foam column; Δp_m is the differential pressure measurement between two consecutive transducers; g is the acceleration due to gravity; and h is the height of foam column between two consecutive differential pressure transducers (0.152 m or 6 in.). Similar average foam density determinations are made by a computer program for the seven 152 mm segments of the annular section (Fig. 5.11) at various times. Density curves are then prepared for each segment as a function of time for the foams allowed to drain in the annulus. The density curve of 50% quality aqueous foam is shown in Fig. 5.12.

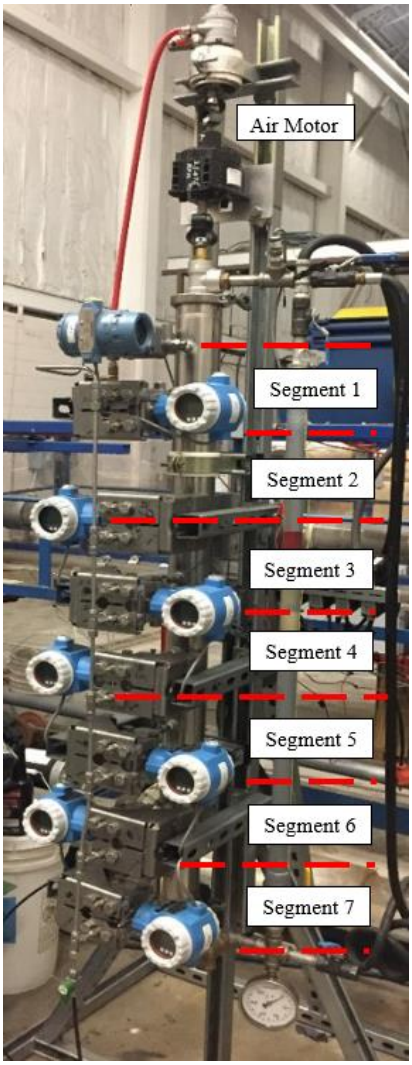

Figure 5. 11: Annular section of foam stability testing cell

Foam density across all segments was initially uniform due to the homogeneity of foam. This value was measured and used to determine initial foam quality. From the density data, the drainage is obtained as a function of time for each quality foam trapped in the annulus. This is accomplished by generating a data point each time density value approached to that of the liquid phase and indicated the level of accumulating drained liquid in the annulus at the corresponding time. The process of generating drainage curves for foams trapped in straight pipe section is much simpler by contrast. Drained liquid volume was measured by recording height of liquid level at the bottom of the pipe using a measuring tape and stopwatch. A flashlight was used to enhance the

visibility of foam-liquid interface which is characterized by the absence of bubbles in the liquid. The test was deemed to have concluded when density profiles obtained from annulus flattened out and there was no increase in liquid level in the pipe.

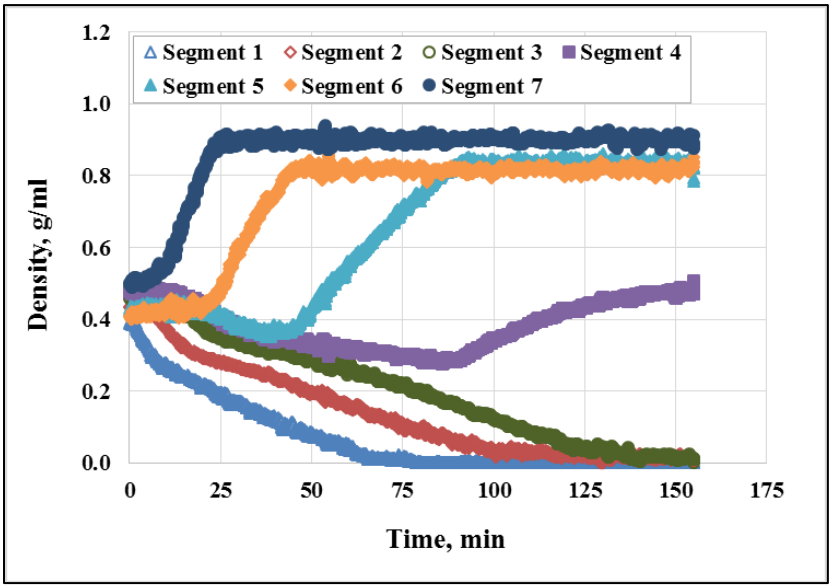

Figure 5. 12: Density curves of 50% quality aqueous foam

The test procedure detailed so far was used to obtain drainage curves of foams trapped in vertical annulus and pipe as well. When tests conducted in inclined configuration, compass feature of smartphone (maximum error of 1°) and level balance were used to measure the angle of inclination. Prior to gathering any test data, the differential pressure cells were recalibrated after inclining the stability testing cell.

Finally, experiments were conducted by rotating the inner pipe in the annular section to measure foam stability under dynamic condition. For these experiments, the foam trapped in the annular section was allowed to rest for one minute before turning on the air motor, shown in Fig. 5.13, to rotate the inner pipe at approximately 0.42 and 0.73 radian/s (4 and 7 rpm). These values were chosen as they represent the minimum rotational speed required to rotate the inner pipe, and the maximum rotational speed achieved when the air-supply valve of the motor was completely

open. The shear exerted on foam column of various foams is presented in Table 5.4.These experiments were conducted at intervals of 10% quality, starting with 40%. Dynamic foam stability experiments were limited to the annular section. Drainage curves of foams subject to rotating inner pipe in annulus were produced.

Figure 5. 13: Air motor used to rotate PTFE inner pipe of annulus

Table 5. 4: Shear rate range exerted on foam column

Foam type	Shear rate, s^{-1}
Aqueous	1.5 – 1.8
Polymer	1.5 – 1.8
Oil	1.6 – 1.7

5.6 Bubble Size Measurements

The foam flow loop also consisted of a horizontal visual port (Fig. 5.14), where foam could be seen flowing or static. A microscopic camera was used to capture images of stationary foam at this port. These images were captured periodically for aqueous and polymer foams from the moment the foam was trapped (designated by time, t = 0). A total of nine images were taken for each quality of foam at times, t = 0, 2, 4, 8, 16, 32, 64, 128, and 256 minutes. From these images, the coarsening/coalescence of bubbles in foam structure with time could be clearly seen. A thin wire

of 160 μm, carefully taped across the visual port was used as a frame of reference to scale the captured images. Specifically, this scale was used to approximately measure the diameters of bubbles captured in images using scientific image analysis software (Image J).

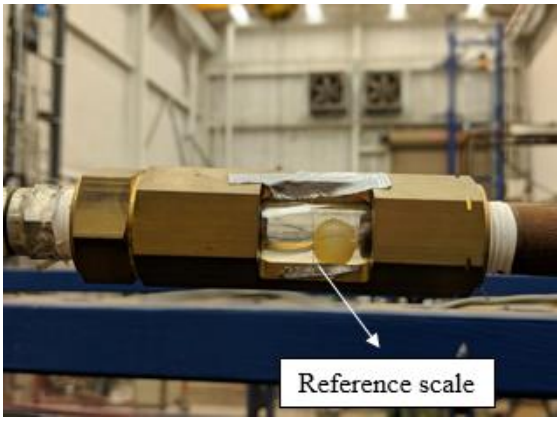

Figure 5. 14: Horizontal visual port with a reference scale of 0.16 mm thickness

5.7 Reproducibility of Measurements and Error Analysis

It is important to be able to reproduce the drainage curves generated from measured data. To ensure this, a few tests were repeated by entrapment of foam in pipe and annulus as shown in Fig. 5.15.

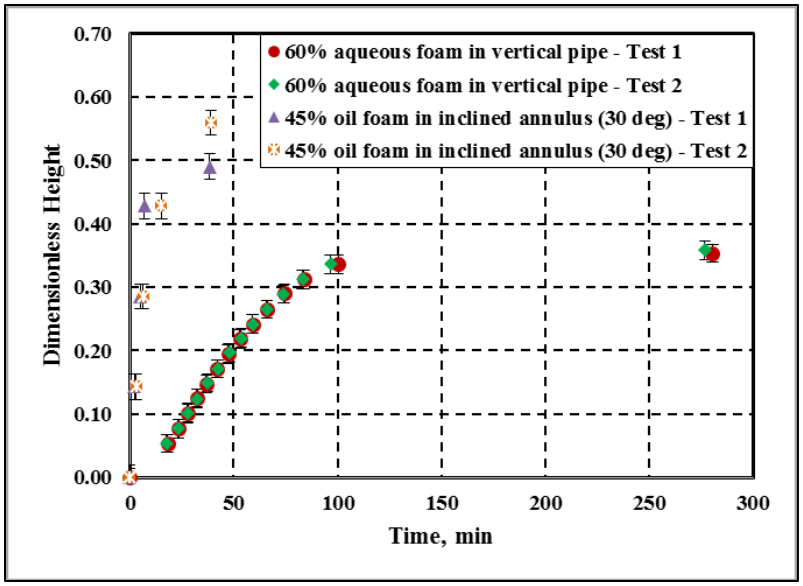

Figure 5. 15: Reproducibility of experimental data

On comparing the drainage curves obtained in above figure, it can be concluded that the experimental results presented here can be reasonably reproduced. Furthermore, error analysis was undertaken to estimate the uncertainty in measurements with 95% confidence. Fixed or bias errors in measurements are unavoidable due to limitations of equipment used (pressure transducers, flow meter, measuring tape, level balance, compass, tachometer). Some random or precision errors that may have influenced measurements were due to visual inspection of foam column, misrepresentation of very small bubbles in images captured, and in estimations of volumetric average bubble diameter.

CHAPTER 6

RESULTS AND DISCUSSION

The results obtained from various experiments that were detailed in the previous chapter are presented here. These include results from foam drainage experiments performed with foams prepared using three base liquids. Drainage experiments were primarily performed in vertical pipe and annular test cell where foam was first circulated and trapped to measure its drainage volume as a function of time. These experiments enabled the comparison of various drainage curves generated using measurements obtained from the stability cell. The curves are a good indicator of foam stability. Particularly, the influences of geometry, foam quality, and inclination on the drainage were examined under static conditions.

Varying geometry from pipe to annulus changes the way container walls affect the upward motion of gas bubbles in the liquid and downward flow of liquid through the foam network. Quality determines the density of the foam as well as its basic bubble structure and consequently its rheology. The effect of inclination is more complex. In inclined conduits, liquid has to travel very short distance vertically to reach the low-side of the conduit wall. Once the liquid reaches the low-side of an inclined pipe or annulus wall, it forms a fluid layer that flows down to the bottom without facing the hydraulic resistance of complex bubble structure which hinders the drainage process.

In addition to the static foam drainage tests, dynamic tests were performed by subjecting the foam trapped in the annulus to shear by rotating the inner cylindrical rod. Therefore, these tests were limited to the annulus. The inner rod was rotated by an air motor at two different rotational speeds that were selected based on system limitations. Intuitively, one can expect

inducing turbulence within the conduit due to the rotation of the inner cylinder could result in re-generation of foam and extend the drainage time. However, if the rotation happens at low speed without inducing turbulence, then the shearing may induce degradation of foam structure that would facilitate drainage of foam.

Drainage curve analysis of various foams enabled one to understand the half-life of foam under various conditions. This is an important parameter and should be considered when designing any oilfield jobs with foam. However, the complete decay of foam is dependent on the rate of bubble coarsening and collapse. Photographic images and videos of static foam in a horizontal viewport taken using a microscopic camera enabled analyzing the bubble size distribution at various qualities and times. The effect of quality, time, and base liquid composition on the drainage rate and how these factors affect foam structure and result in total foam collapse can be studied through changes in bubble size distribution.

6.1 Foam Drainage

As discussed in previous chapters, drainage always precedes total foam collapse due to the combined effects of drainage and decay. Therefore, a high rate of drainage is followed by a quick collapse of foam structure and vice versa. Hence, the rate of drainage is a good indication of stability when comparing different foams.

6.1.1 Aqueous Foam

The drainage curves of aqueous foams in the vertical pipe and annular sections are shown in Fig. 6.1. Three distinct drainage regimes can be observed from each curve, which can be termed as: (i) early drainage, (ii) intermediate drainage, and (iii) late drainage. In each of this regime, the slope of the curve indicates the rate of liquid drainage. The first regime is characterized by an

initial delay or very slow drainage of liquid from the foam column followed by a rapid increase in the drainage rate. In the intermediate regime, the rate of drainage is more or less constant leading to an almost linear relationship between liquid column height and time. Most of the liquid phase drains during the first two regimes. Therefore, the rate of drainage gradually decreases and approaches zero asymptotically in the late drainage regime. The drainage curves produced, and the three regimes identified are consistent with previously published literature on drainage behavior of standing foams in cylindrical conduits under atmospheric conditions (Miles et al. 1945; Jacobi et al. 1956; Bhakta and Ruckenstein 1995; Argillier et al. 1998; Hilgenfeldt et al. 2001; Saint-Jalmes and Langevin 2002).

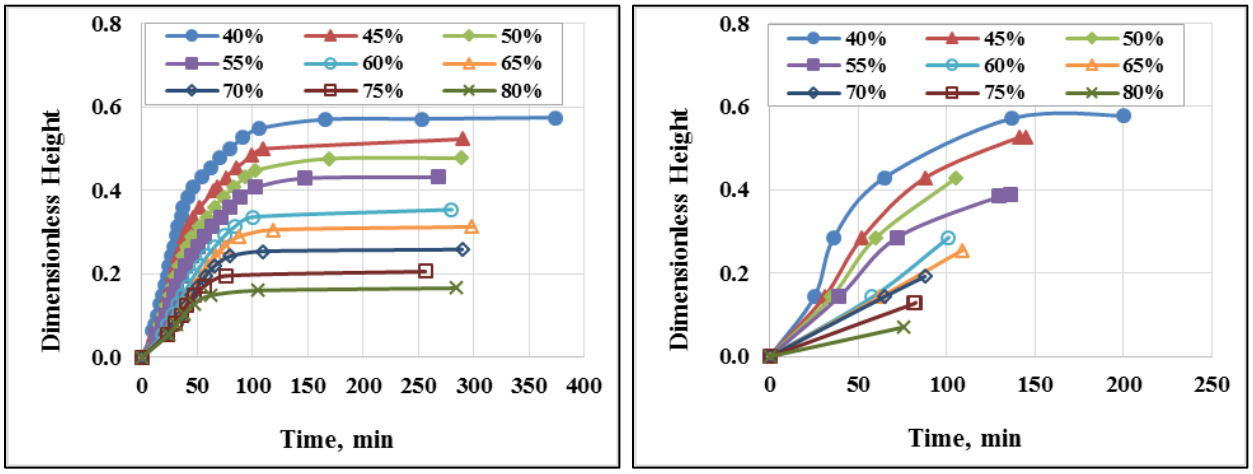

(a) **(b)**

Figure 6. 1: Drainage curves of aqueous foam in vertical – (a) pipe and (b) annulus

Furthermore, for both vertical pipe and annulus, it can be observed from the drainage curves that the drainage rate decreases with increasing foam quality. This indicates that less liquid is collected at the bottom of the foam column within a given period of time as the quality is increased. Higher quality foams have a lower liquid volume fraction. This means that for given foam volume, less liquid is available to drain as the quality is increased. In addition, the hydraulic resistance of foam structure increases with quality due to the reduction in film thickness or decline in the permeability of foam structure. The liquid drainage in foam occurs across liquid films, which

separate the trapped gas bubbles. As quality increases these liquid films thin hindering drainage due to reduced flow area. In addition, factors impeding flow such as viscous properties of base liquid, capillary forces, electrical forces, dispersion, steric forces, disjoining pressure, and other interfacial effects are very significant in thin films (Derjaguin et al. 1941; Verwey and Overbeek 1948; Schramm and Wassmuth 1994; Barigou et al. 2001; Saint-Jalmes et al. 2004; Saint-Jalmes 2006; Karakashev 2017). The dependence of drainage curve on foam quality observed in present work with aqueous foams is consistent with measurements reported in previously published literature (Hilgenfeldt et al. 2001; Saint-Jalmes and Langevin 2002).

At low qualities (40-55%), the drainage curves obtained from the vertical pipe and annulus are very similar. The half-lives of 40% and 55% foams are a good indication of this. For 40% foam, this value is approximately 31 minutes in the pipe and 37 minutes in the annulus. Approximate values of half-lives for 55% foam was 40 minutes in the pipe and 60 minutes in the annulus. With increasing quality the discrepancy between drainage curves obtained from pipe versus annulus increases. At 80% quality, it takes less than 30 minutes for the drained liquid to fill 8% of initial foam height in the vertical pipe, while that value is approximately 76 minutes in the annulus. This difference between drainage curves obtained from pipe versus annulus can be explained by wall effects on bubble motion and liquid movement. In the annulus, the foam is in contact with a larger container area as compared to the pipe: the inner surface area of the outer pipe and surface area of the inner rod. Therefore, the hindrance effects of container walls on the motion of bubbles and drainage of liquid are more significant in the annulus as compared to the pipe, resulting in reduced liquid drainage in the annulus.

Results obtained by inclining the test sections up to 30^{o} (measured from vertical) are shown in Fig. 6.2. The drainage behavior observed in inclined conduits is very similar to that observed in

vertical pipe and annulus. The three regimes with varying drainage rates were observed in inclined conduits as well. The rate of drainage slows down with increasing quality, as was also observed for vertical pipe and annulus. For the same quality, as observed earlier in vertical sections, the drainage rate is slower in annulus compared to the pipe. However, for the same quality, the rate of drainage is much faster in inclined pipe and annulus as compared to vertical ones.

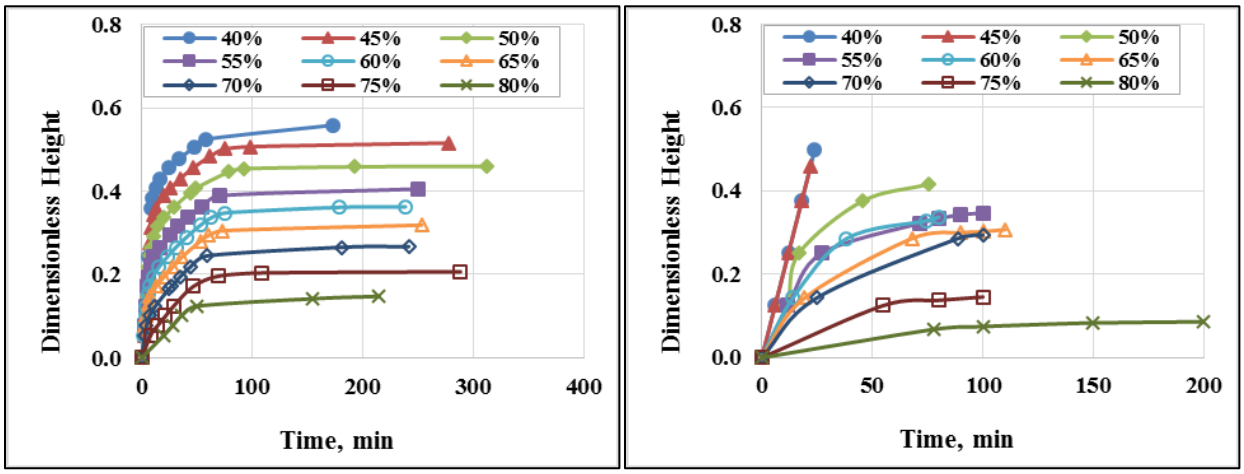

(a) **(b)**

Figure 6. 2: Drainage curves of aqueous foam in inclined - (a) pipe and (b) annulus

In the inclined conduit, the liquid does not drain purely axially. Instead, it drains vertically downward and it has to travel a very short distance to reach the conduit wall, where it starts to flow along the wall and collects at the lower end of the test section. In case of vertical pipe and annulus, the drained liquid is forced to travel downward axially through the bubble structure flowing in thin films between bubbles until it reaches the lower end of the pipe and annular section where it accumulates. In this case, the travel distance is the distance between the top of the conduit to the top of drained liquid collected at the bottom of the conduit. For inclined sections, this distance can be very short depending on the radius (or hydraulic radius) of the conduit as the drained liquid travels both in vertical and lateral directions reaching the conduit wall in a short time and flowing down to the bottom of the conduit like a layer of liquid. Therefore, in inclined sections, draining

liquid experiences substantially reduced flow resistance from the bubble structure. Half-lives of 40, 55, and 70% foam in pipe and annulus when vertical and when inclined at 30° from vertical are shown in a bar graph below (Fig. 6.3).

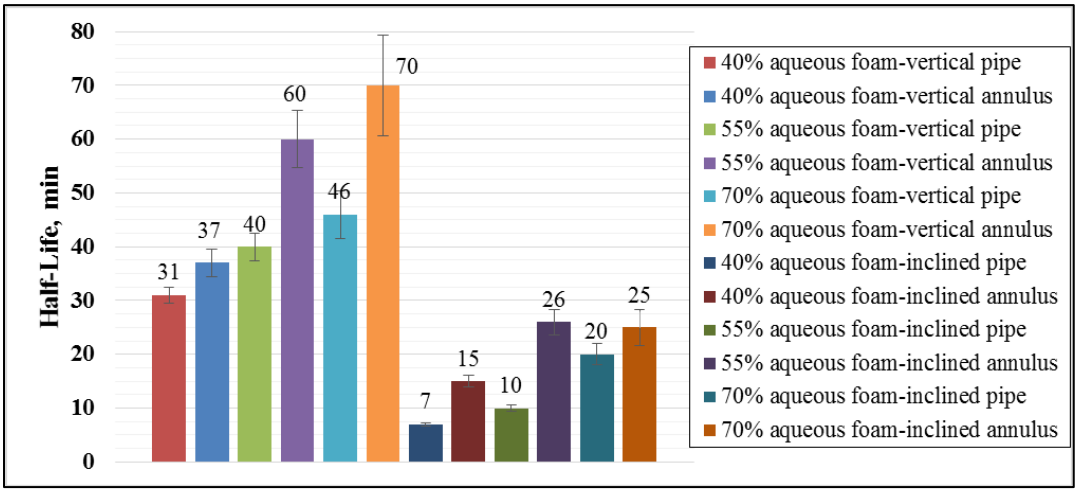

Figure 6. 3: Half-lives of aqueous foams in vertical and inclined tubing

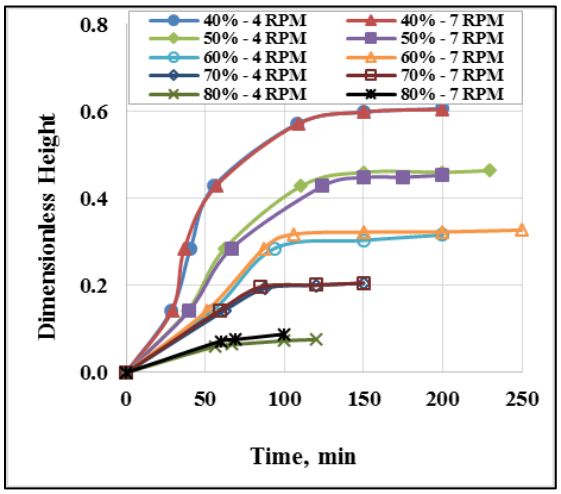

Figure 6. 4: Drainage curves of aqueous foam in a vertical annulus with a rotating inner rod

The drainage curves of aqueous foam trapped in the annulus while rotating the inner rod at 4 and 7 rpm are shown in Fig. 6.4. These set of experiments were performed to examine the effect of shearing on the drainage of foam. Intuitively, it was expected that the shear exerted on trapped foam to either break down the foam structure, resulting in enhanced drainage, or supply turbulent

energy to regenerate the drained foam. However, these experiments were limited by the capacity of the air motor used to rotate the inner rod. On comparing drainage curves in Figs. 6.4 and 6.1b, it can be seen the shear rate applied to the foam column was not sufficient to produce any measurable difference on drainage curves at various qualities.

6.1.2 Polymer Foam

The drainage curves of polymer-based foams obtained from vertical pipe and annulus are shown in Fig. 6.5. Similar curves obtained in inclined configuration (30^o from vertical) are shown in Fig. 6.6. Figure 6.7 shows the drainage curves obtained from annulus while rotating the inner rod at two different speeds. These curves (Figs. 6.5 - 6.7) show the drainage behavior of polymer foams which follow patterns similar to those observed with aqueous foams in Figs. 6.1-6.4. However, comparing Fig. 6.1 and 6.5, it can be seen that although the three drainage regimes established with aqueous foam exist in case of polymer foam as well, they are less distinct. Similarly, it is difficult to distinguish between these regimes in Fig. 6.6, as liquid drained at a higher rate in inclined sections as compared to the vertical ones. From these figures, it can be clearly observed that polymer foams display better stability than aqueous foam at all qualities.

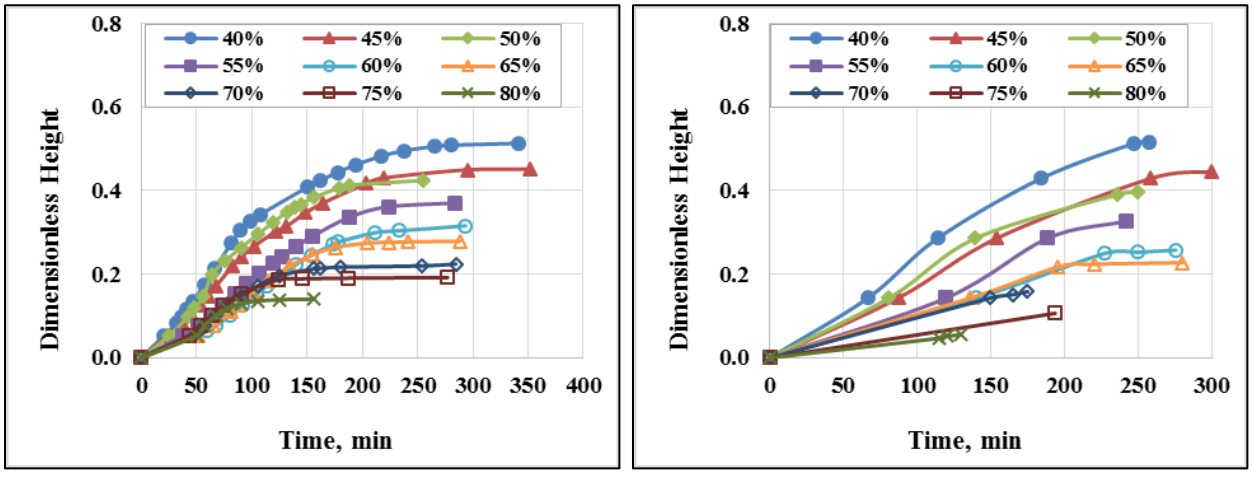

Figure 6. 5: Drainage curves of polymer foam in vertical - (a) pipe and (b) annulus

The half-life of 40% aqueous foam in the vertical pipe was approximately 31 minutes while that of the polymer foam was 90 minutes (Figs. 6.1 and 6.4a). Similarly, in the annulus, the half-life of 45% aqueous foam was approximately 53 minutes while that of the polymer foam was more than 154 minutes. The enhanced stability of polymer foam is expected because the base fluid used to prepare polymer foam was more viscous than water. As this fluid drains down through the foam structure, it experiences much higher viscous resistance than water.

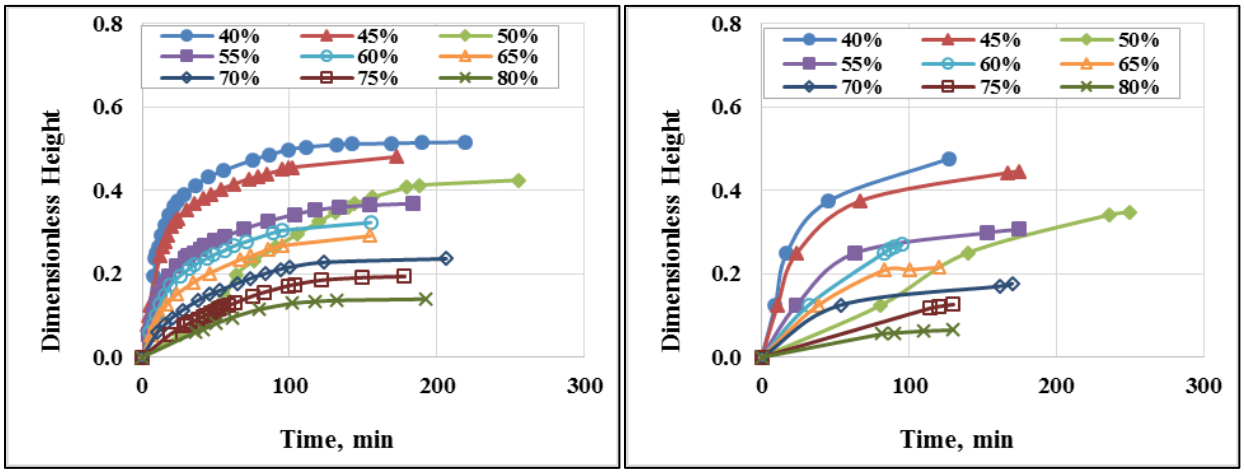

(a) (b)

Figure 6. 6: Drainage curves of polymer foam in inclined - (a) pipe and (b) annulus

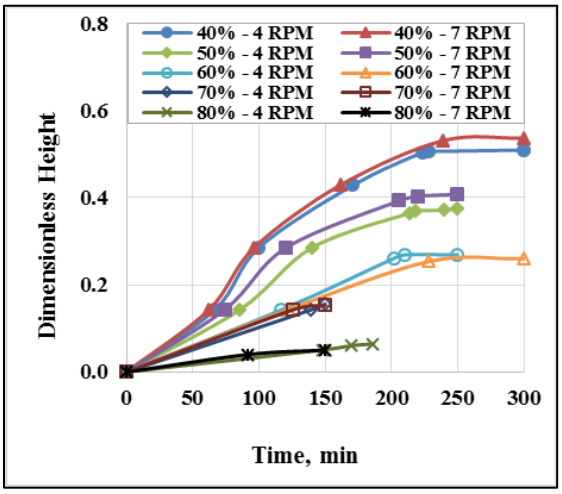

Figure 6. 7: Drainage curves of polymer foam in a vertical annulus with a rotating inner pipe

The drainage curves of polymer-based foam obtained from the annulus under dynamic conditions (rotating inner pipe at two different speeds) exhibit no noticeable difference when compared with those obtained from under static conditions (comparing Fig. 6.7 and 6.5b). Any appreciable difference might be observed if a higher shear rate is applied to the foams.

6.1.3 Oil-based foam

A mixture of mineral oil and diesel was used to prepare oil-based foam. The addition of light mineral oil enhanced the viscosity of base oil (0.0046 Pa-s). However, comparing Fig. 6.8, which shows drainage curves obtained with oil-based foam in pipe and annulus to Fig. 6.1, it can be seen that oil-based foam drained much quicker than aqueous foam. The half-life of 40% oil-based foam in a vertical pipe was approximately 26 minutes. When this half-life is compared with those of aqueous (31 minutes) and polymer (90 minutes) foams, it can be seen that oil-based foam clearly displayed the least stability. Regardless of conduit geometry and inclination angle, oil-based foam showed the lowest stability at all qualities when compared with aqueous and polymer foams (Fig. 6.9). The three drainage regimes described earlier are much more distinctly observed in the drainage curves of oil-based foams as compared to either aqueous or polymer foam. This shows that although base liquid viscosity is an important parameter that affects the stability of foam by slowing drainage rate, clearly, there are other factors which contribute to the rapid break down of oil-based foam structure.

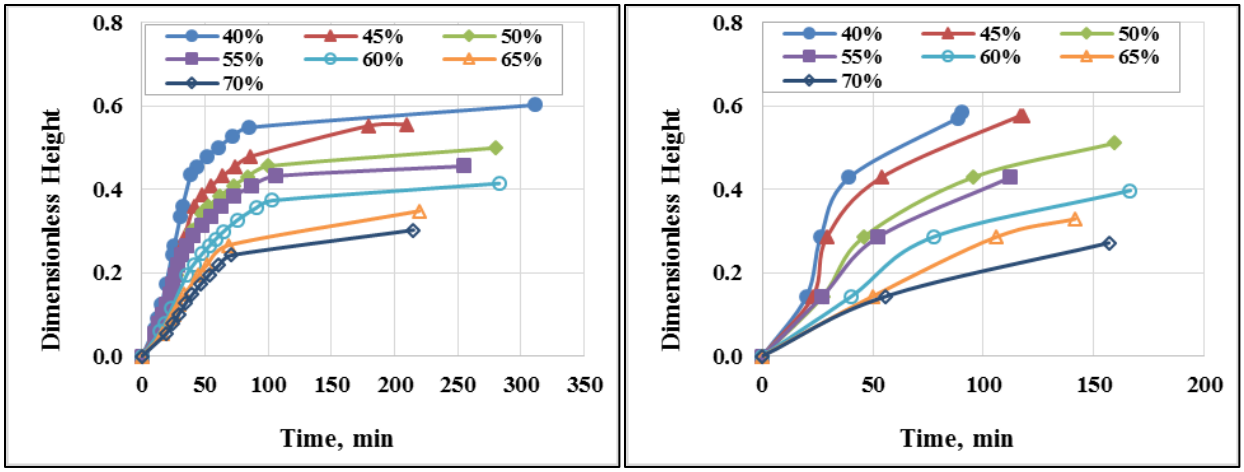

(a) **(b)**

Figure 6. 8: Drainage curves of oil-based foam in vertical - (a) pipe and (b) annulus

Mechanisms of foam decay such as bubble coalescence and collapse (Ostwald ripening) might have played a larger role in oil-based foam destabilization than in case of aqueous or polymer foams. Break down of bubble structure would result in much quicker drainage while rheology of the base liquid has a limited effect on decay mechanisms. As a result, oil-based foam quality was restricted to 70%. Above this quality, it was not possible to obtain meaningful measurements as the foam was highly unstable. Within the quality range of 40-70%, drainage curves of oil-based foams followed similar patterns that were established in aqueous and polymer foams. Drainage rate at each quality was higher in a pipe as compared to annulus for both vertical and inclined cases. When compared to aqueous and polymer-based foams, this difference in drainage rate is minimal, especially at low qualities (less than 45%).

Clearly, wall effects are least consequential in oil-based foams while they influenced polymer foams to the greatest degree. This can be explained by the highest stability exhibited by polymer foams as compared to aqueous or oil-based foams. By comparison, low-quality oil-based foams (40-45%) degraded very quickly masking the influence of container walls on liquid droplets or gas bubbles. As quality increased, wall effects played a larger role. For instance, 70% quality

oil-based foam in annulus drained approximately 20% of its liquid in 100 minutes whereas it took about 50 minutes in the pipe to drain the same percentage of liquid. At higher qualities, bubbles are coarser, increasing the Particle-to-Container Diameter Ratio (PCDR). Higher PCDRs are associated with greater wall effects on fluid motion (Clift et al. 1978). However, it is very difficult to calculate PCDR for annulus. Therefore, an exact comparison between pipe and annulus cannot be made.

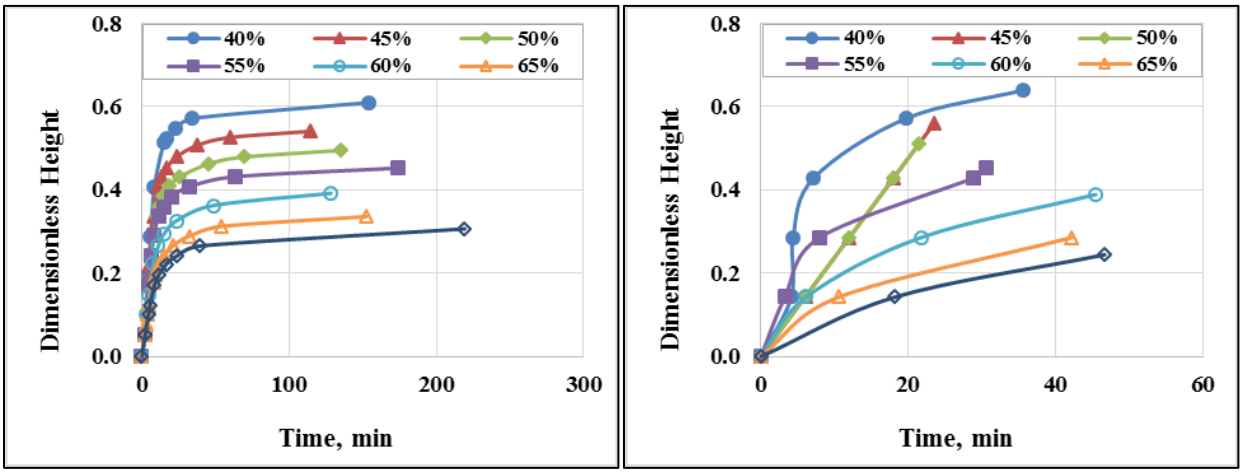

(a) **(b)**

Figure 6. 9: Drainage curves of oil-based foam in inclined - (a) pipe and (b) annulus

Similar to those of aqueous or polymer foams, the drainage of oil-based foams was higher in inclined section than in the vertical one regardless of foam quality and conduit geometry (Figs. 6.8 and 6.9). At low qualities (less than 50%), the drainage rate difference between pipe and annulus was the greatest. As compared to aqueous and polymer-based foams, for each quality and test section geometry, the difference in the rate of drainage between vertical and inclined cases was the highest for oil-based foam. This again can be explained by relatively poor stability of oil-based foam in particular and lower quality foams in general. For easy comparison of drainage behavior and, therefore, stability, half-lives of aqueous, polymer, and oil foams (40, 55, 70%

quality) are shown in Fig. 6.10. Superior stability is indicated by higher half-life in the bar graph below.

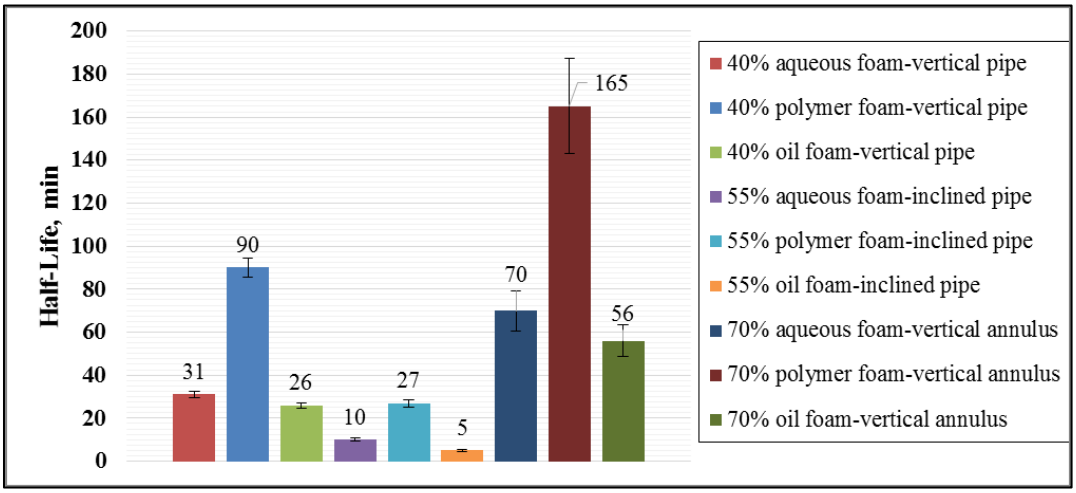

Figure 6. 10: Half-lives of aqueous, oil, and polymer foams in pipe and annulus

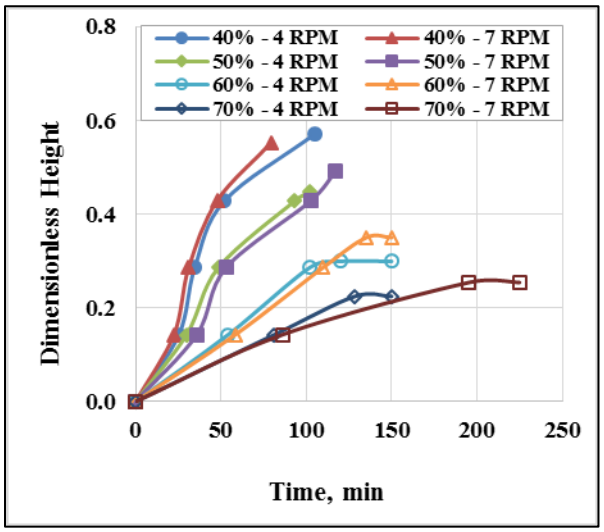

Figure 6. 11: Drainage curves of oil foam in a vertical annulus with a rotating inner cylinder

No appreciable difference could be observed for oil-based foam trapped in a vertical annulus with and without rotating inner pipe (Figs. 6.8b and 6.11). Higher rotational speeds may be required to observe the effect of shear on drainage behavior of oil-based foam.

6.2 Foam Decay

Drainage removes the liquid from the foam network while decay results in coarsening and coalescence of foam bubble structure, eventually resulting in the total collapse of the foam. The rates of coarsening and coalescence are indicative of the level of foam decay. A microscopic camera was used to capture images of aqueous and polymer foams. The first image was taken as soon as each foam was trapped in the viewport and was denoted as t = 0. Following this, eight more images were captured at various times (2, 4, 8, 16, 32, 64, 128, and 256 seconds) in a geometric progression. Eight consecutive images of aqueous and polymer-based foams (at different qualities) that were taken using a microscopic camera are shown in Figs. 6.12 and 6.13, respectively. A reference scale of 500 microns is provided for each set of images enabling clear visualization of bubble coarsening with time.

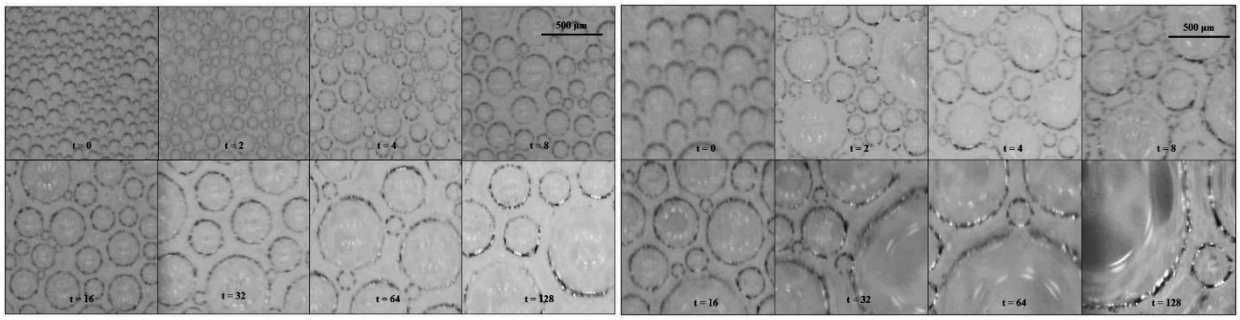

(a) **(b)**

Figure 6. 12: Bubble coarsening in aqueous foams - (a) 45% and (b) 75%

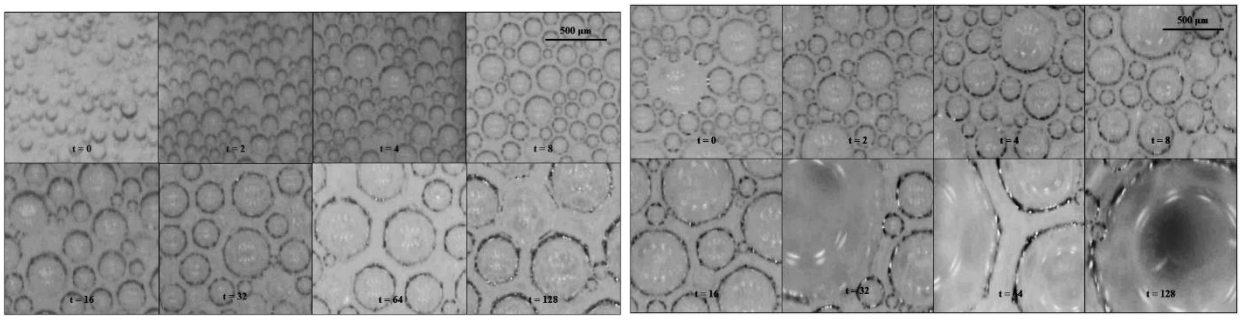

(a) **(b)**

Figure 6. 13: Bubble coarsening in polymer foams - (a) 45% and (b) 75%

Comparing aqueous and polymer foams for a given quality and aging time, aqueous foams had larger average bubble diameters. Although none of the images show perfectly spherical bubbles, for bubbles size analysis, spherical bubbles are assumed. The mean bubble diameters of aqueous and polymer foams were determined as a function of time using image processing software (Image J). Plots of mean bubble size with time for aqueous and polymer foams are shown in Fig. 6.14. These plots quantitatively show that the average bubble size increases with foam quality. This can be explained by considering the low-liquid-content of high-quality foams and a relatively large volume of gas trapped in a fixed volume pipe or annulus test section. Consequently, in high-quality foams, limited liquid is available to each gas bubble. For each quality and in both types of foams, the rate of increase in mean bubble size (coarsening rate) rose sharply in the beginning (within the first eight minutes) and reduced gradually with increasing time. The highest quality foams (80%) underwent the most change in mean bubble size. This can be seen in Fig. 6.14 as a sharp increase in slope within the first four minutes was observed with 80% quality foams.

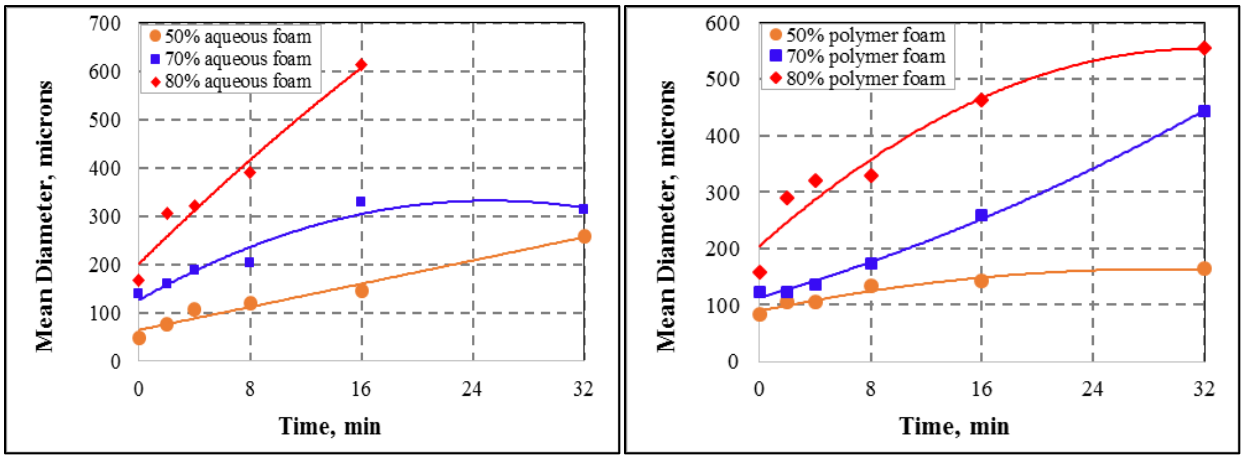

(a) **(b)**

Figure 6. 14: Mean bubble diameter with time - (a) aqueous and (b) polymer foams

Furthermore, the results shown in Fig. 6.14 might indicate that, at various qualities, the initial rate of foam decay represented by the rate of change in mean bubble size is high before

gradually stabilizing. The drainage curves presented in Section 6.1 demonstrated that the rate of drainage from foam is high initially before plateauing with increasing time. Therefore, foam destabilization processes of drainage and bubble coarsening follow similar rate patterns even though the mechanisms associated with each process are different. Hence, foam drainage information could be used to comparatively judge stability of different foams even if there is no information on bubble coarsening which is one of the mechanisms of foam degradation.

The initial high rate of bubble size increase can be explained using the two main mechanisms of foam decay: coarsening and coalescence. Due to the pressure difference between bubbles and the formation of foam structure with thin liquid films, coarsening and coalescence occur simultaneously once the foam is formed. This pressure difference exists across a curved surface due to interfacial tension. The pressure inside the bubble is higher than that of the outside. This differential pressure leads to mass transfer in lamellae, forcing liquid to be collected at Plateau borders and thinning the films. If film between bubbles thins to the point of rupturing, gas bubbles merge to form a larger bubble. When all the thin liquid films between gas bubbles have ruptured, it results in the formation of bulk liquid and gas separated by a single interface, i.e. a complete collapse of the foam. The driving force for these mechanisms is described using the Young-Laplace equation (Eq. 3.3). The equation shows that pressure differential increases with decreasing bubble size. Therefore, foams made of small bubbles coarsen at a much higher rate than the ones formed by large bubbles. This can be seen in Fig. 6.14 where for a given quality, polymer foam coarsens at a greater rate, initially as compared to aqueous foam.

The change in bubble size distribution due to foam decay is shown in Fig. 6.15 as a cumulative distribution. The number of fine bubbles significantly reduced for both aqueous and polymer-based foams as displayed by a large gap between distribution plots. As overall bubble

size increases initially, the driving force behind the decay mechanism of coalescence and coarsening decreases, resulting in a declining rate of bubble size increase as more time elapses.

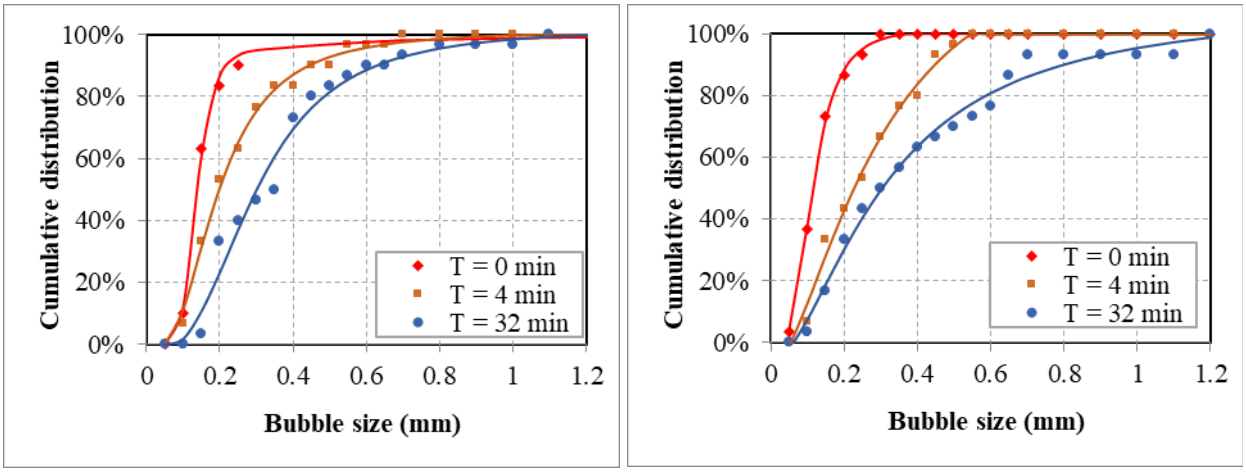

Figure 6. 15: Cumulative bubble size distribution at various elapsed times: (a) aqueous and (b) polymer foams (80% quality)

The average bubble sizes of aqueous and polymer foams are correlated with time and liquid volume fraction (Eq. 6.1). The purpose of developing these simple and easy to use correlations is to include the effect of coarsening/coalescence in the mathematical models developed in Chapter 4. The correlation constants for aqueous and polymer foams are shown in Table 6.1.

$$d_b = Ae^{-B\varepsilon} \qquad (at\ t = 0) \tag{6.1}$$

$$d_b = Ce^{-Dt^{-E}\varepsilon} \qquad (at\ t > 0) \tag{6.2}$$

where d_b is the average bubble diameter in m; t is the time in seconds; ε is the liquid volume fraction; and, A, B, C, D, E, are the correlation constants.

Table 6. 1: Correlation constants for aqueous and polymer foams

Correlation Constants	Aqueous foams	Polymer foams
A, m	0.0003	0.0002
B	-3.4	-1.9

C, m	0.0005	0.0003
D, s^E	14.838	3.394
E	0.284	0.124

In Fig. 6.16, the predictions of the correlations are compared with measurements. The correlations are more accurate as liquid volume fraction decreases and when the base liquid phase is water. To visualize the deviation of correlation predictions from actual measured values, Fig. 6.17 was generated. Predictions lie within the error margin of +/- 25%, except for a few outliers. Non-Newtonian behavior of the liquid phase was not considered in the correlation development of polymer foams. This might account for the greater deviation of correlation predictions from the measured values.

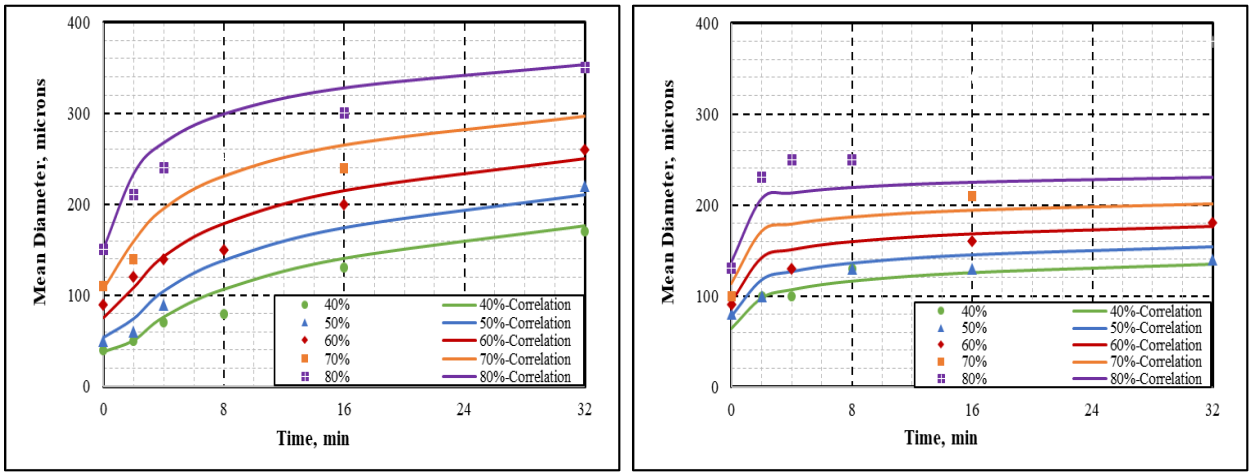

(a) **(b)**

Figure 6. 16: Mean bubble diameter correlation for – (a) aqueous; and, (b) polymer foams

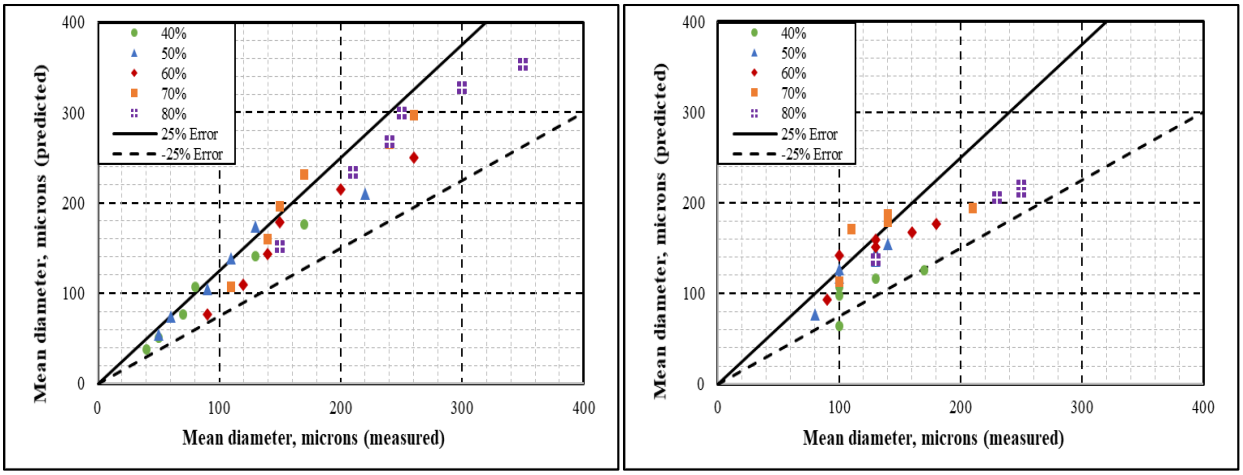

(a) **(b)**

Figure 6. 17: Error % of correlations developed for – (a) aqueous; and, (b) polymer foams

6.3 Results of Mathematical Models

The results obtained from the mathematical models developed in Chapter 4 are presented in this part along with the experimental measurements of aqueous and polymer foams. For the comparison, only 40, 60, and 80% quality foams are considered. Oil-based foams were not included in this study as any such models developed for these foams would not include the effect of bubble coarsening. Models for various quality oil-based foams have previously been developed by Ibizugbe (2012) using Koehler et al. (2000) node dominated drainage equation.

In this study, both channel and node dominated models are developed that include the effect of change in bubble size distribution as drainage progresses. Models predict the change in liquid volume fraction over time in a foam column.

6.3.1 Aqueous Foam

The model predictions obtained for 40% aqueous foam are validated with experimental measurements in Fig. 6.18. These figures show variation in liquid volume fraction with height at different times. For 40% quality aqueous foam, node dominated model over predicts the liquid

volume fraction at early times. Channel dominated model predictions are more closely related to experimental results for this foam.

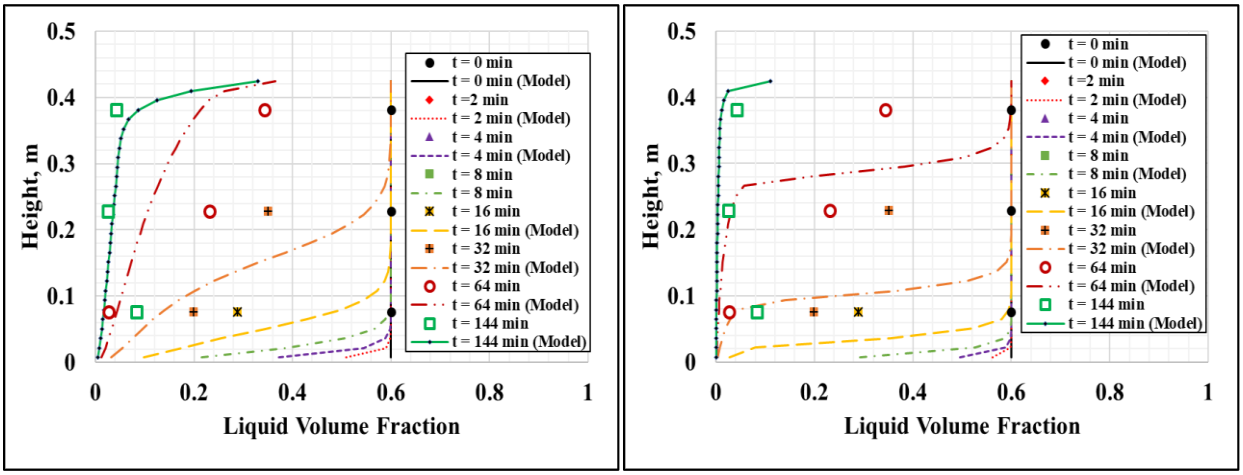

(a) **(b)**

Figure 6. 18: Model predictions and experimental measurements for 40% aqueous foams – (a) channel dominated; and, (b) node dominated models

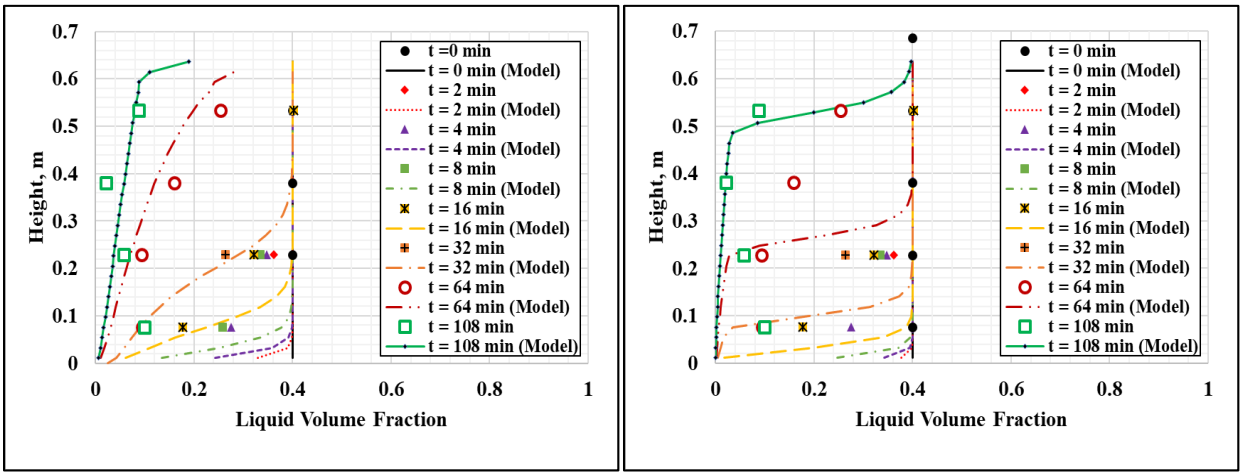

(a) **(b)**

Figure 6. 19: Model predictions and experimental measurements for 60% aqueous foams – (a) channel dominated; and, (b) node dominated models

In Fig. 6.19, predictions from channel and node dominated models are presented along with experimental measurements for 60% quality aqueous foams. Here as well node dominated model over-predicted liquid volume fractions while channel dominated model provided reasonable predictions. Similarly, in Fig. 6.20, model predictions and experimental measurements for 80%

quality foams are presented. Both models provided reasonable predictions. By comparison, channel dominated model appears to be a better fit for 80% aqueous foam.

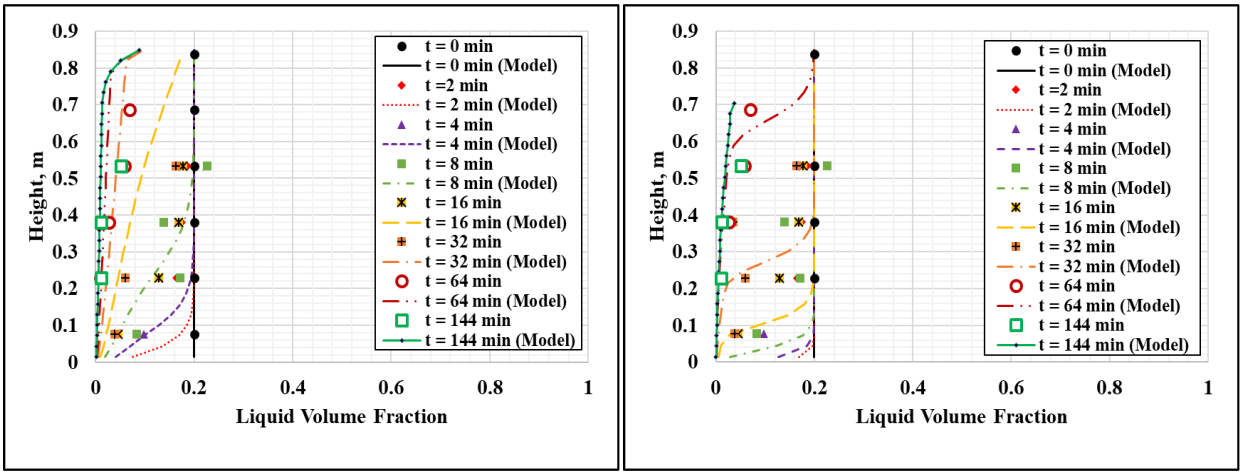

(a) **(b)**

Figure 6. 20: Model predictions and experimental measurements for 80% aqueous foams – (a) channel dominated; and, (b) node dominated models

6.3.2 Polymer Foam

For polymer-based foams, numerical solutions are obtained for all qualities (40, 60, and 80%) considered. Results for 40% quality foam are presented in Fig. 6.21. Node dominated model slightly over predicts liquid volume fraction. For this quality of polymer foam, channel dominated model is more accurate than the node dominated model. Node dominated model predictions deviate widely for early time steps in predicting liquid volume fraction. Similar observations can be made from Fig. 6.22, which shows channel and node dominated model predictions as well as experimental measurements for 60% quality polymer foams. For this quality as well, it is preferable to use the channel dominated model. For 80% quality foam, both model models make reasonable predictions, but clearly channel dominated model is a better fit as can be seen in Fig. 6.22. Node dominated model slightly over predicts liquid volume fraction at early time steps.

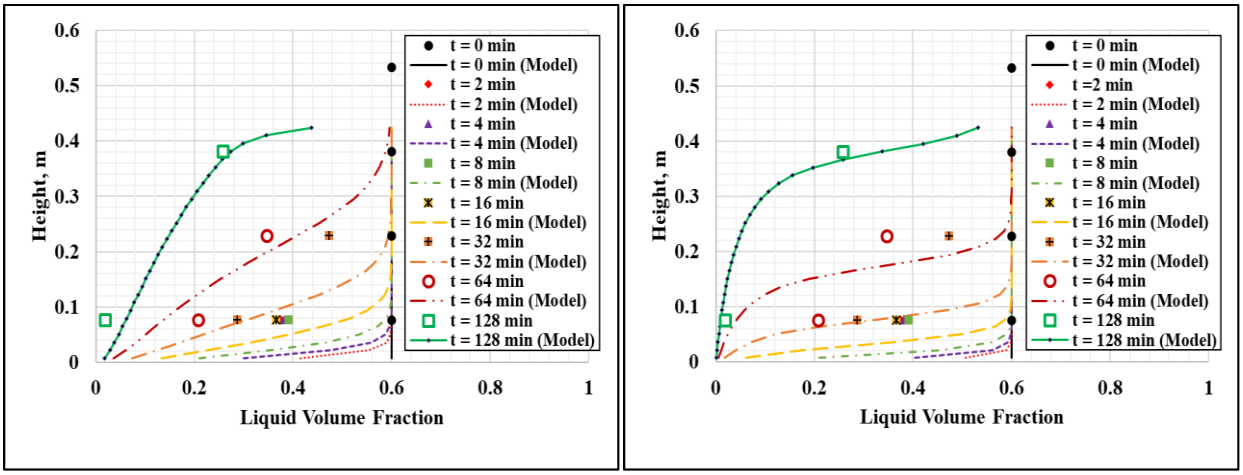

(a) **(b)**

Figure 6. 21: Model predictions and experimental measurements for 40% polymer foams – (a) channel dominated; and, (b) node dominated models

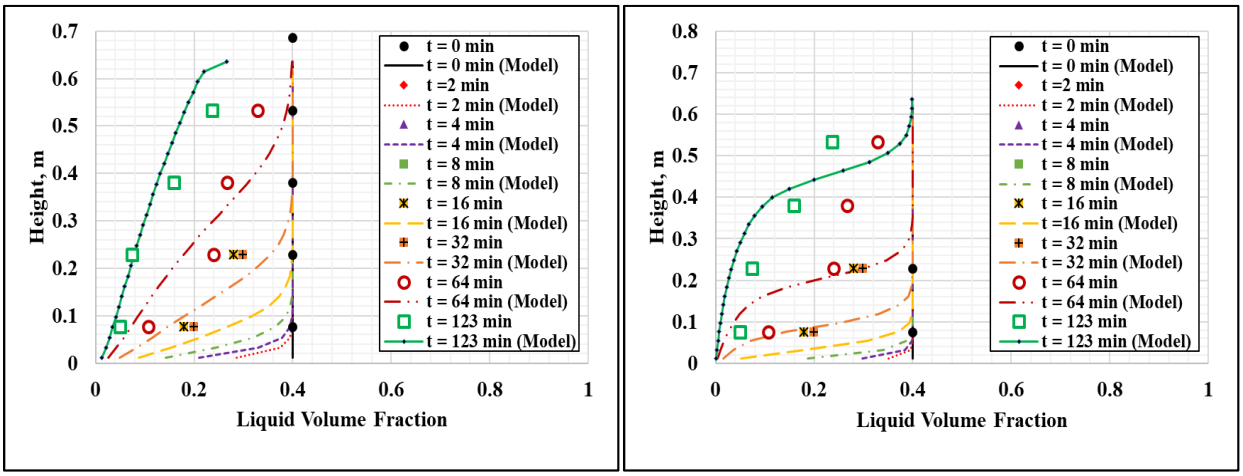

(a) **(b)**

Figure 6. 22: Model predictions and experimental measurements for 60% polymer foams – (a) channel dominated; and, (b) node dominated models

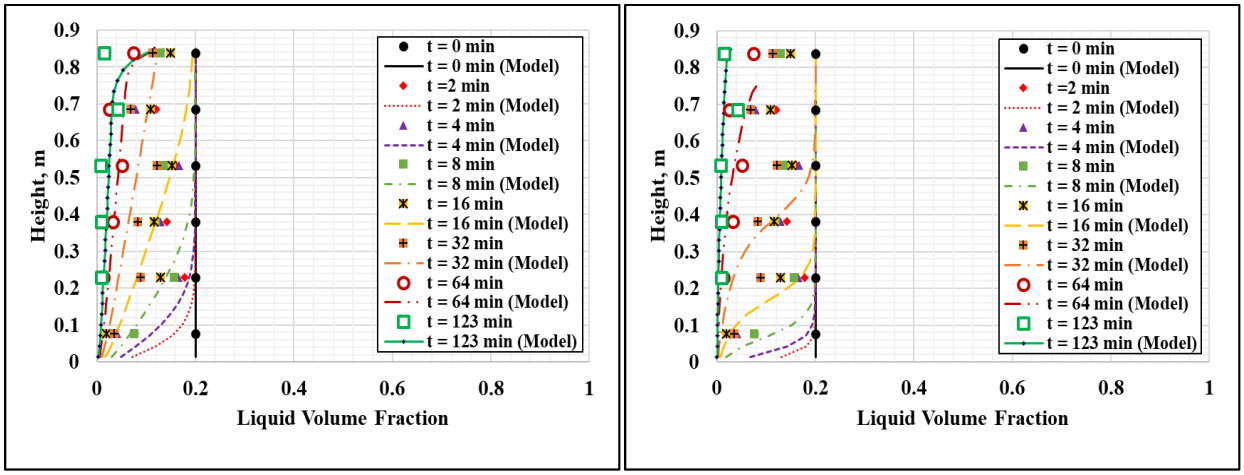

(a) **(b)**

Figure 6. 23: Model predictions and experimental measurements for 80% polymer foams – (a) channel dominated; and, (b) node dominated models

For both aqueous and polymer foams, channel dominated model performs better at predicting liquid volume fraction at all three qualities considered (40, 60, and 80%). Node dominated model widely over predicts liquid volume fraction at early time steps for wet foams (40-60%). For dry foam, this model provides better predictions but still slightly over predicts liquid volume fraction at early time steps. Overall, it is not recommended to use node dominated model for the qualities of foams studied (40-80%). The channel dominated model reasonably predicts the liquid volume fractions of all foams considered.

CHAPTER 7

CONCLUSIONS AND RECOMMENDATIONS

In this chapter, the various conclusions drawn from the experimental and mathematical modeling studies are presented. Recommendations are outlined based on of outcomes of these studies.

7.1 Conclusions

An innovative method was developed to investigate the drainage behavior of foams. The method is reasonably accurate, cost-effective, and comparable to other methods available in the literature. Experimentally, the effects of quality, conduit geometry, inclination angle, and shearing, on the liquid drainage of foam were investigated. There was not much information available in the literature regarding these parameters and this study aims to rectify this. Furthermore, mathematical models are developed taking into consideration change in the bubble sizes of aqueous and polymer foams. The models are evaluated using experimental measurements. Based on the outcomes of these studies, the following conclusions can be made:

I. Polymer foam exhibited the highest stability and tests with these foams required prolonged times to complete. Regardless of conduit geometry and inclination angle, oil-based foam showed the lowest stability at all qualities when compared with aqueous and polymer-based foams.

II. The hindrance effects of container walls on the motion of bubbles and drainage of liquid are more significant in the annulus as compared to the pipe, resulting in reduced liquid drainage in the annulus.

III. The rate of foam drainage is much higher in inclined conduits than the vertical ones. In inclined conduits, draining liquid experiences substantially reduced flow resistance from the bubble

structure. The highest difference in drainage between vertical and inclined cases was observed with oil-based foam.

IV. Even though base liquid viscosity is an important parameter that affects the drainage behavior of foams, there are other factors such as coalescence and coarsening which contribute to the rapid break down of foam structure and severe drainage. As a result, although the base liquid of oil-based foam was more viscous than water, oil-based foam drained much quicker than aqueous foam.

V. At the shear rates exerted on foam column, no appreciable difference could be observed in the drainage behavior of foams.

VI. Mathematical models developed by Koehler et al. (2000) were modified to account for change in channel length as bubbles coarsen with decreasing liquid volume fraction and increasing time.

VII. Models developed for drainage from unbounded foam fluid were incorporated to the case of foam trapped in annulus by adjusting the sensitivity of permeability terms.

VIII. Channel-dominated model developed in this study is suitable for all foams considered (40 to 80%). Node dominated model over predicts liquid volume fraction at early time steps.

7.2 Recommendations

It was not possible to obtain experimental information on the effect of shear on drainage behavior of foam. Modifying the existing experimental apparatus to exert reasonably high-shear rates might provide useful insights, especially as very little information is available regarding this parameter in the literature. Also, it would be interesting to see the effect of conduit diameter on the drainage

behavior of foams. Very limited studies (Brannigan and De Alcantara Bonfim 2001) are available related to conduit size.

Models developed in the current study successfully incorporated the effect of increasing bubble size on drainage behavior. In addition to this effect, the drainage model should be upgraded to include the effect of inclination. A mathematical model that predicts half-life of foam in wellbore containing vertical, inclined, and horizontal sections would be of great practical value. To accomplish this, foam drainage equations need to be modified to include additional liquid drainage by virtue of inclination angle. Furthermore, additional drainage due to various factors (geometry, inclination, diameter effect) can be accounted for by defining 'enhanced liquid velocity' term in previously developed drainage equations.

NOMENCLATURE

A – interfacial area

A, B, C, D – constants in channel-dominated foam drainage equation

A, B, C, D, E – correlations constants

dA – incremental area of film

d_b – average bubble diameter

dh – incremental liquid height

dt – incremental drainage time

dx – incremental width of film

E – surface energy

g – acceleration due to gravity

h – height between consecutive differential pressure transducers on stability testing cell

H – height of foam column portion

$i_{1\text{-}30}$ – grid designation

I_o – maximum intensity of incident monochromatic light

I_R – intensity of refracted monochromatic light

j_{dave} – average superficial drainage velocity

K – flow consistency index

L – length of channel

l – length of film

m_g – mass of gas

m_l – mass of liquid

n – flow behavior index

N – number of time step

n_F – number of foam lamellae in unit length

p – pressure in foam structure due to liquid phase

P_A – pressure at A

P_B – pressure at B

P_G – static pressure acting at the interface due to gas phase

p_{gas} – pressure of gas phase in bubbles

P_L – static pressure acting at the interface due to liquid phase

r – characteristic radius of curvature for channels

R_1 – radius of curvature of bubble #1

R_{1A} – radius of curvature of bubble #1 at A

R_{1B} – radius of curvature of bubble #1 at B

R_2 – radius of curvature of bubble #2

R_{2A} – radius of curvature of bubble #2 at A

R_{2B} – radius of curvature of bubble #2 at B

t – time

t_f – film thickness

V_f – volume of foam

z – coordinate axis

ΔP – pressure gradient

Δp_m – measured differential pressure between consecutive transducers on stability testing cell

Δt – time step

Δz – grid length

GREEK LETTERS

α, β, χ – constants in node dominated foam drainage equation

δ_e – constant relating shape of channel to liquid volume fraction

ε – liquid volume fraction

φ – foam quality

λ – wavelength of monochromatic light

θ – angle of reflection

ρ_f – foam density

$\overline{\rho_f}$ – average density of foam between two consecutive pressure transducers on stability cell

ρ_l – liquid density

σ – interfacial tension

ABBREVIATIONS

ADM – Adomian decomposition method

B-GFCF – bivariate generalized fractional order of Cheybyshev functions

FDE – foam drainage equation

gpm – gallons per minute

HEC – hydroxyethyl cellulose

HPTM – homotopy perturbation transform method

HWM – Haar wavelets method

LDM – Laplace decomposition method

lpm – liters per minute

MRI – magnetic resonance imaging

PCDR – particle-to-container diameter ratio

ppg – pounds per gallon

PTFE – polytetrafluoroethylene

PVC – polyvinyl chloride

RDTM – reduced differential transform method

rpm – revolutions per minute

REFERENCES

Abbott, W.K. 1974. An Analysis of Slip Velocities of Spherical Particles in Foam Drilling Fluid. MSc. Thesis, Colorado School of Mines, Golden, Colorado.

Abdolhamid, A., Rezaee, N., Naser, J. 2017. Numerical modelling of flow through foam's node. Journal of Colloid and Interface Science, Vol. 504, p. 485 – 491.

Akhtar, T. 2017. Rheology of Aqueous and Polymer-based Nitrogen Foams at High Pressure and High Temperature (HPHT) Conditions. Master's Thesis, University of Oklahoma.

Anderson, G.W. 1984. Use of Preformed Foam in Low Pressure Reservoir Wells. Proceedings, 5th Offshore SPE South East Asia Offshore Technology Conference, pp. 121 – 129.

Arbabi, S., Nazari, A., Darvishi, M.T. 2016. A semi-analytical solution of foam drainage equation by Haar wavelets method. International Journal for Light and Electron Optics, Optik 127 (2016) 5443 – 5447.

Argillier, J. F., Saintpere, S., Herzhaft, B., Toure, A. 1998. Stability and Flowing Properties of Aqueous Foams for Underbalanced Drilling. SPE 48982, presented at the SPE Annual Technical Conference and Exhibition, New Orleans, Louisiana, September 27-30.

Babatola, F. 2014. Rheology of PAC Polymer-based Foams using Pipe Viscometers. Master's Thesis, University of Oklahoma.

Barigou, M., Crawshaw, J.P., Davidson, J.F., Gladden, L.F., Hollewand, M.P., Paterson, W.R., Scott, D.M. 1993. Applications of magnetic resonance imaging in Chemical Engineering: foam drainage and packed beds. Proceedings of The Institute of Chemical Engineers Research Event, January 6 – 7, Birmingham, p. 552 – 554.

Barigou, M., Davidson, J.F. 1994. Soap film drainage: theory and experiment. Chemical Engineering Science, 49: 1807–1819.

Barigou, M., Deshpande, N.S., Wiggers, F.N. 2001. An enhanced electrical resistance technique for foam drainage measurement. Colloids and Surfaces A: Physiochemical and Engineering Aspects, Vol. 189, p. 237 – 246.

Bart E. 1968. The slow unsteady settling of a fluid sphere toward a flat fluid interface. Chemical Engineering Science, 23(3):193-210, June 1.

Belorgey, O., Benattar, J.J. 1991. Structural properties of soap black films investigated by X-ray reflectivity. Physical Review Letters 66 (3) 313 – 316.

Benion, D.B., Thomas, F.B. 1994. Underbalanced Drilling of Horizontal Wells: Does It Really Eliminate Formation Damage?. SPE 27352, presented at the SPE International Symposium on Formation Damage Control, Lafayette, Louisiana, February 7-10.

Bentsen, N.W., Veny, J.N. 1976. Preformed Stable Foam Performance in Drilling and Evaluating Shallow Gas Wells in Alberta. Journal of Petroleum Technology, pp. 1237 – 1240, August.

Bernard, G.G., Holm, L.W., Harvey, C.P. 1980. Use of Surfactant to Reduce CO2 Mobility in Oil Displacement. SPEJ, August, 281 – 292.

Beyer, A.H., Millhone, R.S., Foote, R.W. 1972. Flow Behavior of Foam as a Well Circulation Fluid. SPE 3986, paper presented at the 1972 SPE Annual Fall Meeting, San Antonio, Texas, October.

Bhakta, A., Ruckenstein, E. 1995. Drainage of Standing Foam. Langmuir, Vol. 11, p. 1486 – 1492.

Bhakta, A., Ruckenstein, E. 1996. Modeling of the Generation and Collapse of Aqueous Foams. Langmuir, 12, 3089-3099.

Bhakta, A., Ruckenstein, E. 1997. Decay of standing foams: drainage, coalescence and collapse. Advances in Colloid and Interface Science, 70 (1997) 1 – 124.

Bikerman, J.J. 1938. The Unit of Foaminess. Transactions of the Faraday Society, 34 (1938) 634 – 638.

Bikerman, J.J. 1953. Foams: Theory and Industrial Applications. Reinhold, New York.

Bikerman, J.J., Perri, J.M., Booth, R.B., Currie, C.C. 1973. Foams. Springer, Berlin.

Bisperink, C.G.J., Ronteltap, A.D., Prins, A. 1992. Adv. Colloid Interface Sci., 38:13.

Bleakley, W.B. 1973. West Texas Workovers with Foam Gain Favor. Oil & Gas Journal, pp. 5 – 17, March 22.

Bonilla, L.F., Shah, S.N. 2000. Experimental Investigation on the Rheology of Foams. SPE 59752, paper presented at the 2000 SPE/CERI Gas Technology Symposium, Calgary, Alberta, Canada, April 3 – 5.

Brewster, D. 1867. On the colors of soap bubbles. The Royal Society of Edinburgh, 24:491.

Bundy, F. 1980. The P, T phase and reaction diagram for elemental carbon, 1979. JGR Solid Earth, Vol. 85, Issue B12, December 10.

Burcik, E. J. 1950. The Rate of Surface Tension Lowering and its Role in Foaming. Journal of Colloidal Science, (1950) 5, 421.

Cantan, I., Cohen-Addad, S., Elias, F., Graner, F., Höhler, R., Flatman, R., et al. 2013. Foams: structure and dynamics. OUP Oxford.

Carrier, V., Colin, A. 2003. Coalescence in draining foams. Langmuir, 19:4535 – 8.

Cawiezel, K.E., Niles, T.D. 1987. Rheological Properties of Foam Fracturing Fluids Under Downhole Conditions. SPE 16191, paper presented at the SPE Hydrocarbon Economics and Evaluation Symposium, Dallas, Texas, March 2 – 3.

Chang, R.C., Schoen, H.M., Grove, C.S. 1956. Bubble Size and Bubble Size Determination. Industrial & Engineering Chemistry, 48.11 (1956) 2035 – 2039.

Chang, K.S., Lemlich, R. 1980. A study of the electrical conductivity of foam. Journal of Colloid and Interface Science, Vol. 73, p. 224 – 232.

Clark, D.C, Dann, R., Mackie, A.R., Mingins, J., Pinder, A.C., Purdy, P.W., Russell, E.J., Smith, L.J., Wilson, D.R. 1990. Surface-diffusion in sodium dodecyl sulphate-stabilized thin liquid-films. Journal of Colloid Interface Science, 138 (1) 195 – 206.

Clark, N.O. 1947. Special Report No. 6. Department of Scientific and Industrial Research, Her Majesty's Stationary Office, London.

Clift, R., Grace, J. R., & Weber, M. E. (1978). Bubbles, drops, and particles. Courier Corporation.

Clunie, J.S., Goodman, J.F., Ingram, B.T. 1971. Thin Liquid Films. Surface and Colloidal Science, Wiley: New York, Vol. 3, pp. 167 – 239.

Cox, S.J., Bradley, G., Hutzler, S., Weaire, D. 2001. Vertex corrections in the theory of foam drainage. Journal of Physics: Condensate Matter, Vol. 13, 4863.

Czarnecki, J., Malysa, K., Pomianowski, A. 1982. Dynamic Frothability Index. Journal of Colloid and Interface Science, 86.2 (1982) 570 – 572.

Datye, A.K., Lemlich, R. 1983. Liquid distribution and electrical conductivity in foam. International Journal of Multiphase Flow, Vol. 9, p. 627 – 636.

Desai, D., Kumar, R. 1982. Flow through a plateau border of cellular foam. Vol. 37, Issue 9, p. 1361 – 1370.

Deshpande, N.S, Barigou, M. 1999. Foam formation, drainage and collapse in presence of antifoams. AIDIC-Italian Association of Chemical Engineering Conference Series, Vol. 4, p. 295 – 301.

Derjaguin, B., Landau, L. 1941. Theory of the Stability of Strongly Charged Lyophobic Sols and of the Adhesion of Strongly Charged Particles in Solutions of Electrolytes. Academy of Sciences of the USSR, Institute of Colloid and Electrochemistry, Laboratory of Thin Films, Institute of Physical Problems, Moscow.

Dickinson, J.E., Laskovski, D., Stevenson, P., Galvin, K.P. 2010. Enhanced foam drainage using parallel inclined channels in a single-stage foam fractionating column. Chemical Engineering Science, Vol. 65, p. 2481 – 2490.

Drenckhan, W., Hutzler, S. 2015. Strcuture and energy of liquid foams. Advanced Colloid Interface Science, 224:1 – 16.

Drenckhan, W., Saint-Jalmes, A. 2015. The science of foaming. Advances in Colloid and Interface Science, 222 (2015) 228 – 259.

Durian, D.J., Weitz, D.A., Pine, D.J. 1991. Multiple Light-Scattering Probes of Foam Structures and Dynamics. Science, 252:686.

Essary, R.L., Rogers E.E. 1976. Techniques and Results of Foam Redrilling Operations–San Joaquin Valley, California. Proceedings, Symposium on Formation Damage Control, Society of Petroleum Engineers of AIME, pp. 237 – 244.

Gonatas, C.P, Leigh, J.S, Yodh, A.G, Glazier, J.A, Prause, B. 1995. Magnetic resonance images of coarsening inside a foam. Physical Review Letters, 75:573 – 6.

Gol'dfarb, I.I., Kann, K.B., Shreiber, I.R. 1988. Liquid flow in foams. Vol. 23, Issue 2, p. 244 – 249.

Goyon, J., Bertrand, F., Pitois, O., Ovarlez, G. 2010. Shear Induced Drainage in Foamy Yield-Stress Fluids. Physical Review Letters, 104, 128301, 22 March.

Gubes, M., Keskin, Y., Oturane, G. 2015. Numerical solution of time-dependent Foam Drainage Equation (FDE). Computational Methods for Differential Equations, Vol. 3, No. 2, pp. 111 – 122.

Guo, B., Ghalambor, A. 2002. Gas Volume Requirements for Underbalanced Drilling: Deviated Holes. PennWell Corporation, Tulsa, Oklahoma.

Happel, J., Brenner, H. 1965. Low Reynolds Number Hydrodynamics, with Special Applications to Particulate Media. Prentice-Hall.

Harris, P.C. 1989. Effects of Texture on Rheology of Foam Fracturing Fluids. SPE Production Engineering, August.

Heller, J.P., Kuntamukkula, M.S. 1987. Critical Review of the Foam Rheology Literature. Industrial Engineering and Chem. Res., 26, 318-325.

Herzaft, B., Kakadjian, S., Moan, M. 2005. Measurement and modeling of the flow behavior of aqueous foams using a recirculating pipe rheometer. Colloids and Surfaces A: Physicochem. Eng. Aspects 263 920050 153 – 164.

Hill, C., Eastoe, J. 2017. Foams: From nature to industry. Advanced in Colloid and Interface Science, 247 (2017) 496 – 513.

Hilgenfeldt, S., Koehler, S.A., Stone, H.A. 2001. Dynamics of Coarsening Foams: Accelerated and Self-Limiting Drainage. Physical Review Letters, Vol. 86, No. 20.

Hollinger, H.B. 1991. Thermodynamics of Foam. Journal of Colloid Interface Science, 143.1 (1991) 278 – 286.

Holt, T., Vassenden, F., Svorstol, I. 1996. Effects of Pressure on Foam Stability; Implications for Foam Screening. SPE 35398, paper presented at the 1996 SPE/DOE Tenth Symposium on Improved Oil Recovery, Tulsa, Oklahoma, April 21 – 24.

Hooke, R. 1672. On holes (black film) in soap bubbles. Royal Society of Chemistry, March, p. 28.

Hutchins, R.D., Miller, M.J. 2003. A Circulating Foam Loop for Evaluating Foam at Conditions of Use. SPE 80242, presented at the SPE International Symposium on Oilfield Chemistry, Houston, Texas, USA, February 5-7.

Hutchison, S.O., Anderson, G.W. 1972. Preformed Stable Foam Aids Workover, Drilling. Oil and Gas Journal, September 25, pp. 13 – 18.

Hutzler, S., Verbist, G., Weaire, D., van der Steen, J.A. 1995. Measurement of foam density profiles using AC capacitance. Europhysics Letters, 31 (8), p. 497 – 502.

Ibizugbe, N.O. 2012. Drainage Behavior of Oil-based Drilling Foam under Ambient Conditions. Master's Thesis, University of Oklahoma.

Isenberg, C. 1992. The Science of Soap Films and Soap Bubbles. Courier Corporation.

Jacobi, W.M., Woodcock, K.E., Grove, C.S. 1956. Theoretical Investigation of Foam Drainage. Industrial and Engineering Chemistry, Vol. 48, No. 11.

Jiang, C.S., Wu, Z.L., Li, R., Liu, Q. 2011. Technology of protein separation from whey wastewater by two-stage foam separation. Biochemical Engineering Journal, Vol. 55, p. 43 – 48.

Joly, M. 1964. Surface Viscosity. Recent Progress in Surface Science, Academic, Orlando, Florida, Vol. 1, pp 1 – 50.

Koehler, S.A., Stone, H.A., Brenner, M.P., Eggers, J. 1998. Dynamics of foam drainage. Physical Review E, American Physical Society, Volume 58, Number 2.

Koehler, S.A., Hilgenfeldt, S., Stone, H.A. 1999a. Liquid Flow through Aqueous Foams: The Node-Dominated Foam Drainage Equation. Physical Review Letters, American Physical Society, Volume 82, Number 21.

Koehler, S.A., Hilgenfeldt, S., Stone, H.A. 1999b. Foam Drainage: Experiments and a New Model. In Foams and Films: Proceedings of the International Workshop on Foams and Films, Leuven, Belgium.

Koehler, S.A., Hilgenfeldt, S., Stone, H.A. 2000. A Generalized View of Foam Drainage: Experiment and Theory. Langmuir 2000, 16, 6327-6341.

Koehler, S.A., Hilgenfeldt, S., Stone, H. 2004. Foam drainage on the microscale: II. Imaging flow through single plateau borders. Journal of Colloid and Interface Science, Vol. 276, p. 439 – 449.

Kraynik, A.M. 1983. Foam drainage. Sandia National Laboratories, Internal Report, 83 – 0844.

Kruglyakov, P.M., Taube, P.R. 1965. Zh. Prikl. Khim., 38:2258.

Lachaise, J., Graciaa, A., Marion, G., Salager, J.L. 1990. A New Reflectometry Method to Measure a Liquid Foam Stability. Journal of Dispersion Science and Technology, 11.4 (1990) 409 – 430.

Lambert, J., Cantat, I., Delannay, R., Renault, A., Graner, F., Glazier, J.A, et al. 2005. Extraction of relevant physical parameters from 3D images of foams obtained by X-ray tomography. Colloids and Surfaces A: Physiochemical and Engineering Aspects, Vol. 263, Issues 1 – 3, p. 295 – 302.

Larson, R.E., Higdon, J.J. 1989. A periodic grain consolidation model of porous media. Physics of Fluids A: Fluid Dynamics, Vol. 1, Issue 1, p. 38 – 46.

Leonard, R.A., Lemlich, R. 1965. A study of interstitial liquid flow in foam. Part I. Theoretical model and application to foam fractionation. The American Institute of Chemical Engineers Journal, Vol. 11, Issue 1, p. 18 – 25.

Lincicome, J.D. 1984. Using Foam to Drill Deep, Underpressured Zones. World Oil, pp. 11 – 14, December 15.

Lyuke, S.E., Daramola, M.O, Mokena, P., Marshall, A. 2015. Thermodynamic stability of graphitic diamond films produced from catalytic chemical vapour deposition reactor. Journal of Industrial and Engineering Chemistry, Vol. 30, pgs. 336 – 341, October 25.

Maini, B.B., Ma, V. 1986. Laboratory evaluation of foaming agents for high-temperature applications–I. Measurements of foam stability at elevated temperatures and pressures. JCPT, November – December, 65 – 69.

Malysa, K. 1992. Wet Foams: Formation, Properties And Mechanism Of Stability. In: Advances in Colloid and Interface Science, 40, 37-83.

McCarthy, M.J. 1990. Interpretation of the magnetic-resonance-imaging signal from a foam. American Institute of Chemical Engineers Journal, Vol. 36, p. 287 – 290.

Miles, G.D., Shedlovsky, L., Ross, J. 1945. Foam Drainage. Presented at the 108th Meeting of the American Chemical Society, New York, September 13.

Mitchell, B.J. 1971. Test Data Fill Theory Gap on Using Foam as a Drilling Fluid. Oil and Gas Journal, September, 96 – 100.

Monnereau, C., Vignes-Adler, M., Kronberg, B. 1999. Influence of gravity on foams. Journal de Chimie Physique et de Physico-Chimie Biologique, 96:958 – 67.

Monsalve, A., Schechter, R. 1984. The Stability of Foams: Dependence of Observation on Bubble Size Distribution. Journal of Colloid and Interface Science, 97.2 (1984) 327 – 335.

Mukhopadhyay, G., Khanam, J., Nanda, A. 2010. Protein removal from whey waste water by foam fractionation in batch process. Separation Science and Technology, Vol. 45, p. 1331 – 1339.

Myagotin, A., Helfen, L., Baumbach, T. 2009. Coalescence measurements for evolving foams monitored by real-time projection imaging. Measurement Science and Technology, Vol. 20, Number 5.

Mysels, K.J., Shinoda, K., Frankel, S. 1959. Soap films: studies of their thinning and a bibliography. Pergamon, New York.

Narsimhan, G., Ruckenstein, E. 1996. Structure, Drainage, and Coalescence of Foams and Concentrated Emulsions. In Foams, Theory, Measurements and Applications, Chapter 2,

Newton, I. 1730. Optics. London, 17044th edition, corrected in 1952, Dover.

Nishioka, G.M., Ross, S. 1981. A New Method and Apparatus for Measuring Foam Stability. Journal of Colloid and Interface Science, 81.1 (1981) 1 – 7.

Nishioka, G.M., Ross, S., Whitworth, M. 1983. The Stability of Foam: Comparison of Experimental Data and Computed Results. Journal of Colloid and Interface Science, Vol. 95, No. 2, October.

Nishioka, G.M., Ross, S., Kornbrekke, R.E. 1996. Fundamental Methods for Measuring Foam Stability. In Foams: theory, measurements, and applications, Surfactant Science Series, v. 57, pp. 275 – 285.

Okpobiri, G.A., Ikoku, C.U. 1986. Volumetric Requirements for Foam and Mist Drilling Operations. SPEDE, February, 71 – 88.

Papara, M., Zabulis, X., Karapantsios, T.D. 2009. Container effects on the free drainage of wet foams. Chemical Engineering Science, Vol. 64, p. 1404 – 1415.

Parand, K., Delkhosh, M. 2017. An efficient numerical method for solving nonlinear foam drainage equation. Indian Journal of physics, DOI 10.1007/s12648-017-1098-8.

Pitois, O., Fritz, C., Vignes-Adler, M. 2005. Hydrodynamic resistance of a single foam channel. Colloids and Surfaces A: Physicochemical and Engineering Aspects, Vol. 261, p. 109 – 114.

Platikanov, D., Graf, H.A., Weiss, A., Clemens, D. 1993. X-ray scattering by black foam films-new data analysis. Colloid and Polymer Science, 271 (1) 106 – 107.

Prause, B.A, Glazier, J.A., Gravina, S.J., Montemagno, C.D. 1995. 3-Dimensional magnetic-resonance-imaging of a liquid foam. Journal of Physics: Condensate Matter, Vol. 7, p. L511 – L516.

Princen, H.M. 1988. Rheology of Foams and Highly Concentrated Emulsions. II. Experimental Study of the Yield Stress and Wall Effects for Concentrated Oil-in-Water Emulsions. Langmuir, 4:164.

Princen, H.M. 1990. Gravitational syneresis in foams and concentrated emulsions. Journal of Colloid and Interface Science, Vol. 134, Issue 1, p. 188 – 197.

Prud'homme, R.K., Khan, S.A. 1996. Foams: theory, measurements, and applications. Surfactant Science Series, v. 57.

Ramadan, A., Kuru, E., Saasen, A. 2003. Critical Review of Drilling Foam Rheology. Annual Transactions of the Nordic Rheology Society, Vol. 11.

Rankin, M.D., Friesenhahn, T.J., Price, W.R. 1989. Lightened Fluid Hydraulics and Inclined Boreholes. SPE/IADC 18670, paper presented at the 1989 SPE/IADC Drilling Conference, New Orleans, Louisiana, February 28 – March 3.

Raza, S.H., Marsden, S.S. 1967. The Streaming Potential and the Rheology of Foam. Society of Petroleum Engineers, December 12.

Reduced Pressure Drilling Systems. Bachman Drilling and Production Specialties, Inc., Oklahoma City, Oklahoma.

Rio, E., Drenckhan, W., Salonen, A., Langevin, D. 2014. Unusually stable liquid foams. Advance Colloid Interface Science, 205:74 – 86.

Ross, S., Cutillas, M.J. 1955. The Transmission of Light by Stable Foams. The Journal of Physical Chemistry, 59.9 (1955) 863 – 866.

Ross, S. 1969. Bubbled and Foams – New General Law. Industrial & Engineering Chemistry, 61.10 (1969) 48 – 57.

Ross, S., Nishioka G. 1975. Foaminess of Binary and Ternary Solutions. The Journal of Physical Chemistry 79.15 (1975): 1561 – 1565.

Ross, S., Nishioka G. 1976. Foaming Behavior of Partially Miscible Liquids as related to their Phase Diagrams. Foams, proceedings of a symposium organized by the Society of Chemical Industry, Colloid and Surface Chemistry Group, and held at Brunei University, Academic Press, London.

Ross, S., Suzin, Y. 1985. Retardation of the Ascent of Gas Bubbles by Surface-Active Solutes in Nonaqueous Solutions. Journal of Colloid and Interface Science, 103.2 (1985): 578 – 585.

Ross, S., Morrison, I.D. 1988. Size and Surface Area. Colloidal Systems and Interfaces, Wiley, New York, 31 – 54.

Russell, B.A. 1993. How Surface Hole Drilling Performance was Improved 65 Percent. Paper SPE/IADC 25766 presented at the 1993 SPE/IADC Drilling Conference, Amsterdam, The Netherlands, February 23–25.

Ruckenstein, E., Jain, R.K. 1974. Spontaneous Rupture of Thin Liquid Films. Journal of Colloid Science, (1974) 70, 132 – 147.

Sanghani, V., Ikoku, C.U. 1983. Rheology of Foam and Its Implications in Drilling and Cleaout Operations. Journal of Energy Resources Technology, Vol. 105/353, September.

Saint-Jalmes, A., Vera, M.U., Durian, D. 1999. Uniform foam production by turbulent mixing: new results on free drainage vs. liquid content. The European Physical Journal b – Condensed Matter and Complex Systems, Vol. 12, Issue 1, p. 67 – 73.

Saint-Jalmes, A., Langevin, D. 2002. Time evolution of aqueous foam: drainage and coarsening. Journal of Physics: Condensate Matter, Vol. 14, p. 9397 – 9412.

Saint-Jalmes, A., Zhang, Y., Langevin, D. 2004. Quantitative description of foam drainage: transitions with surface mobility. European Physical Journal E: Soft Matter and Biological Physics, Vol. 15, p. 53 – 60.

Saint-Jalmes, A., Durian, D., Weitz, D. 2005. Kirk-Othmer Encyclopedia of Chemical Technology. Fifth edition, vol. 12, p. 1.

Saint-Jalmes, A. 2006. Physical chemistry in foam drainage and coarsening. The Royal Society of Chemistry, Soft Matter, 2, p. 836 – 849.

Schramm, L.L. 1994. Foams: Fundamentals and Applications in the Petroleum Industry. Advances in Chemistry Series 242, American Chemical Society, Washington DC.

Sebba, F. 1987. Foams and Biliquid Foams – Aphrons. J. Wiley and Sons, Chichester, Chapter 4.

Sherif, T., Ahmed, R., Shah, S., Amani, M. 2015. Rheological behavior of oil-based drilling foams. Journal of Natural Gas Science and Engineering, 26(2015) 873 – 882.

Sepulveda, J.J., Falana, O.M., Kakadjian, S., Morales, J.D., Zamora, F. 2008. Oil-Based Foam and Proper Underbalanced-Drilling Practices Improve Drilling Efficiency in a Deep Gulf Coast Well. SPE 115536, presented at the 2008 SPE Annual Technical Conference and Exhibition, Denver, Colorado, September 21-24.

Sherif, Testi. 2015. Rheology of Drilling Foams Using Pipe Viscometer. Master's Thesis, University of Oklahoma.

Stevenson, P. 2007. On the forced drainage of foam. Colloids and Surfaces A: Physiochemical Engineering Aspects, Vol. 305, p. 1 – 9.

Stone, H.A., Koehler, S.A., Hilgenfeldt, S., Durand, M. 2002. Perspectives on foam drainages and the influence of interfacial rheology. Journal of Physics: Condensation Matter 15 (2003) S283-S290.

Underbalanced Drilling Manual. 1997. Gas Research Institute, Chicago, Illonois.

Vera, M.U., Durian, D.J. 2002. Enhanced Drainage and Coarsening in Aqueous Foams. Physical Review Letters, Vol. 88, No. 8.

Verbist, G., Weaire, D., Kraynik, A.M. 1996. The foam drainage equation. Journal of Physics, Matter 8 (1996) 3715 – 3731.

Verwey, E. J. W. and Overbeek, J. T. G. 1948. Theory of Stability of Lyophobic Colloids. Elsevier Amsterdam.

Wang, G.C. 1984. A laboratory Study of CO2 Foam Properties and Displacement Mechanism. SPE/DOE 12645, paper presented at the 1984 EOR Symposium, Tulsa, April 15 – 18.

Wang, Y., Wu, Z., Li, R., Zhang, Z. 2013. Enhancing foam drainage using inclined foam channels of different angles for recovering the protein from whey wastewater. Colloids and Surfaces A: Physicochemical and Engineering Aspects, Vol. 419, p. 28 – 36.

Wang, J., Nguyen, A.V., Farrokhpay, S. 2016. A critical review of the growth, drainage, and collapse of foams. Advances in Colloid and Interface Science, Vol. 228, pgs. 55 – 70, February.

Wasan, D.T., Koczo, K., Nikolov, A.D. 1994. Mechanisms of Aqueous Foam Stability and Antifoaming Action with and without Oil: A Thin-Film Approach. Foams: Fundamentals and Applications in the Petroleum Industry, Advances in Chemistry Series 242, American Chemical Society, Washington DC.

Watkins, R.C. 1973. An Improved Foam Testing for Lubricating Oils. Journal of the Institute of Petroleum, 106 – 113.

Weaire, D., Pageron, V. 1990. Frustrated froth: evolution of foam inhibited by an insoluble gaseous component. Philosophical Magazine Letters, 62:417 – 21.

Weaire, D., Findlay, S., Verbist, G. 1995. Measurement of foam drainage using AC conductivity. Journal of Physics: Condensed Matter, 7 (16), L217 – L222.

Weaire, D., Hutzler, S., Verbist, G., Peters, E. 1997. A Review of Foam Drainage. Advances in Chemical Physics, Volume 102, John Wiley & Sons, Inc.

Weaire, D.L., Hutzler, S. 1999. The physics of foams. Oxford University Press.

Wendorff, C.L., Ainley, B.R. 1981. Massive Hydraulic Fracturing of High-Temperature Wells with Stable Frac Foam. SPE 10257, presented at the 1981 SPE Annual Fall Meeting, San Antonio, Texas.

Wheeler, A. J., Ganji, A. R. 1996. Introduction to Engineering Experimentation. Prentice Hall, Upper Saddle River, New Jersey, p. 160-178.

Wilde, P.J. 1996. Foam measurement by the microconductivity technique: An assessment of its sensitivity to interfacial and environmental factors. Journal of Colloid and Interface Science, 178, p. 733 – 739.

Yamanaka, T., Tano, T., Kamegaya, O., Exerowa, D., Cohen, R.D. Effects of metal-ions on the equilibrium thicknesses of foam films stabilized by lysophosphatidylcholine as studied by FT-IR spectroscopy. Langmuir 10 (6) 1871–1876.

Zayed, E.M., Al-Nowehy, A.G. 2016. Exact solutions for nonlinear foam drainage equation. Indian Journal Physics, February, 91(2): 209 – 218.

Zick, A.A., Homsy, G.M. 1982. Stokes flow through periodic arrays of spheres. Journal of Fluid Mechanics, Vol. 115, February, pp. 13 – 26.

APPENDIX A: BASE LIQUID CHARACTERIZATION

Table A. 1: Derivation of base liquid gradient for oil foams

Water gradient	0.433 psi/ft (14.7 psi = 407.2 in. of water; 1 psi = 27.7 in. of water)
Oil gradient	= 0.8 x 0.433 psi/ft or 0.8 x 0.465 psi/ft = 0.3464 psi/ft or 0.372 psi/ft = 0.3464 x 27.7 in. of water/ft = 9.59528 in./ft = 4.79764 in./0.5 ft = 4.8 in. per ½ ft

Table A. 2: Density calculation of base liquid for oil foams

Mass of empty density bottle, g	14.9
Mass of liquid, g	8.3
Volume of liquid, ml	10
Density, g/ml	0.83

Test was repeated five times and exact same measurements were obtained for mass.

Table A. 3: Rheology data of base liquid for oil foams

Shear Rate, s^{-1}	Shear Stress, Pa	Viscosity, Pa-s
0.00426	0.204*	0.0399
0.00640	0.306*	0.0300
0.01919	0.919*	0.0054
0.03411	1.633	0.0048
0.04904	2.348	0.0046
0.09168	4.389	0.0043

***** - shear stress values too low to obtain reasonable data for viscosity estimation. Measurements made at 21.2 ^{o}C.

Table A. 4: Rheology data of base liquid for polymer foams

Shear Rate, s^{-1}	Shear Stress, Pa	Viscosity, Pa-s
51.09	0.510	0.0251
102.18	0.715	0.0232
153.27	1.021	0.0214
170.30	1.123	0.0210
306.54	1.735	0.0190
340.60	1.940	0.0185
510.90	2.756	0.0171
1021.80	4.900	0.0150

APPENDIX B: FOAM RHEOLOGY DATA

Table B. 1: Aqueous foam rheology measurements – 40%

Pipe #	Flowrate, lpm	Wall Sheart Stress, Pa	Wall Shear Rate, s^{-1}
1	5.45	0.2704	58.10
	8.23	0.6296	87.72
	12.24	1.0466	130.57
	18.52	1.7067	197.46
	27.83	3.7969	296.82
	41.48	8.0150	442.30
	54.17	13.1217	577.66
2	5.50	0.0829	26.10
	8.24	0.1461	39.07
	12.28	0.2318	58.26
	18.53	0.6039	87.88
	27.92	1.0500	132.43
	41.70	2.2057	197.82
	54.53	3.8481	258.67

Table B. 2: Aqueous foam rheology measurements – 45%

Pipe #	Flowrate, lpm	Wall Sheart Stress, Pa	Wall Shear Rate, s^{-1}
1	5.39	0.2813	57.83
	8.19	0.6405	87.84
	12.22	1.2216	131.04
	18.43	2.0856	197.70
	27.75	3.5038	297.65
	41.43	7.7008	444.44
	54.14	12.7130	580.83
2	5.45	0.0722	25.96
	8.23	0.2009	39.23
	12.24	0.3499	58.36
	18.42	0.6725	87.81
	27.79	1.1405	132.47
	41.59	2.2949	198.25
	54.37	3.7848	259.18

Table B. 3: Aqueous foam rheology measurements – 50%

Pipe #	Flowrate, lpm	Wall Sheart Stress, Pa	Wall Shear Rate, s^{-1}
1	5.40	0.7675	62.77
	8.19	1.2719	95.21
	12.17	1.8491	141.41
	18.38	2.8262	213.61
	27.66	3.9685	321.34
	41.31	6.2047	479.98
	53.92	10.6166	626.47
2	5.56	0.2810	28.80
	8.25	0.4636	42.73
	12.27	0.6556	63.57
	18.46	1.1273	95.60
	27.81	1.5951	144.04
	41.55	2.5269	215.26
	54.37	3.4222	281.67

Table B. 4: Aqueous foam rheology measurements – 55%

Pipe #	Flowrate, lpm	Wall Sheart Stress, Pa	Wall Shear Rate, s^{-1}
1	5.47	1.1658	65.11
	8.26	1.7962	98.40
	12.20	2.7487	145.29
	18.26	4.0955	217.50
	27.47	5.8756	327.10
	40.93	8.4209	487.51
	53.47	10.8041	636.81
2	5.42	0.4914	28.77
	8.27	0.7085	43.84
	12.24	1.0834	64.89
	18.31	1.5789	97.12
	27.56	2.3274	146.18
	41.07	3.5518	217.82
	53.79	4.6135	285.29

Table B. 5: Aqueous foam rheology measurements – 60%

Pipe #	Flowrate, lpm	Wall Sheart Stress, Pa	Wall Shear Rate, s^{-1}
1	5.414	1.4942	64.65
	8.212	2.9866	98.08
	12.205	4.5682	145.76
	18.238	6.0320	217.81
	27.238	8.2029	325.30
	40.423	11.7215	482.77
	52.734	15.7050	629.79
2	5.490	0.6830	29.03
	8.231	0.9910	43.53
	12.276	1.8220	64.91
	18.141	2.6943	95.93
	27.366	4.0627	144.71
	40.727	5.0443	215.36
	53.335	6.2878	282.03

Table B. 6: Aqueous foam rheology measurements – 65%

Pipe #	Flowrate, lpm	Wall Sheart Stress, Pa	Wall Shear Rate, s^{-1}
1	5.54	2.2050	67.24
	8.36	3.4714	101.43
	12.39	5.0527	150.34
	18.04	6.0332	218.97
	27.14	9.7454	329.37
	40.14	13.5496	487.09
	52.34	17.7299	635.19
2	5.42	1.1707	29.30
	8.35	1.7838	45.10
	12.40	2.6349	66.99
	18.32	4.0329	99.02
	27.12	5.4733	146.58
	40.10	7.4182	216.67
	52.63	9.2878	284.38

Table B. 7: Aqueous foam rheology measurements – 70%

Pipe #	Flowrate, lpm	Wall Sheart Stress, Pa	Wall Shear Rate, s^{-1}
1	5.16	5.0984	66.92
	8.02	6.5464	104.08
	12.02	8.4622	155.99
	17.77	11.6274	230.53
	26.86	14.4439	348.50
	39.34	20.1908	510.45
	50.77	27.5498	658.69
2	5.35	3.2687	32.14
	8.22	3.9890	49.36
	12.30	5.2032	73.87
	18.13	6.6178	108.89
	27.04	8.6715	162.39
	39.80	10.6873	239.02
	51.43	14.5345	308.85

Table B. 8: Aqueous foam rheology measurements – 75%

Pipe #	Flowrate, lpm	Wall Sheart Stress, Pa	Wall Shear Rate, s^{-1}
1	4.98	8.1152	69.67
	7.92	10.4142	110.87
	11.77	12.4610	164.67
	17.45	15.7259	244.15
	26.34	18.3520	368.55
	40.06	25.6902	560.53
	50.05	32.6663	700.33
2	5.27	6.3476	34.66
	7.94	7.8322	52.28
	11.86	9.5738	78.07
	17.63	11.6703	116.03
	26.47	13.8395	174.21
	40.41	17.1713	265.92
	50.87	20.7049	334.78

Table B. 9: Aqueous foam rheology measurements – 80%

Pipe #	Flowrate, lpm	Wall Sheart Stress, Pa	Wall Shear Rate, s^{-1}
1	5.03	10.8963	66.23
	7.62	14.0735	100.27
	11.30	18.0562	148.69
	16.95	23.8417	223.01
	24.17	33.5366	318.12
	36.18	41.5869	476.10
	46.72	48.5119	614.93
2	5.04	9.1821	32.72
	7.65	10.0967	49.68
	11.36	12.3788	73.77
	16.94	14.7558	110.04
	25.24	18.1480	163.99
	36.75	24.4343	238.73
	47.60	28.8818	309.26

Table B. 10: Polymer foam rheology measurements – 40%

Pipe #	Flowrate, lpm	Wall Sheart Stress, Pa	Wall Shear Rate, s^{-1}
1	5.48	1.6342	64.32
	8.24	2.4879	96.79
	12.19	3.7942	143.14
	18.34	5.7570	215.42
	27.47	8.8267	322.67
	40.89	12.6699	480.30
	53.48	17.0536	628.15
2	5.50	0.5856	28.71
	8.23	0.9629	42.97
	12.19	1.4354	63.63
	18.37	2.1996	95.90
	27.55	3.3527	143.78
	41.09	4.9277	214.45
	53.87	6.6052	281.16

Table B. 11: Polymer foam rheology measurements – 45%

Pipe #	Flowrate, lpm	Wall Sheart Stress, Pa	Wall Shear Rate, s^{-1}
1	5.59	1.9193	66.02
	8.23	2.8785	97.18
	12.17	4.3257	143.81
	18.28	6.4442	215.94
	27.33	9.8081	322.84
	40.58	14.1523	479.39
	53.06	18.3311	626.84
2	5.64	0.7670	29.69
	8.28	1.1454	43.63
	12.23	1.7422	64.40
	18.36	2.6134	96.69
	27.59	3.8464	145.34
	40.95	5.7826	215.68
	53.61	7.4690	282.39

Table B. 12: Polymer foam rheology measurements – 50%

Pipe #	Flowrate, lpm	Wall Sheart Stress, Pa	Wall Shear Rate, s^{-1}
1	5.56	2.6642	65.77
	8.23	3.8879	97.23
	12.18	5.6514	143.91
	18.23	8.3354	215.50
	27.20	12.2714	321.47
	40.26	17.9033	475.89
	52.44	23.2587	619.88
2	5.56	1.0632	29.34
	8.25	1.5774	43.55
	12.19	2.3428	64.36
	18.28	3.4822	96.52
	27.33	5.1431	144.28
	40.57	7.4734	214.14
	52.97	9.6825	279.64

Table B. 13: Polymer foam rheology measurements – 55%

Pipe #	Flowrate, lpm	Wall Sheart Stress, Pa	Wall Shear Rate, s^{-1}
1	5.56	3.8239	66.75
	8.23	5.4768	98.71
	12.18	7.8477	146.17
	18.19	11.4062	218.26
	27.09	16.6531	324.97
	40.00	24.2893	479.90
	51.90	31.5884	622.64
2	5.54	1.6002	29.79
	8.22	2.2933	44.17
	12.22	3.3168	65.65
	18.29	4.8263	98.27
	27.29	7.0842	146.65
	40.46	10.1436	217.42
	52.75	13.0823	283.46

Table B. 14: Polymer foam rheology measurements – 60%

Pipe #	Flowrate, lpm	Wall Sheart Stress, Pa	Wall Shear Rate, s^{-1}
1	5.45	3.8428	64.67
	8.10	6.2287	96.02
	12.02	9.7002	142.57
	17.99	14.1342	213.33
	26.70	19.8398	316.65
	39.24	28.1373	465.42
	50.75	36.6541	601.97
2	5.50	2.2063	29.74
	8.16	3.0845	44.15
	12.16	4.4126	65.81
	18.17	6.4125	98.32
	27.07	9.1841	146.43
	39.96	13.2229	216.16
	51.91	16.8973	280.80

Table B. 15: Polymer foam rheology measurements – 65%

Pipe #	Flowrate, lpm	Wall Sheart Stress, Pa	Wall Shear Rate, s^{-1}
1	5.34	8.9400	63.10
	8.03	11.7388	94.92
	11.90	15.8633	140.63
	17.75	21.1571	209.82
	26.23	29.0994	310.11
	38.27	40.9713	452.35
	49.41	50.7767	584.07
2	5.30	4.7088	27.99
	8.02	6.0984	42.33
	11.92	8.1542	62.91
	17.58	11.7363	92.83
	26.55	14.8665	140.14
	39.08	20.4512	206.31
	50.66	25.2523	267.47

Table B. 16: Polymer foam rheology measurements – 70%

Pipe #	Flowrate, lpm	Wall Sheart Stress, Pa	Wall Shear Rate, s^{-1}
1	5.12	12.6534	60.53
	7.76	16.3353	91.74
	11.50	21.0372	135.96
	17.28	27.4129	204.24
	25.43	36.2707	300.66
	37.25	47.6997	440.37
	48.12	56.3741	568.81
2	5.18	7.3734	27.35
	7.80	9.5316	41.19
	11.66	12.2529	61.54
	17.47	15.6105	92.22
	25.96	19.8967	137.07
	38.26	26.0061	201.96
	49.70	30.7729	262.41

Table B. 17: Polymer foam rheology measurements – 75%

Pipe #	Flowrate, lpm	Wall Sheart Stress, Pa	Wall Shear Rate, s^{-1}
1	4.97	18.0255	58.81
	7.53	22.4276	89.01
	11.17	29.1479	132.01
	16.65	35.1948	196.77
	24.33	44.2484	287.57
	34.97	59.9557	413.39
	45.42	68.6483	536.95
2	4.93	11.2807	26.02
	7.64	13.8363	40.32
	11.39	16.9075	60.11
	17.06	20.7228	90.07
	24.42	29.0325	128.91
	36.36	35.6665	191.97
	47.34	37.8880	249.94

Table B. 18: Polymer foam rheology measurements – 80%

Pipe #	Flowrate, lpm	Wall Sheart Stress, Pa	Wall Shear Rate, s^{-1}
1	10.770	35.6686	127.31
	15.826	44.9111	187.08
	23.465	56.0902	277.38
	32.330	70.0728	382.18
	41.640	75.0983	492.23
2	4.994	9.2916	26.36
	7.662	10.1742	40.45
	11.357	12.3780	59.96
	16.881	14.7777	89.12
	25.249	18.1533	133.30
	36.745	24.4678	193.99
	47.532	28.9034	250.94

APPENDIX C: BUBBLE SIZE MEASUREMENTS

Table C. 1: Volumetric average bubble diameter of aqueous foam – 40%

d, mm	t, s	ε
0.0452	0	0.6
0.0500	120	0.6
0.0742	240	0.6
0.0928	480	0.6
0.1425	960	0.6
0.1956	1920	0.6

Table C. 2: Volumetric average bubble diameter of aqueous foam – 50%

d, mm	t, s	ε
0.0472	0	0.5
0.0765	120	0.5
0.1071	240	0.5
0.1203	480	0.5
0.1445	960	0.5
0.2592	1920	0.5

Table C. 3: Volumetric average bubble diameter of aqueous foam – 60%

d, mm	t, s	ε
0.1006	0	0.4
0.1369	120	0.4
0.1523	240	0.4
0.1759	480	0.4
0.2643	960	0.4
0.2912	1920	0.4

Table C. 4: Volumetric average bubble diameter of aqueous foam – 70%

d, mm	t, s	ε
0.1375	0	0.3
0.1583	120	0.3
0.1864	240	0.3
0.2024	480	0.3
0.3290	960	0.3
0.3129	1920	0.3

Table C. 5: Volumetric average bubble diameter of aqueous foam – 80%

d, mm	t, s	ε
0.1665	0	0.2
0.3052	120	0.2
0.3203	240	0.2
0.3895	480	0.2
0.6133	960	0.2
0.4549	1920	0.2

Table C. 6: Volumetric average bubble diameter of polymer foam – 40%

d, mm	t, s	ε
0.1030	0	0.6
0.1032	120	0.6
0.1057	240	0.6
0.1322	480	0.6
0.1872	960	0.6
0.2485	1920	0.6

Table C. 7: Volumetric average bubble diameter of polymer foam – 50%

d, mm	t, s	ε
0.0830	0	0.5
0.1045	120	0.5
0.1060	240	0.5
0.1331	480	0.5
0.1418	960	0.5
0.1638	1920	0.5

Table C. 8: Volumetric average bubble diameter of polymer foam – 60%

d, mm	t, s	ε
0.1022	0	0.4
0.1065	120	0.4
0.1573	240	0.4
0.1437	480	0.4
0.2001	960	0.4
0.2192	1920	0.4

Table C. 9: Volumetric average bubble diameter of polymer foam – 70%

d, mm	t, s	ε
0.1232	0	0.3
0.1225	120	0.3
0.1365	240	0.3
0.1736	480	0.3
0.2586	960	0.3
0.4439	1920	0.3

Table C. 10: Volumetric average bubble diameter of polymer foam – 80%

d, mm	t, s	ε
0.1578	0	0.2
0.2894	120	0.2
0.3203	240	0.2
0.3301	480	0.2
0.4630	960	0.2
0.5562	1920	0.2

APPENDIX D: MATHEMATICAL MODELING RESULTS

D1. MATLAB script of channel-dominated model

```
clear all;
mu = ?; %viscosity of base liquid with surfactant (kg/ms)
rho = 1000; %density of base liquid with surfactant (kg/m3)
g = 9.81; %acceleration due to gravity (m/s2)
deltaE = 0.1711; %constant proposed by Koehler et al. (2000)
K1 = ?; %permeability is user input; determined by experimental validation
gamma = ?; %surface tension (kg/s2)

%constants below:
A = mu;
B = 2*K1*rho*g;
C = gamma*deltaE^0.5*K1;
D = gamma*deltaE^0.5*K1;

%model parameters:
deltaT = 60; %timestep (s)
grids = 32; %thirty grids + two imaginary grids
H = ?; %x percent of total height of foam column (m)
z = H/(grids-2); %each grid length
E = zeros(grids,1);
E(:,1) = ?; %initializing model by specifying liquid vol. fraction at t = 0

%computations:
for index = 1 : grids
x1(index) = E (index, 1);
y1 (index) = grids - index;
end
figure(1)
plot(x1,y1);
hold on;

for n = 1:? %n chosen based on total length of experiment
E(1, 1) = 0;
for i = 2:grids-1
L = (0.0005*exp(-14.84*((n*deltaT)^-0.284)*E(i,1)))/3; %foam length (m)
E(i,1) = (deltaT/A)*(C*L*(E(i,1)^-0.5)*((E(i+1,1)-E(i,1))/z)^2 +
D*L*(E(i,1)^0.5)*(E(i+1,1)-2*E(i,1)+E(i-1,1))/(z^2) -
B*(L^2)*E(i,1)*(E(i+1,1)-E(i,1))/z) + E(i,1);
end
for index = 1 : grids;
x1 (index) = E (index, 1);
y1 (index) = index;
end
figure (1)
plot(x1, y1); hold on;
end
```

D2. MATLAB script of node-dominated model

```
clear all;
mu = ?; %viscosity of base liquid with surfactant at 1 1/s (kg/ms)
rho = 1000; %density of base liquid with surfactant (kg/m3)
g = 9.81; %acceleration due to gravity (m/s2)
deltaE = 0.1711; %constant proposed by Koehler et al. (2000)
K2 = ?; %permeability is user input; determined by experimental validation
gamma = ?; %surface tension (kg/s2)

%constants below:
A = mu;
B = 1.5*K2*rho*g;
C = gamma*deltaE^0.5*K2/2;

%model parameters:
deltaT = 60; %timestep (s)
grids = 32; %thirty grids + two imaginary grids
H = ?; %x percent of total height of foam column
z = H/(grids-2); %each grid length
E = zeros(grids,1);
E(:,1) = ?; %initializing model by specifying liquid vol. fraction at t = 0

%computations:
for index = 1 : grids
x1(index) = E (index, 1);
y1 (index) = grids - index;
end
figure(2)
plot(x1,y1);
hold on;
for n = 1:? %n chosen based on total length of experiment
E(1, 1) = 0;
for i = 2:grids-1
L = (0.0003*exp(-3.4*((n*deltaT)^-0.124)*E(i,1)))/3; %foam length (m)
E(i,1) = (deltaT/A)*(C*L*(E(i+1,1)-2*E(i,1)+E(i-1,1))/z^2 -
B*(L^2)*(E(i,1)^0.5)*(E(i+1,1)-E(i,1))/z) + E(i,1);
end
for index = 1 : grids;
x1 (index) = E (index, 1);
y1 (index) = index;
end
figure (2)
plot(x1, y1); hold on;
end
```

Table D. 1: Channel dominated model results for 40% aqueous foam

Mathematical Modeling Results - Channel Dominated							K_1 = 0.0035		
Grids	**y, m**	**t = 0 min**	**t = 2 min**	**t = 4 min**	**t = 8 min**	**t = 16 min**	**t = 32 min**	**t = 64 min**	**t = 144 min**
1	0.007	0.6000	0.5091	0.3720	0.2162	0.0981	0.0325	0.0121	0.0049
2	0.022	0.6000	0.5897	0.5439	0.3854	0.1745	0.0549	0.0201	0.0081
3	0.036	0.6000	0.5989	0.5886	0.5058	0.2557	0.0751	0.0268	0.0107
4	0.050	0.6000	0.5999	0.5979	0.5653	0.3439	0.0954	0.0329	0.0130
5	0.065	0.6000	0.6000	0.5996	0.5886	0.4291	0.1171	0.0387	0.0152
6	0.079	0.6000	0.6000	0.5999	0.5965	0.4977	0.1412	0.0444	0.0172
7	0.093	0.6000	0.6000	0.6000	0.5990	0.5442	0.1688	0.0500	0.0192
8	0.108	0.6000	0.6000	0.6000	0.5997	0.5717	0.2011	0.0556	0.0212
9	0.122	0.6000	0.6000	0.6000	0.5999	0.5865	0.2390	0.0612	0.0231
10	0.137	0.6000	0.6000	0.6000	0.6000	0.5938	0.2831	0.0669	0.0249
11	0.151	0.6000	0.6000	0.6000	0.6000	0.5973	0.3325	0.0727	0.0268
12	0.165	0.6000	0.6000	0.6000	0.6000	0.5989	0.3846	0.0786	0.0286
13	0.180	0.6000	0.6000	0.6000	0.6000	0.5995	0.4353	0.0847	0.0304
14	0.194	0.6000	0.6000	0.6000	0.6000	0.5998	0.4802	0.0909	0.0322
15	0.209	0.6000	0.6000	0.6000	0.6000	0.5999	0.5169	0.0974	0.0340
16	0.223	0.6000	0.6000	0.6000	0.6000	0.6000	0.5446	0.1041	0.0358
17	0.237	0.6000	0.6000	0.6000	0.6000	0.6000	0.5643	0.1111	0.0376
18	0.252	0.6000	0.6000	0.6000	0.6000	0.6000	0.5777	0.1185	0.0393
19	0.266	0.6000	0.6000	0.6000	0.6000	0.6000	0.5864	0.1262	0.0411
20	0.280	0.6000	0.6000	0.6000	0.6000	0.6000	0.5919	0.1344	0.0429
21	0.295	0.6000	0.6000	0.6000	0.6000	0.6000	0.5953	0.1431	0.0447
22	0.309	0.6000	0.6000	0.6000	0.6000	0.6000	0.5973	0.1525	0.0466
23	0.324	0.6000	0.6000	0.6000	0.6000	0.6000	0.5985	0.1626	0.0487
24	0.338	0.6000	0.6000	0.6000	0.6000	0.6000	0.5992	0.1735	0.0517
25	0.352	0.6000	0.6000	0.6000	0.6000	0.6000	0.5995	0.1855	0.0570
26	0.367	0.6000	0.6000	0.6000	0.6000	0.6000	0.5998	0.1987	0.0675
27	0.381	0.6000	0.6000	0.6000	0.6000	0.6000	0.5999	0.2133	0.0876
28	0.395	0.6000	0.6000	0.6000	0.6000	0.6000	0.5999	0.2299	0.1251
29	0.410	0.6000	0.6000	0.6000	0.6000	0.6000	0.6000	0.2619	0.1948
30	0.424	0.6000	0.6000	0.6000	0.6000	0.6000	0.6000	0.3656	0.3300

Table D. 2: Node dominated model results for 40% aqueous foam

Mathematical Modeling Results - Node Dominated							K_2 = 0.0011		
Grids	**y, m**	**t = 0 min**	**t = 2 min**	**t = 4 min**	**t = 8 min**	**t = 16 min**	**t = 32 min**	**t = 64 min**	**t = 144 min**
1	0.007	0.6000	0.5627	0.4957	0.2931	0.0270	0.0037	0.0008	0.0002
2	0.022	0.6000	0.5983	0.5893	0.5272	0.0799	0.0079	0.0016	0.0003
3	0.036	0.6000	0.5999	0.5991	0.5871	0.3552	0.0131	0.0025	0.0005
4	0.050	0.6000	0.6000	0.5999	0.5980	0.5230	0.0197	0.0035	0.0007
5	0.065	0.6000	0.6000	0.6000	0.5997	0.5796	0.0290	0.0046	0.0009
6	0.079	0.6000	0.6000	0.6000	0.6000	0.5951	0.0410	0.0058	0.0011
7	0.093	0.6000	0.6000	0.6000	0.6000	0.5989	0.1400	0.0072	0.0014
8	0.108	0.6000	0.6000	0.6000	0.6000	0.5998	0.3666	0.0086	0.0016
9	0.122	0.6000	0.6000	0.6000	0.6000	0.6000	0.5098	0.0103	0.0018
10	0.137	0.6000	0.6000	0.6000	0.6000	0.6000	0.5690	0.0121	0.0021
11	0.151	0.6000	0.6000	0.6000	0.6000	0.6000	0.5900	0.0141	0.0024
12	0.165	0.6000	0.6000	0.6000	0.6000	0.6000	0.5969	0.0164	0.0027
13	0.180	0.6000	0.6000	0.6000	0.6000	0.6000	0.5991	0.0190	0.0030
14	0.194	0.6000	0.6000	0.6000	0.6000	0.6000	0.5997	0.0219	0.0033
15	0.209	0.6000	0.6000	0.6000	0.6000	0.6000	0.5999	0.0254	0.0036
16	0.223	0.6000	0.6000	0.6000	0.6000	0.6000	0.6000	0.0295	0.0039
17	0.237	0.6000	0.6000	0.6000	0.6000	0.6000	0.6000	0.0347	0.0043
18	0.252	0.6000	0.6000	0.6000	0.6000	0.6000	0.6000	0.0412	0.0047
19	0.266	0.6000	0.6000	0.6000	0.6000	0.6000	0.6000	0.0574	0.0051
20	0.280	0.6000	0.6000	0.6000	0.6000	0.6000	0.6000	0.1922	0.0055
21	0.295	0.6000	0.6000	0.6000	0.6000	0.6000	0.6000	0.3823	0.0059
22	0.309	0.6000	0.6000	0.6000	0.6000	0.6000	0.6000	0.5039	0.0064
23	0.324	0.6000	0.6000	0.6000	0.6000	0.6000	0.6000	0.5611	0.0069
24	0.338	0.6000	0.6000	0.6000	0.6000	0.6000	0.6000	0.5849	0.0075
25	0.352	0.6000	0.6000	0.6000	0.6000	0.6000	0.6000	0.5943	0.0084
26	0.367	0.6000	0.6000	0.6000	0.6000	0.6000	0.6000	0.5979	0.0096
27	0.381	0.6000	0.6000	0.6000	0.6000	0.6000	0.6000	0.5992	0.0116
28	0.395	0.6000	0.6000	0.6000	0.6000	0.6000	0.6000	0.5997	0.0163
29	0.410	0.6000	0.6000	0.6000	0.6000	0.6000	0.6000	0.5999	0.0245
30	0.424	0.6000	0.6000	0.6000	0.6000	0.6000	0.6000	0.6000	0.1110

Table D. 3: Channel dominated model results for 60% aqueous foam

Mathematical Modeling Results - Channel Dominated							K_1 = 0.0025		
Grids	**y, m**	**t = 0 min**	**t = 2 min**	**t = 4 min**	**t = 8 min**	**t = 16 min**	**t = 32 min**	**t = 64 min**	**t = 108 min**
1	0.011	0.4000	0.3302	0.2424	0.1345	0.0617	0.0247	0.0108	0.0062
2	0.032	0.4000	0.3908	0.3591	0.2505	0.1102	0.0420	0.0181	0.0104
3	0.054	0.4000	0.3989	0.3913	0.3356	0.1628	0.0578	0.0244	0.0138
4	0.075	0.4000	0.3999	0.3984	0.3770	0.2237	0.0737	0.0302	0.0170
5	0.097	0.4000	0.4000	0.3997	0.3928	0.2851	0.0905	0.0359	0.0201
6	0.119	0.4000	0.4000	0.4000	0.3979	0.3345	0.1089	0.0415	0.0230
7	0.140	0.4000	0.4000	0.4000	0.3994	0.3666	0.1297	0.0471	0.0259
8	0.162	0.4000	0.4000	0.4000	0.3999	0.3844	0.1536	0.0528	0.0288
9	0.183	0.4000	0.4000	0.4000	0.4000	0.3932	0.1816	0.0585	0.0316
10	0.205	0.4000	0.4000	0.4000	0.4000	0.3972	0.2141	0.0644	0.0344
11	0.226	0.4000	0.4000	0.4000	0.4000	0.3989	0.2498	0.0704	0.0373
12	0.248	0.4000	0.4000	0.4000	0.4000	0.3996	0.2861	0.0766	0.0401
13	0.270	0.4000	0.4000	0.4000	0.4000	0.3999	0.3190	0.0830	0.0430
14	0.291	0.4000	0.4000	0.4000	0.4000	0.4000	0.3460	0.0896	0.0458
15	0.313	0.4000	0.4000	0.4000	0.4000	0.4000	0.3660	0.0966	0.0487
16	0.334	0.4000	0.4000	0.4000	0.4000	0.4000	0.3797	0.1038	0.0517
17	0.356	0.4000	0.4000	0.4000	0.4000	0.4000	0.3884	0.1114	0.0546
18	0.377	0.4000	0.4000	0.4000	0.4000	0.4000	0.3936	0.1194	0.0576
19	0.399	0.4000	0.4000	0.4000	0.4000	0.4000	0.3966	0.1280	0.0606
20	0.421	0.4000	0.4000	0.4000	0.4000	0.4000	0.3983	0.1371	0.0636
21	0.442	0.4000	0.4000	0.4000	0.4000	0.4000	0.3991	0.1469	0.0667
22	0.464	0.4000	0.4000	0.4000	0.4000	0.4000	0.3996	0.1574	0.0698
23	0.485	0.4000	0.4000	0.4000	0.4000	0.4000	0.3998	0.1690	0.0730
24	0.507	0.4000	0.4000	0.4000	0.4000	0.4000	0.3999	0.1816	0.0762
25	0.528	0.4000	0.4000	0.4000	0.4000	0.4000	0.4000	0.1957	0.0795
26	0.550	0.4000	0.4000	0.4000	0.4000	0.4000	0.4000	0.2104	0.0827
27	0.572	0.4000	0.4000	0.4000	0.4000	0.4000	0.4000	0.2299	0.0866
28	0.593	0.4000	0.4000	0.4000	0.4000	0.4000	0.4000	0.2415	0.0884
29	0.615	0.4000	0.4000	0.4000	0.4000	0.4000	0.4000	0.2802	0.1100
30	0.636	0.4000	0.4000	0.4000	0.4000	0.4000	0.4000		0.1893

Table D. 4: Node dominated model results for 60% aqueous foam

Mathematical Modeling Results - Node Dominated							K_2 = 0.002		
Grids	**y, m**	**t = 0 min**	**t = 2 min**	**t = 4 min**	**t = 8 min**	**t = 16 min**	**t = 32 min**	**t = 64 min**	**t = 108 min**
1	0.011	0.4000	0.3774	0.3431	0.2468	0.0176	0.0047	0.0013	0.0006
2	0.032	0.4000	0.3990	0.3952	0.3722	0.1980	0.0103	0.0028	0.0012
3	0.054	0.4000	0.4000	0.3997	0.3962	0.3414	0.0166	0.0045	0.0018
4	0.075	0.4000	0.4000	0.4000	0.3996	0.3869	0.0347	0.0064	0.0026
5	0.097	0.4000	0.4000	0.4000	0.4000	0.3975	0.1781	0.0086	0.0034
6	0.119	0.4000	0.4000	0.4000	0.4000	0.3996	0.3142	0.0110	0.0043
7	0.140	0.4000	0.4000	0.4000	0.4000	0.3999	0.3732	0.0136	0.0053
8	0.162	0.4000	0.4000	0.4000	0.4000	0.4000	0.3925	0.0162	0.0064
9	0.183	0.4000	0.4000	0.4000	0.4000	0.4000	0.3981	0.0189	0.0076
10	0.205	0.4000	0.4000	0.4000	0.4000	0.4000	0.3995	0.0215	0.0088
11	0.226	0.4000	0.4000	0.4000	0.4000	0.4000	0.3999	0.0282	0.0102
12	0.248	0.4000	0.4000	0.4000	0.4000	0.4000	0.4000	0.0904	0.0116
13	0.270	0.4000	0.4000	0.4000	0.4000	0.4000	0.4000	0.2264	0.0131
14	0.291	0.4000	0.4000	0.4000	0.4000	0.4000	0.4000	0.3260	0.0146
15	0.313	0.4000	0.4000	0.4000	0.4000	0.4000	0.4000	0.3725	0.0162
16	0.334	0.4000	0.4000	0.4000	0.4000	0.4000	0.4000	0.3905	0.0178
17	0.356	0.4000	0.4000	0.4000	0.4000	0.4000	0.4000	0.3969	0.0195
18	0.377	0.4000	0.4000	0.4000	0.4000	0.4000	0.4000	0.3990	0.0211
19	0.399	0.4000	0.4000	0.4000	0.4000	0.4000	0.4000	0.3997	0.0227
20	0.421	0.4000	0.4000	0.4000	0.4000	0.4000	0.4000	0.3999	0.0243
21	0.442	0.4000	0.4000	0.4000	0.4000	0.4000	0.4000	0.4000	0.0258
22	0.464	0.4000	0.4000	0.4000	0.4000	0.4000	0.4000	0.4000	0.0277
23	0.485	0.4000	0.4000	0.4000	0.4000	0.4000	0.4000	0.4000	0.0355
24	0.507	0.4000	0.4000	0.4000	0.4000	0.4000	0.4000	0.4000	0.0856
25	0.528	0.4000	0.4000	0.4000	0.4000	0.4000	0.4000	0.4000	0.1997
26	0.550	0.4000	0.4000	0.4000	0.4000	0.4000	0.4000	0.4000	0.3009
27	0.572	0.4000	0.4000	0.4000	0.4000	0.4000	0.4000	0.4000	0.3574
28	0.593	0.4000	0.4000	0.4000	0.4000	0.4000	0.4000	0.4000	0.3829
29	0.615	0.4000	0.4000	0.4000	0.4000	0.4000	0.4000	0.4000	0.3937
30	0.636	0.4000	0.4000	0.4000	0.4000	0.4000	0.4000	0.4000	0.3972

Table D. 5: Channel dominated model results for 80% aqueous foam

Mathematical Modeling Results - Channel Dominated							K_1 = 0.011		
Grids	**y, m**	**t = 0 min**	**t = 2 min**	**t = 4 min**	**t = 8 min**	**t = 16 min**	**t = 32 min**	**t = 64 min**	**t = 144 min**
1	0.014	0.2000	0.0758	0.0409	0.0193	0.0094	0.0049	0.0026	0.0013
2	0.043	0.2000	0.1346	0.0696	0.0322	0.0157	0.0081	0.0043	0.0021
3	0.072	0.2000	0.1689	0.0994	0.0436	0.0210	0.0108	0.0057	0.0028
4	0.101	0.2000	0.1860	0.1291	0.0547	0.0258	0.0132	0.0070	0.0034
5	0.129	0.2000	0.1939	0.1539	0.0661	0.0305	0.0155	0.0082	0.0040
6	0.158	0.2000	0.1974	0.1719	0.0784	0.0350	0.0177	0.0093	0.0045
7	0.187	0.2000	0.1989	0.1836	0.0917	0.0394	0.0198	0.0104	0.0051
8	0.216	0.2000	0.1996	0.1908	0.1064	0.0438	0.0219	0.0115	0.0056
9	0.244	0.2000	0.1998	0.1950	0.1217	0.0483	0.0239	0.0126	0.0061
10	0.273	0.2000	0.1999	0.1974	0.1370	0.0527	0.0259	0.0136	0.0066
11	0.302	0.2000	0.2000	0.1986	0.1512	0.0573	0.0279	0.0146	0.0070
12	0.331	0.2000	0.2000	0.1993	0.1635	0.0619	0.0299	0.0156	0.0075
13	0.359	0.2000	0.2000	0.1996	0.1736	0.0666	0.0319	0.0166	0.0080
14	0.388	0.2000	0.2000	0.1998	0.1814	0.0714	0.0338	0.0175	0.0084
15	0.417	0.2000	0.2000	0.1999	0.1873	0.0764	0.0357	0.0185	0.0089
16	0.446	0.2000	0.2000	0.2000	0.1915	0.0816	0.0377	0.0195	0.0093
17	0.475	0.2000	0.2000	0.2000	0.1944	0.0870	0.0396	0.0204	0.0098
18	0.503	0.2000	0.2000	0.2000	0.1964	0.0927	0.0415	0.0214	0.0102
19	0.532	0.2000	0.2000	0.2000	0.1977	0.0986	0.0434	0.0223	0.0106
20	0.561	0.2000	0.2000	0.2000	0.1986	0.1049	0.0453	0.0232	0.0111
21	0.590	0.2000	0.2000	0.2000	0.1991	0.1116	0.0473	0.0242	0.0115
22	0.618	0.2000	0.2000	0.2000	0.1995	0.1185	0.0491	0.0251	0.0120
23	0.647	0.2000	0.2000	0.2000	0.1997	0.1258	0.0512	0.0260	0.0124
24	0.676	0.2000	0.2000	0.2000	0.1998	0.1333	0.0530	0.0269	0.0130
25	0.705	0.2000	0.2000	0.2000	0.1999	0.1409	0.0549	0.0278	0.0141
26	0.733	0.2000	0.2000	0.2000	0.1999	0.1484	0.0573	0.0287	0.0164
27	0.762	0.2000	0.2000	0.2000	0.2000	0.1558	0.0583	0.0298	0.0212
28	0.791	0.2000	0.2000	0.2000	0.2000	0.1620	0.0617	0.0348	0.0301
29	0.820	0.2000	0.2000	0.2000	0.2000	0.1712	0.0631	0.0513	0.0510
30	0.848	0.2000	0.2000	0.2000	0.2000		0.0963	0.0925	0.0885

Table D. 6: Node dominated model for 80% aqueous foam

Mathematical Modeling Results - Node Dominated							K_2 = 0.0011		
Grids	**y, m**	**t = 0 min**	**t = 2 min**	**t = 4 min**	**t = 8 min**	**t = 16 min**	**t = 32 min**	**t = 64 min**	**t = 144 min**
1	0.014	0.2000	0.1696	0.1273	0.0293	0.0048	0.0015	0.0005	0.0004
2	0.043	0.2000	0.1966	0.1852	0.1223	0.0101	0.0032	0.0011	0.0008
3	0.072	0.2000	0.1997	0.1976	0.1764	0.0263	0.0052	0.0017	0.0013
4	0.101	0.2000	0.2000	0.1997	0.1942	0.0867	0.0075	0.0024	0.0019
5	0.129	0.2000	0.2000	0.2000	0.1987	0.1481	0.0101	0.0032	0.0025
6	0.158	0.2000	0.2000	0.2000	0.1998	0.1809	0.0129	0.0041	0.0032
7	0.187	0.2000	0.2000	0.2000	0.2000	0.1939	0.0163	0.0051	0.0040
8	0.216	0.2000	0.2000	0.2000	0.2000	0.1982	0.0241	0.0062	0.0049
9	0.244	0.2000	0.2000	0.2000	0.2000	0.1995	0.0512	0.0073	0.0058
10	0.273	0.2000	0.2000	0.2000	0.2000	0.1999	0.1011	0.0086	0.0068
11	0.302	0.2000	0.2000	0.2000	0.2000	0.2000	0.1474	0.0100	0.0079
12	0.331	0.2000	0.2000	0.2000	0.2000	0.2000	0.1760	0.0114	0.0090
13	0.359	0.2000	0.2000	0.2000	0.2000	0.2000	0.1902	0.0130	0.0103
14	0.388	0.2000	0.2000	0.2000	0.2000	0.2000	0.1963	0.0146	0.0117
15	0.417	0.2000	0.2000	0.2000	0.2000	0.2000	0.1987	0.0164	0.0131
16	0.446	0.2000	0.2000	0.2000	0.2000	0.2000	0.1995	0.0182	0.0147
17	0.475	0.2000	0.2000	0.2000	0.2000	0.2000	0.1999	0.0201	0.0163
18	0.503	0.2000	0.2000	0.2000	0.2000	0.2000	0.2000	0.0221	0.0181
19	0.532	0.2000	0.2000	0.2000	0.2000	0.2000	0.2000	0.0244	0.0199
20	0.561	0.2000	0.2000	0.2000	0.2000	0.2000	0.2000	0.0279	0.0219
21	0.590	0.2000	0.2000	0.2000	0.2000	0.2000	0.2000	0.0360	0.0240
22	0.618	0.2000	0.2000	0.2000	0.2000	0.2000	0.2000	0.0559	0.0259
23	0.647	0.2000	0.2000	0.2000	0.2000	0.2000	0.2000	0.0904	0.0289
24	0.676	0.2000	0.2000	0.2000	0.2000	0.2000	0.2000	0.1291	0.0291
25	0.705	0.2000	0.2000	0.2000	0.2000	0.2000	0.2000	0.1598	0.0380
26	0.733	0.2000	0.2000	0.2000	0.2000	0.2000	0.2000	0.1793	
27	0.762	0.2000	0.2000	0.2000	0.2000	0.2000	0.2000	0.1901	
28	0.791	0.2000	0.2000	0.2000	0.2000	0.2000	0.2000	0.1954	
29	0.820	0.2000	0.2000	0.2000	0.2000	0.2000	0.2000	0.1981	
30	0.848	0.2000	0.2000	0.2000	0.2000	0.2000	0.2000	0.1990	

Table D. 7: Channel dominated model results for 40% polymer foam

Mathematical Modeling Results - Channel Dominated						K_1 = 0.035			
Grids	**y, m**	**t = 0 min**	**t = 2 min**	**t = 4 min**	**t = 8 min**	**t = 16 min**	**t = 32 min**	**t = 64 min**	**t = 128 min**
1	0.0072	0.6000	0.4147	0.2997	0.2093	0.1329	0.0735	0.0360	0.0172
2	0.0216	0.6000	0.5550	0.4784	0.3551	0.2280	0.1247	0.0602	0.0284
3	0.0359	0.6000	0.5901	0.5590	0.4655	0.3142	0.1713	0.0811	0.0378
4	0.0503	0.6000	0.5979	0.5876	0.5354	0.3935	0.2176	0.1009	0.0463
5	0.0647	0.6000	0.5996	0.5965	0.5722	0.4614	0.2650	0.1205	0.0545
6	0.0791	0.6000	0.5999	0.5991	0.5890	0.5139	0.3135	0.1405	0.0623
7	0.0935	0.6000	0.6000	0.5998	0.5959	0.5503	0.3622	0.1612	0.0701
8	0.1078	0.6000	0.6000	0.5999	0.5986	0.5732	0.4093	0.1827	0.0779
9	0.1222	0.6000	0.6000	0.6000	0.5995	0.5863	0.4528	0.2054	0.0856
10	0.1366	0.6000	0.6000	0.6000	0.5998	0.5934	0.4909	0.2293	0.0935
11	0.1510	0.6000	0.6000	0.6000	0.6000	0.5969	0.5224	0.2545	0.1015
12	0.1654	0.6000	0.6000	0.6000	0.6000	0.5986	0.5469	0.2811	0.1096
13	0.1797	0.6000	0.6000	0.6000	0.6000	0.5994	0.5650	0.3089	0.1179
14	0.1941	0.6000	0.6000	0.6000	0.6000	0.5998	0.5778	0.3376	0.1264
15	0.2085	0.6000	0.6000	0.6000	0.6000	0.5999	0.5863	0.3669	0.1352
16	0.2229	0.6000	0.6000	0.6000	0.6000	0.6000	0.5919	0.3964	0.1442
17	0.2373	0.6000	0.6000	0.6000	0.6000	0.6000	0.5953	0.4252	0.1535
18	0.2516	0.6000	0.6000	0.6000	0.6000	0.6000	0.5974	0.4529	0.1631
19	0.2660	0.6000	0.6000	0.6000	0.6000	0.6000	0.5985	0.4786	0.1731
20	0.2804	0.6000	0.6000	0.6000	0.6000	0.6000	0.5992	0.5019	0.1835
21	0.2948	0.6000	0.6000	0.6000	0.6000	0.6000	0.5996	0.5224	0.1943
22	0.3092	0.6000	0.6000	0.6000	0.6000	0.6000	0.5998	0.5398	0.2055
23	0.3235	0.6000	0.6000	0.6000	0.6000	0.6000	0.5999	0.5543	0.2173
24	0.3379	0.6000	0.6000	0.6000	0.6000	0.6000	0.5999	0.5660	0.2296
25	0.3523	0.6000	0.6000	0.6000	0.6000	0.6000	0.6000	0.5752	0.2426
26	0.3667	0.6000	0.6000	0.6000	0.6000	0.6000	0.6000	0.5822	0.2567
27	0.3811	0.6000	0.6000	0.6000	0.6000	0.6000	0.6000	0.5875	0.2735
28	0.3954	0.6000	0.6000	0.6000	0.6000	0.6000	0.6000	0.5913	0.2985
29	0.4098	0.6000	0.6000	0.6000	0.6000	0.6000	0.6000	0.5941	0.3454
30	0.4242	0.6000	0.6000	0.6000	0.6000	0.6000	0.6000	0.5964	0.4371

Table D. 8: Node dominated model results for 40% polymer foam

Mathematical Modeling Results - Node Dominated							K_2 = 0.03		
Grids	**y, m**	**t = 0 min**	**t = 2 min**	**t = 4 min**	**t = 8 min**	**t = 16 min**	**t = 32 min**	**t = 64 min**	**t = 128 min**
1	0.0072	0.6000	0.5067	0.4042	0.2101	0.0602	0.0174	0.0048	0.0014
2	0.0216	0.6000	0.5893	0.5617	0.4559	0.1738	0.0398	0.0103	0.0028
3	0.0359	0.6000	0.5989	0.5939	0.5612	0.3627	0.0713	0.0166	0.0044
4	0.0503	0.6000	0.5999	0.5991	0.5912	0.5026	0.1214	0.0240	0.0062
5	0.0647	0.6000	0.6000	0.5999	0.5982	0.5667	0.2140	0.0329	0.0080
6	0.0791	0.6000	0.6000	0.6000	0.5997	0.5899	0.3500	0.0438	0.0101
7	0.0935	0.6000	0.6000	0.6000	0.5999	0.5972	0.4695	0.0574	0.0123
8	0.1078	0.6000	0.6000	0.6000	0.6000	0.5993	0.5414	0.0751	0.0148
9	0.1222	0.6000	0.6000	0.6000	0.6000	0.5998	0.5761	0.0991	0.0175
10	0.1366	0.6000	0.6000	0.6000	0.6000	0.6000	0.5909	0.1342	0.0204
11	0.1510	0.6000	0.6000	0.6000	0.6000	0.6000	0.5968	0.1904	0.0237
12	0.1654	0.6000	0.6000	0.6000	0.6000	0.6000	0.5989	0.2786	0.0273
13	0.1797	0.6000	0.6000	0.6000	0.6000	0.6000	0.5996	0.3843	0.0313
14	0.1941	0.6000	0.6000	0.6000	0.6000	0.6000	0.5999	0.4746	0.0357
15	0.2085	0.6000	0.6000	0.6000	0.6000	0.6000	0.6000	0.5342	0.0407
16	0.2229	0.6000	0.6000	0.6000	0.6000	0.6000	0.6000	0.5678	0.0463
17	0.2373	0.6000	0.6000	0.6000	0.6000	0.6000	0.6000	0.5850	0.0527
18	0.2516	0.6000	0.6000	0.6000	0.6000	0.6000	0.6000	0.5933	0.0601
19	0.2660	0.6000	0.6000	0.6000	0.6000	0.6000	0.6000	0.5971	0.0687
20	0.2804	0.6000	0.6000	0.6000	0.6000	0.6000	0.6000	0.5988	0.0789
21	0.2948	0.6000	0.6000	0.6000	0.6000	0.6000	0.6000	0.5995	0.0914
22	0.3092	0.6000	0.6000	0.6000	0.6000	0.6000	0.6000	0.5998	0.1070
23	0.3235	0.6000	0.6000	0.6000	0.6000	0.6000	0.6000	0.5999	0.1274
24	0.3379	0.6000	0.6000	0.6000	0.6000	0.6000	0.6000	0.6000	0.1555
25	0.3523	0.6000	0.6000	0.6000	0.6000	0.6000	0.6000	0.6000	0.1966
26	0.3667	0.6000	0.6000	0.6000	0.6000	0.6000	0.6000	0.6000	0.2576
27	0.3811	0.6000	0.6000	0.6000	0.6000	0.6000	0.6000	0.6000	0.3375
28	0.3954	0.6000	0.6000	0.6000	0.6000	0.6000	0.6000	0.6000	0.4203
29	0.4098	0.6000	0.6000	0.6000	0.6000	0.6000	0.6000	0.6000	0.4888
30	0.4242	0.6000	0.6000	0.6000	0.6000	0.6000	0.6000	0.6000	0.5319

Table D. 9: Channel dominated model results for 60% polymer foam

Mathematical Modeling Results - Channel Dominated						K_1 = 0.06			
Grids	**y, m**	**t = 0 min**	**t = 2 min**	**t = 4 min**	**t = 8 min**	**t = 16 min**	**t = 32 min**	**t = 64 min**	**t = 128 min**
1	0.0108	0.4000	0.2866	0.2095	0.1420	0.0883	0.0490	0.0252	0.0128
2	0.0324	0.4000	0.3746	0.3289	0.2435	0.1523	0.0833	0.0422	0.0212
3	0.0539	0.4000	0.3949	0.3781	0.3192	0.2114	0.1146	0.0571	0.0284
4	0.0755	0.4000	0.3990	0.3940	0.3642	0.2665	0.1457	0.0711	0.0349
5	0.0971	0.4000	0.3998	0.3985	0.3860	0.3137	0.1775	0.0850	0.0412
6	0.1186	0.4000	0.4000	0.3996	0.3950	0.3492	0.2101	0.0991	0.0473
7	0.1402	0.4000	0.4000	0.3999	0.3983	0.3727	0.2431	0.1134	0.0534
8	0.1618	0.4000	0.4000	0.4000	0.3995	0.3864	0.2754	0.1283	0.0594
9	0.1833	0.4000	0.4000	0.4000	0.3998	0.3937	0.3054	0.1437	0.0655
10	0.2049	0.4000	0.4000	0.4000	0.4000	0.3973	0.3317	0.1597	0.0716
11	0.2265	0.4000	0.4000	0.4000	0.4000	0.3989	0.3531	0.1764	0.0777
12	0.2481	0.4000	0.4000	0.4000	0.4000	0.3996	0.3694	0.1939	0.0840
13	0.2696	0.4000	0.4000	0.4000	0.4000	0.3998	0.3811	0.2120	0.0903
14	0.2912	0.4000	0.4000	0.4000	0.4000	0.3999	0.3888	0.2307	0.0968
15	0.3128	0.4000	0.4000	0.4000	0.4000	0.4000	0.3937	0.2498	0.1034
16	0.3343	0.4000	0.4000	0.4000	0.4000	0.4000	0.3966	0.2691	0.1102
17	0.3559	0.4000	0.4000	0.4000	0.4000	0.4000	0.3982	0.2880	0.1171
18	0.3775	0.4000	0.4000	0.4000	0.4000	0.4000	0.3991	0.3063	0.1242
19	0.3990	0.4000	0.4000	0.4000	0.4000	0.4000	0.3996	0.3235	0.1315
20	0.4206	0.4000	0.4000	0.4000	0.4000	0.4000	0.3998	0.3390	0.1390
21	0.4422	0.4000	0.4000	0.4000	0.4000	0.4000	0.3999	0.3527	0.1467
22	0.4637	0.4000	0.4000	0.4000	0.4000	0.4000	0.4000	0.3644	0.1546
23	0.4853	0.4000	0.4000	0.4000	0.4000	0.4000	0.4000	0.3739	0.1628
24	0.5069	0.4000	0.4000	0.4000	0.4000	0.4000	0.4000	0.3814	0.1712
25	0.5285	0.4000	0.4000	0.4000	0.4000	0.4000	0.4000	0.3871	0.1799
26	0.5500	0.4000	0.4000	0.4000	0.4000	0.4000	0.4000	0.3913	0.1889
27	0.5716	0.4000	0.4000	0.4000	0.4000	0.4000	0.4000	0.3943	0.1982
28	0.5932	0.4000	0.4000	0.4000	0.4000	0.4000	0.4000	0.3963	0.2077
29	0.6147	0.4000	0.4000	0.4000	0.4000	0.4000	0.4000	0.3977	0.2203
30	0.6363	0.4000	0.4000	0.4000	0.4000	0.4000	0.4000	0.3985	0.2667

Table D. 10: Node dominated model results for 60% polymer foam

Mathematical Modeling Results - Node Dominated						K_2 = 0.03			
Grids	**y, m**	**t = 0 min**	**t = 2 min**	**t = 4 min**	**t = 8 min**	**t = 16 min**	**t = 32 min**	**t = 64 min**	**t = 128 min**
1	0.0108	0.4000	0.3513	0.2978	0.1874	0.0510	0.0154	0.0048	0.0015
2	0.0324	0.4000	0.3956	0.3843	0.3389	0.1782	0.0364	0.0104	0.0032
3	0.0539	0.4000	0.3996	0.3981	0.3871	0.3082	0.0705	0.0173	0.0051
4	0.0755	0.4000	0.4000	0.3998	0.3977	0.3711	0.1443	0.0256	0.0073
5	0.0971	0.4000	0.4000	0.4000	0.3996	0.3923	0.2499	0.0360	0.0097
6	0.1186	0.4000	0.4000	0.4000	0.3999	0.3982	0.3312	0.0493	0.0124
7	0.1402	0.4000	0.4000	0.4000	0.4000	0.3996	0.3733	0.0672	0.0154
8	0.1618	0.4000	0.4000	0.4000	0.4000	0.3999	0.3908	0.0951	0.0188
9	0.1833	0.4000	0.4000	0.4000	0.4000	0.4000	0.3971	0.1455	0.0225
10	0.2049	0.4000	0.4000	0.4000	0.4000	0.4000	0.3991	0.2205	0.0268
11	0.2265	0.4000	0.4000	0.4000	0.4000	0.4000	0.3998	0.2947	0.0316
12	0.2481	0.4000	0.4000	0.4000	0.4000	0.4000	0.3999	0.3466	0.0370
13	0.2696	0.4000	0.4000	0.4000	0.4000	0.4000	0.4000	0.3756	0.0431
14	0.2912	0.4000	0.4000	0.4000	0.4000	0.4000	0.4000	0.3896	0.0501
15	0.3128	0.4000	0.4000	0.4000	0.4000	0.4000	0.4000	0.3959	0.0582
16	0.3343	0.4000	0.4000	0.4000	0.4000	0.4000	0.4000	0.3984	0.0678
17	0.3559	0.4000	0.4000	0.4000	0.4000	0.4000	0.4000	0.3994	0.0793
18	0.3775	0.4000	0.4000	0.4000	0.4000	0.4000	0.4000	0.3998	0.0943
19	0.3990	0.4000	0.4000	0.4000	0.4000	0.4000	0.4000	0.3999	0.1157
20	0.4206	0.4000	0.4000	0.4000	0.4000	0.4000	0.4000	0.4000	0.1497
21	0.4422	0.4000	0.4000	0.4000	0.4000	0.4000	0.4000	0.4000	0.2002
22	0.4637	0.4000	0.4000	0.4000	0.4000	0.4000	0.4000	0.4000	0.2594
23	0.4853	0.4000	0.4000	0.4000	0.4000	0.4000	0.4000	0.4000	0.3123
24	0.5069	0.4000	0.4000	0.4000	0.4000	0.4000	0.4000	0.4000	0.3502
25	0.5285	0.4000	0.4000	0.4000	0.4000	0.4000	0.4000	0.4000	0.3737
26	0.5500	0.4000	0.4000	0.4000	0.4000	0.4000	0.4000	0.4000	0.3868
27	0.5716	0.4000	0.4000	0.4000	0.4000	0.4000	0.4000	0.4000	0.3936
28	0.5932	0.4000	0.4000	0.4000	0.4000	0.4000	0.4000	0.4000	0.3970
29	0.6147	0.4000	0.4000	0.4000	0.4000	0.4000	0.4000	0.4000	0.3987
30	0.6363	0.4000	0.4000	0.4000	0.4000	0.4000	0.4000	0.4000	0.3993

Table D. 11: Channel dominated model results for 80% polymer foam

Mathematical Modeling Results - Channel Dominated							K_1 = 0.3		
Grids	**y, m**	**t = 0 min**	**t = 2 min**	**t = 4 min**	**t = 8 min**	**t = 16 min**	**t = 32 min**	**t = 64 min**	**t = 123 min**
1	0.0144	0.2000	0.0721	0.0482	0.0294	0.0170	0.0095	0.0053	0.0031
2	0.0431	0.2000	0.1195	0.0798	0.0488	0.0281	0.0157	0.0087	0.0050
3	0.0719	0.2000	0.1523	0.1063	0.0652	0.0375	0.0209	0.0116	0.0066
4	0.1007	0.2000	0.1730	0.1295	0.0804	0.0460	0.0256	0.0141	0.0081
5	0.1294	0.2000	0.1852	0.1491	0.0948	0.0541	0.0300	0.0165	0.0094
6	0.1582	0.2000	0.1921	0.1648	0.1087	0.0619	0.0342	0.0188	0.0107
7	0.1869	0.2000	0.1959	0.1765	0.1220	0.0696	0.0382	0.0209	0.0119
8	0.2157	0.2000	0.1979	0.1848	0.1346	0.0771	0.0422	0.0231	0.0131
9	0.2445	0.2000	0.1989	0.1905	0.1463	0.0846	0.0461	0.0251	0.0142
10	0.2732	0.2000	0.1995	0.1942	0.1570	0.0920	0.0500	0.0272	0.0153
11	0.3020	0.2000	0.1997	0.1965	0.1663	0.0994	0.0538	0.0292	0.0164
12	0.3307	0.2000	0.1999	0.1979	0.1742	0.1067	0.0576	0.0311	0.0175
13	0.3595	0.2000	0.1999	0.1988	0.1807	0.1140	0.0613	0.0331	0.0186
14	0.3883	0.2000	0.2000	0.1993	0.1859	0.1212	0.0651	0.0350	0.0197
15	0.4170	0.2000	0.2000	0.1996	0.1899	0.1283	0.0688	0.0369	0.0207
16	0.4458	0.2000	0.2000	0.1998	0.1929	0.1353	0.0725	0.0388	0.0217
17	0.4745	0.2000	0.2000	0.1999	0.1951	0.1421	0.0763	0.0407	0.0228
18	0.5033	0.2000	0.2000	0.1999	0.1967	0.1487	0.0800	0.0426	0.0238
19	0.5321	0.2000	0.2000	0.2000	0.1978	0.1550	0.0837	0.0445	0.0248
20	0.5608	0.2000	0.2000	0.2000	0.1985	0.1609	0.0874	0.0464	0.0258
21	0.5896	0.2000	0.2000	0.2000	0.1991	0.1665	0.0911	0.0482	0.0269
22	0.6183	0.2000	0.2000	0.2000	0.1994	0.1716	0.0949	0.0501	0.0279
23	0.6471	0.2000	0.2000	0.2000	0.1996	0.1762	0.0986	0.0519	0.0290
24	0.6758	0.2000	0.2000	0.2000	0.1998	0.1804	0.1023	0.0538	0.0302
25	0.7046	0.2000	0.2000	0.2000	0.1999	0.1840	0.1061	0.0556	0.0319
26	0.7334	0.2000	0.2000	0.2000	0.1999	0.1871	0.1098	0.0575	0.0350
27	0.7621	0.2000	0.2000	0.2000	0.1999	0.1898	0.1136	0.0598	0.0412
28	0.7909	0.2000	0.2000	0.2000	0.2000	0.1920	0.1174	0.0653	0.0531
29	0.8196	0.2000	0.2000	0.2000	0.2000	0.1939	0.1205	0.0813	0.0752
30	0.8484	0.2000	0.2000	0.2000	0.2000	0.1948	0.1354	0.1191	0.1167

Table D. 12: Node dominated model results for 80% polymer foam

Mathematical Modeling Results - Node Dominated							K_2 = 0.1		
Grids	**y, m**	**t = 0 min**	**t = 2 min**	**t = 4 min**	**t = 8 min**	**t = 16 min**	**t = 32 min**	**t = 64 min**	**t = 123 min**
1	0.0144	0.2000	0.1313	0.0678	0.0189	0.0064	0.0022	0.0007	0.0003
2	0.0431	0.2000	0.1826	0.1423	0.0524	0.0142	0.0046	0.0015	0.0005
3	0.0719	0.2000	0.1961	0.1801	0.1050	0.0243	0.0074	0.0024	0.0008
4	0.1007	0.2000	0.1992	0.1940	0.1513	0.0383	0.0107	0.0034	0.0012
5	0.1294	0.2000	0.1998	0.1983	0.1787	0.0600	0.0145	0.0044	0.0015
6	0.1582	0.2000	0.2000	0.1996	0.1917	0.0921	0.0189	0.0056	0.0019
7	0.1869	0.2000	0.2000	0.1999	0.1970	0.1280	0.0240	0.0068	0.0023
8	0.2157	0.2000	0.2000	0.2000	0.1990	0.1580	0.0300	0.0082	0.0027
9	0.2445	0.2000	0.2000	0.2000	0.1997	0.1780	0.0372	0.0098	0.0031
10	0.2732	0.2000	0.2000	0.2000	0.1999	0.1894	0.0460	0.0114	0.0036
11	0.3020	0.2000	0.2000	0.2000	0.2000	0.1952	0.0573	0.0132	0.0041
12	0.3307	0.2000	0.2000	0.2000	0.2000	0.1980	0.0725	0.0151	0.0046
13	0.3595	0.2000	0.2000	0.2000	0.2000	0.1992	0.0925	0.0173	0.0052
14	0.3883	0.2000	0.2000	0.2000	0.2000	0.1997	0.1163	0.0196	0.0058
15	0.4170	0.2000	0.2000	0.2000	0.2000	0.1999	0.1403	0.0221	0.0064
16	0.4458	0.2000	0.2000	0.2000	0.2000	0.2000	0.1608	0.0248	0.0071
17	0.4745	0.2000	0.2000	0.2000	0.2000	0.2000	0.1761	0.0277	0.0078
18	0.5033	0.2000	0.2000	0.2000	0.2000	0.2000	0.1863	0.0309	0.0085
19	0.5321	0.2000	0.2000	0.2000	0.2000	0.2000	0.1925	0.0344	0.0093
20	0.5608	0.2000	0.2000	0.2000	0.2000	0.2000	0.1961	0.0383	0.0101
21	0.5896	0.2000	0.2000	0.2000	0.2000	0.2000	0.1980	0.0425	0.0109
22	0.6183	0.2000	0.2000	0.2000	0.2000	0.2000	0.1991	0.0472	0.0118
23	0.6471	0.2000	0.2000	0.2000	0.2000	0.2000	0.1996	0.0524	0.0127
24	0.6758	0.2000	0.2000	0.2000	0.2000	0.2000	0.1998	0.0582	0.0137
25	0.7046	0.2000	0.2000	0.2000	0.2000	0.2000	0.1999	0.0654	0.0147
26	0.7334	0.2000	0.2000	0.2000	0.2000	0.2000	0.2000	0.0722	0.0158
27	0.7621	0.2000	0.2000	0.2000	0.2000	0.2000	0.2000	0.0860	0.0169
28	0.7909	0.2000	0.2000	0.2000	0.2000	0.2000	0.2000		0.0181
29	0.8196	0.2000	0.2000	0.2000	0.2000	0.2000	0.2000		0.0199
30	0.8484	0.2000	0.2000	0.2000	0.2000	0.2000	0.2000		0.0265